Institute of Experimental and Clinical Pharmacology and Toxicology
Preclinical Center for Molecular Signaling (PZMS)

Faculty of Medicine

Saarland University, Homburg (Saar)

Ca^{2+}-dependent mechanisms of ADAM10 activation in non-excitable cells

Dissertation

Submitted in Fulfillment of the Requirements for the Degree of

Doctor rerum naturalium (Dr. rer. nat.)

of the Medical Faculty of Saarland University

2025

by

Federico Guillermo Gharzia

born on 18.10.1994 in Argentina

Tag der Promotion: 02.06.2026

Dekan: Univ.-Prof. Dr. med. dent. Matthias Hannig

Berichterstatter: Prof. Dr. Daniela Yildiz

Prof. Dr. David Mick

Doctoral supervisor: Univ.-Prof. Dr. rer. nat. Daniela Yildiz

Table of Content

1 Summary

A disintegrin and metalloproteinase is a family of zinc-dependent metalloproteinases that primarily act on the cellular surface, cleaving their substrates near the surface in a process called shedding. Among their members, ADAM10 is an important metalloproteinase mostly known for its participation in Notch signaling.. Some of its most prominent substrates are the adherens junction(AJ)-forming molecule E-cadherin and the epidermal growth factor betacellulin. It has been proposed that intracellular Ca^{2+} increases can promote the activation of ADAM10 since a stimulation of different cell lines with ionophores like ionomycin has led to an augmentation of ADAM10 activity. Due to ADAM10's involvement in pathologies such as AD, cancer development, acute inflammatory responses and pathogen entry, a deeper understanding of ADAM10 regulation through Ca^{2+} is crucial for more effective treatment of these conditions.

To investigate the Ca^{2+} dependent activation of ADAM10 in more detail, ionomycin, trifluoperazine and ophiobolin A as reagents promoting different manners of Ca^{2+} entry were tested for their ADAM10 activation. Their effects were further investigated under Ca^{2+} free conditions and intracellular Ca^{2+} sequestration to determine the origin of these activating Ca^{2+} ions. Furthermore, time- and threshold dependence were investigated using increasing concentrations of ionomycin and a minimal concentration of ionomycin resulting in intracellular Ca^{2+} increase. In parallel, the effect of these stimulations on membrane-unbound forms and non-cell associated forms such as in exosomes contribute to the activity promotion observed under these conditions. The mentioned stimuli are artificial stimuli. Physiological Ca^{2+} entry pathways would be, as one example, be represented by members of the TRP channel family, which were investigated for their effects on ADAM10 activation. As readout for the activity, the cleavage of E-cadherin was used, and its processing into different fragments was investigated in more detail using various tagged versions of E-cadherin. Finally, *Pseudomonas aeruginosa* infection was used as a natural stimulus, in conjunction with inhibitors of the PQS quorum sensing communication system, to assess the activation of ADAM10 and the potential involvement of Ca^{2+} ions under these conditions.

Stimulation with ionomycin and trifluoperazine under chelating conditions or in the nominal absence of Ca^{2+} revealed a dependency on extracellular Ca^{2+} for the activation of ADAM10 when stimulated with ionomycin. However, trifluoperazine appeared to be only partially dependent on Ca^{2+} in promoting ADAM10 activity. Furthermore, ionomycin stimulation was found to be time-independent and to reach a Ca^{2+} influx threshold when utilizing a concentration of at least 0.6 µM of ionomycin. On the other hand, stimulations with trifluoperazine required longer times to achieve a significant increase in ADAM10 activity. Cell-uncoupled forms of ADAM10 were found to be activated more rapidly by trifluoperazine than by ionomycin, which correlated with the surface expression of ADAM10, also upregulated under trifluoperazine stimulation. Additionally, the release of ADAM10 in exosomes was increased in the presence of extracellular Ca^{2+}. Furthermore, ADAM10 was activated after the opening of members of the TRPC subfamily, but not by TRPM3 as representative of the melastatin subfamily. pointing towards a potential dependence on the formation of certain microdomains. The infection with *Peudomonas aeruginosa* resulted in a subsequent activation of ADAM10. This was only partially reduced when the cells were infected with a pyocyanin knockout mutant and completely abrogated when inhibiting the bacteria with PQS inhibitors overnight. Although Ca^{2+} imaging experiments revealed a slight Ca^{2+} increase when infecting with *Pseudomonas aeruginosa,* which is ablated when using previously incubated bacteria with PQS inhibitors, different mechanisms may account for the observed activation.

The opening of specific Ca^{2+} channels and the temporal dynamics of subsequent Ca^{2+} entry offers novel possibilities to target ADAM10 while circumventing detrimental side-effects of systemic inhibition.

1 Zusammenfassung

Disintegrin und Metalloproteinas e ist eine Familie von zinkabhängigen Metalloproteinasen, die hauptsächlich auf der Zelloberfläche wirken und ihre Substrate in einem als Shedding bezeichneten Prozess nahe der Oberfläche spalten. Unter ihren Mitgliedern ist ADAM10 eine wichtige Metalloprotease, die vor allem für ihre Beteiligung an der Notch-Signalübertragung bekannt ist. Zu ihren wichtigsten Substraten gehören das Adhäsionsmolekül E-Cadherin, das Adhäsionsverbindungen (AJ) bildet, und der epidermale Wachstumsfaktor Betacellulin. Es wurde vermutet, dass ein Anstieg des intrazellulären Ca^{2+} die Aktivierung von ADAM10 fördern kann, da eine Stimulation verschiedener Zelllinien mit Ionophoren wie Ionomycin zu einer Steigerung der ADAM10-Aktivität geführt hat. Aufgrund der Beteiligung von ADAM10 an Pathologien wie Alzheimer, Krebsentwicklung, akuten Entzündungsreaktionen und dem Eindringen von Krankheitserregern ist ein tieferes Verständnis der Regulation von ADAM10 durch Ca^{2+} für eine wirksamere Behandlung dieser Erkrankungen von entscheidender Bedeutung.

Um die Ca^{2+}-abhängige Aktivierung von ADAM10 genauer zu untersuchen, wurden Ionomycin, Trifluoperazin und Ophiobolin A als Reagenzien, die unterschiedliche Arten des Ca^{2+}-Eintritts fördern, auf ihre ADAM10-Aktivierung getestet. Ihre Wirkungen wurden unter Ca^{2+}-freien Bedingungen und bei intrazellulärer Ca^{2+}-Sequestrierung weiter untersucht, um den Ursprung dieser aktivierenden Ca^{2+}-Ionen zu bestimmen. Darüber hinaus wurden die Zeit- und Schwellenwertabhängigkeit unter Verwendung steigender Ionomycin-Konzentrationen und einer minimalen Ionomycin-Konzentration, die zu einem Anstieg des intrazellulären Ca^{2+} führt, untersucht. Parallel dazu wurde untersucht, inwieweit die Wirkung dieser Stimulationen auf membrangebundene und nicht zellassoziierte Formen, wie z. B. in Exosomen, zur unter diesen Bedingungen beobachteten Aktivitätsförderung beiträgt. Bei den genannten Stimuli handelt es sich um künstliche Stimuli. Physiologische Ca^{2+}-Eintrittswege wären beispielsweise durch Mitglieder der TRP-Kanalfamilie repräsentiert, die auf ihre Auswirkungen auf die ADAM10-Aktivierung untersucht wurden. Als Messgröße für die Aktivität wurde die Spaltung von E-Cadherin verwendet, und seine Verarbeitung zu verschiedenen Fragmenten wurde unter Verwendung verschiedener markierter Versionen von E-Cadherin genauer untersucht. Schließlich wurde eine Infektion mit Pseudomonas aeruginosa als natürlicher Stimulus in Verbindung mit Inhibitoren des PQS-Quorum-Sensing-Kommunikationssystems verwendet, um die Aktivierung von ADAM10 und die mögliche Beteiligung von Ca^{2+}-Ionen unter diesen Bedingungen zu bewerten.

Die Stimulation mit Ionomycin und Trifluoperazin unter chelatbildenden Bedingungen oder bei nomineller Abwesenheit von Ca^{2+} zeigte eine Abhängigkeit von extrazellulärem Ca^{2+} für die Aktivierung von ADAM10 bei Stimulation mit Ionomycin. Trifluoperazin schien jedoch nur teilweise von Ca^{2+} abhängig zu sein, um die ADAM10-Aktivität zu fördern. Darüber hinaus wurde festgestellt, dass die Ionomycin-Stimulation zeitunabhängig war und bei Verwendung einer Konzentration von mindestens 0,6 µM Ionomycin einen Ca^{2+}-Einstromschwellenwert erreichte. Andererseits erforderten Stimulationen mit Trifluoperazin längere Zeiten, um einen signifikanten Anstieg der ADAM10-Aktivität zu erreichen. Es wurde festgestellt, dass zellunabhängige Formen von ADAM10 durch Trifluoperazin schneller aktiviert wurden als durch Ionomycin, was mit der Oberflächenexpression von ADAM10 korrelierte, die ebenfalls unter Trifluoperazin-Stimulation hochreguliert wurde. Darüber hinaus war die Freisetzung von ADAM10 in Exosomen in Gegenwart von extrazellulärem Ca^{2+} erhöht. Außerdem wurde ADAM10 nach der Öffnung von Mitgliedern der TRPC-Unterfamilie aktiviert, jedoch nicht durch TRPM3 als Vertreter der Melastatin-Unterfamilie. Dies deutet auf eine mögliche Abhängigkeit von der Bildung bestimmter Mikrodomänen hin. Die Infektion mit Peudomonas aeruginosa führte zu einer anschließenden Aktivierung von ADAM10. Diese wurde nur teilweise reduziert, wenn die Zellen mit einem Pyocyanin-Knockout-Mutanten infiziert wurden, und vollständig aufgehoben, wenn die

Bakterien über Nacht mit PQS-Inhibitoren gehemmt wurden. Obwohl Ca^{2+}-Bildgebungsversuche einen leichten Ca^{2+}-Anstieg bei der Infektion mit Pseudomonas aeruginosa zeigten, der bei Verwendung von zuvor mit PQS-Inhibitoren inkubierten Bakterien abgebaut wurde, könnten unterschiedliche Mechanismen für die beobachtete Aktivierung verantwortlich sein.

Die Öffnung spezifischer Ca^{2+}-Kanäle und die zeitliche Dynamik des anschließenden Ca^{2+}-Eintritts bieten neue Möglichkeiten, ADAM10 gezielt zu beeinflussen und gleichzeitig die nachteiligen Nebenwirkungen einer systemischen Hemmung zu umgehen.

2 Introduction

2.1 Proteases, metalloproteinases and the metzincins superfamily

Proteases are considered in research not only to be important targets for the biopharmaceutical industry (Turk, 2006) but also targets for many pathogens, promoting either directly or indirectly their infective capacities (Agbowuro *et al.*, 2018; Marquart, 2021). Proteases are enzymes catalyzing the cleavage of peptide bonds. They were previously thought to be only involved in the metabolism of misdirected, unassembled, or misfolded proteins (Werb, 1997). However, besides these nonspecific cleavage functions, proteases participate and are relevant in many physiological processes such as fate, localization and activity of many proteins, modulation of protein-protein interactions, creation of new bioactive molecules, contribution to the processing of cellular information and generation, transduction and amplification of molecular signals (López-Otín and Bond, 2008). The size of proteases ranges from a single amino acid chain corresponding to a zinc metalloproteinase of *Streptomyces caespitosus* (Harada *et al.*, 1995) to single-chain multidomain structures like the family of ADAM proteases with around 80 to 130 kilodaltons (kDa) (Giebeler and Zigrino, 2016). Bulkier complexes like the cytosolic 26S proteasome complex with around 2000 kDa in size also exist (Bard et al., 2019).

Proteases can be classified based on their optimal pH activity (Mala *et al.*, 1998) the evolutionary phylogeny based on their sequence similarity (Rawlings, Barrett and Bateman, 2012) and the site of cleavage (Van Der Velden and Hulsmann, 1999). The most important classification is based on their catalytic residue participating in the cleavage, classifying proteases into seven broad groups (López-Otín and Bond, 2008): serine proteases, cysteine proteases, threonine proteases, aspartic proteases, glutamic proteases, asparagine peptide hydrolases and metalloproteinases. Members of the different families have a variable range of specificities, which is determined by the molecular interactions in the protein-protein interface between the protease and its substrate (Schauperl *et al.*, 2015). The nomenclature by Schechter and Berger indicates which amino acids and the probability that they have to occupy the different positions of the cleavage site (Schechter and Berger, 1972) visualized as a "sequence logo" where the more likely an amino acid for a determined position is, the bigger it is graphed (Fig. 2.1) (Ratnikov *et al.*, 2014).

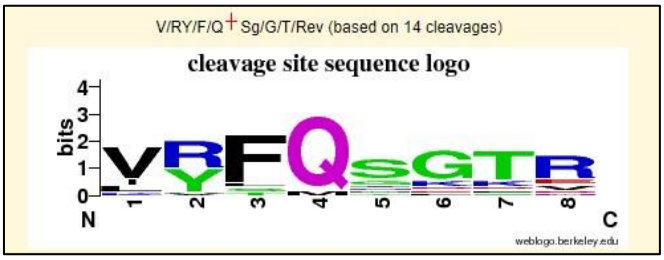

Figure 2.1. Protease specificity matrix.

Example of a specificity matrix taken from the MEROPS database of the tobacco etch virus Nla peptidase (Kapust *et al.*, 2002; Rawlings, Barrett and Bateman, 2012).

The specificity of single proteases ranges from broad-range proteases like trypsin (Olsen, Ong and Mann, 2004) to proteases with more restricted activities like tobacco etch virus peptidases (Kapust *et al.*, 2002) or thrombin since these proteases have to be tightly controlled for a correct physiological activity (Gallwitz *et al.*, 2012).

One important class of physiologically and pathophysiologically important protease are metalloproteinases characterized by a ligated metal ion in their catalytic pockets (Chang and Werb, 2001). The ligated metal ion is usually zinc, although in some cases cobalt or manganese might appear instead (Griffin and Fogarty, 1973; Galindo-Murillo and Cheatham, 2014). The primary characteristic responsible for the binding of the zinc ion is the presence of the motif HEXXHXXGXXH, with the three

histidines acting as ligands to the zinc ion. Metalloproteinases that possess this binding motif are called metzincins (Bode, Gomis-Rüth and Stöckler, 1993), including the matrix metalloproteinases (MMPs) or matrixins, bacterial serralysins, astracins and reprolysins. The reprolysins include snake venom metalloproteinases (e.g., adamalysins, atrolysins) and 'a disintegrin and metalloproteinase' (ADAM) proteases (Nagase, 2001).

2.1.1 A disintegrin and metalloproteinase

ADAM proteases are type 1 transmembrane proteins characterized by the presence of both a disintegrin and a metalloproteinase domain. Their primary function is to cleave other transmembrane proteins near the cell surface. This process is called ectodomain shedding (Giebeler and Zigrino, 2016). However, their multidomain topology allows them to perform different functions aside from the catalysis (Saha et al., 2017). This is particularly important considering that some ADAM members lack their cleavage function and act through the binding of other proteins like integrins through their disintegrin domain (Huang, Bridges and White, 2005). Humans possess 33 different members of the ADAM family, of which 12 are pseudogenes. Of the remaining 21, only 13 members show a catalytic activity (Edwards, Handsley and Pennington, 2009). Like all other proteins allocated to the secretory pathway, ADAMs possess a signal sequence in their N-terminus responsible for this targeting. This is followed by a pro-domain which performs two functions: the correct folding of the protein, acting as an internal chaperone protecting the enzyme from early degradation and it is responsible for keeping the protease in a latent, inactivated state through a cysteine-switch (Milla, Gonzales and Leonard, 2006). The pro-domain is typically removed during transit through the Golgi apparatus by pro-protein convertases like furins (Endres *et al.*, 2003). At this point, two forms in ADAMs are recognized: the pro-form, which contains the pro-domain and the mature form after its cleavage by furins. The catalytic reprolysin domain is responsible for the catalytic function, containing the consensual motif of metzincins HEXXHXXGXXH (Aitken, 1999). Accordingly, mutations in some members in this motif renders them unable to perform their catalytic functions. C-terminal to the catalytic domain is the disintegrin-like domain, known from small proteins in snake venoms containing a similar domain with the ability to bind platelet integrins, subsequently preventing platelet aggregation and blood clotting (Huang, Bridges and White, 2005; Lu *et al.*, 2005). Next to this domain, ADAMs possess a cysteine-rich domain whose functions have been related to integrin adhesion, embryonic development as well as substrate recognition (Peschon *et al.*, 1998). The C-terminal cytoplasmic tail of ADAM proteases varies in length and architecture, resulting in lower sequence identity between ADAM orthologues for the C-terminus compared to the extracellular domains. Some ADAM members can bind different regulatory proteins like calmodulin (CaM) (Nagano *et al.*, 2004), Src homology region-3 (SH3) domain or Synapse Associated Protein-97 (Marcello *et al.*, 2007).

Since a dysregulation of ADAM proteases is responsible for various diseases, tight control with different regulatory checkpoints is required. These regulatory checkpoints include the genetic expression and regulation of their expression by transcription factor activity, as well as their transit through the secretory pathway as signal peptide-containing proteins. Additionally, the activity of ADAMs can be further regulated by their coupling with partner proteins such as tetraspanins (Tspans) (Eschenbrenner *et al.*, 2020) or inactive rhomboid like proteins (iRhoms) (Groth *et al.*, 2016a) further supporting their correct localization or by narrowing their substrate specificity (Matthews *et al.*, 2017). Once metalloproteinases are located on the cell surface, they can still undergo further regulation via their recycling in endosomes or degradation. They can also be released in extracellular vesicles (EVs) which are then released into the extracellular space where they can remodel the extracellular matrix (ECM) (Shimoda, 2019) or cleave other proteins *in trans* located on neighboring cells (Aljohmani *et al.*, 2022). Regulation of their activity constitutes an additional regulatory checkpoint (Guerra *et al.*, 2021). This is achieved through the use of endogenous tissue inhibitors of metalloproteinases (TIMPs), which

can further act on the membrane surface as well (Murphy, 2011). Once located on the membrane surface, metalloproteinase activity can be further regulated by various signaling pathways, such as the (un)coupling of specific binding proteins, like CaM (Pan et al., 2012), or Ca^{2+} influxes (Veit *et al.*, 2018). Ca^{2+} influxes could be part of a controlled process that regulates normal Ca^{2+} homeostasis in the cell, or they may be involved in various pathophysiological processes.

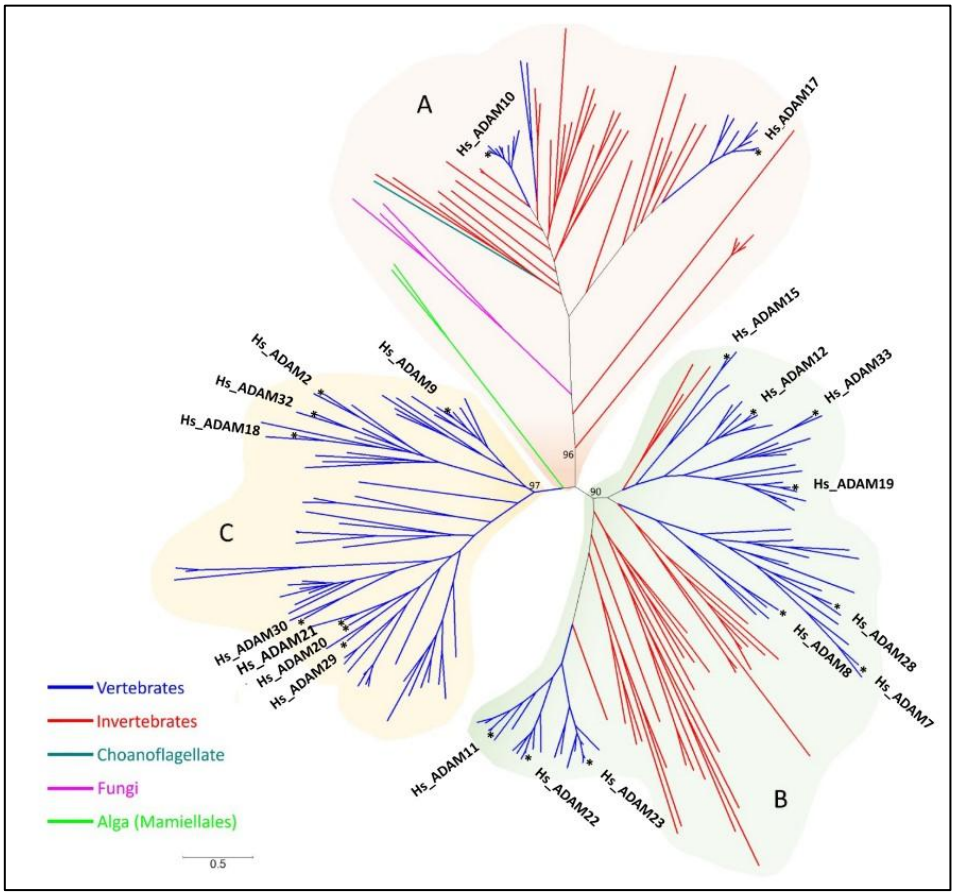

Figure 2.2. ADAMs phylogenic tree.
Phylogenia of different eukaryotic ADAMs clustered in three different clades as shown in Souza *et al.*, 2020.

Among the most important physiological roles played by ADAMs are fertility through sperm-egg interactions, cell fate and formation of central nervous system (CNS), cell migration and several aspects in cell immunity such as orchestration of immune and inflammatory responses (Evans, Schultz and Kopf, 1998; Evans, 2001; Van Der Vorst, Weber and Donners, 2018; Arai *et al.*, 2023 Edwards, Handsley and Pennington, 2009)). The knockout of some ADAM genes has been related to either early to perinatal lethality, as observed in *in vivo* studies with ADAM10 and ADAM17. Therefore, ADAM proteases might be suitable targets for therapeutic interventions, however, a more detailed understanding of their activation mechanisms is necessary.

2.1.1.1 ADAM10

ADAM10, together with ADAM17, is one of the most researched ADAMs. They share the lack of an epidermal growth factor (EGF)-like domain close to the plasma membrane (Giebeler and Zigrino, 2016), clustering them phylogenetically together (Fig. 2.2). ADAM10 covers a broad substrate spectrum, like adhesion molecules, receptors and ligands. One important substrate of ADAM10 is E-cadherin, the most prominent AJ molecule in epithelial tissues (Campbell, L and DeMali, 2017). It plays a crucial role in the formation of the apical-basal polarity of epithelial cells since an ablation of E-

cadherin consequentially randomizes nuclear position and lamellipodial ruffling in kidney epithelial cells (Fig. 2.3) (Desai *et al.*, 2009). Furthermore, studies *in vivo* point towards a disruption of spindle formations and a loss of polarity in prostate luminal cells upon E-cadherin knockout (Wang *et al.*, 2018). In recent years, an additional function has been assigned to the ectodomain of E-cadherins. For example, certain groups have correlated a higher amount of proteolysis-derived soluble ectodomain of E-cadherin with certain cancer types. Additionally, the released ectodomain of E-cadherin has been shown to disrupt cell-cell interactions, promote migration and invasion and also promote the proliferation and survival of certain cancer cells *in vitro* (Grabowska and Day, 2012; Tang *et al.*, 2018).

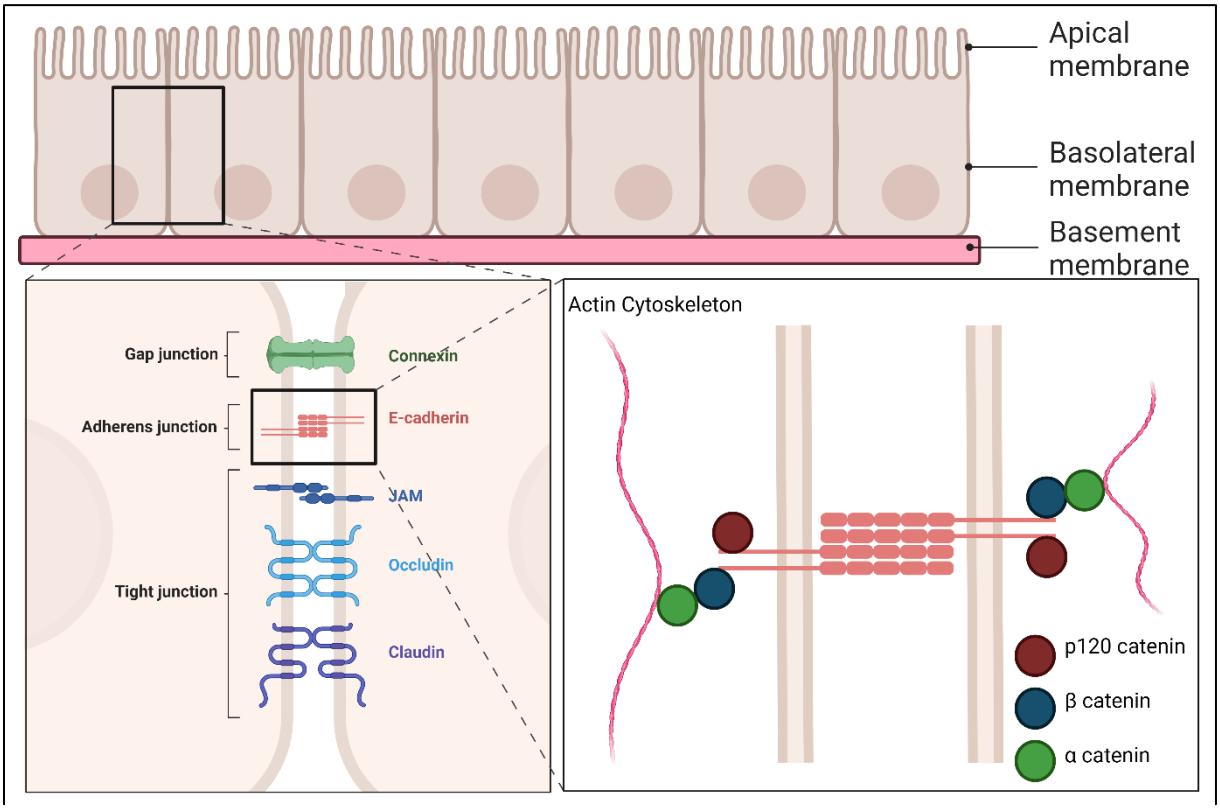

Figure 2.3. Adherens junctions and E-cadherin.

Location of different types of cell-cell interactions on epithelial tissue and schematic representation of AJ formed by E-cadherin.

The processing of E-cadherin by ADAM10 has gained relevance not only in cancer research but also in bacterial infection since cadherins constitute one of the first protective barriers of the organism against pathogens, mediating host-pathogen interaction (Dash, Duraivelan and Samanta, 2021). The cleavage capacity of E-cadherin by ADAM10 is utilized by several bacteria to enhance their infectivity, invasiveness and establishment in additional tissues. This is achieved by Ca^{2+} entry into the cell as an influx from the extracellular space or an efflux from the mitochondria into the cytosol (Reboud *et al.*, 2017; Ramachandran *et al.*, 2020). Additionally, ADAM10 may also function as a virus cofactor, thereby contributing not only to E-cadherin cleavage but also to EGF cleavage, transactivating EGFR members and thus enhancing cell-to-cell infectivity (Carriquí-Madroñal *et al.*, 2023). Cleavage of E-cadherin also leads to the development of an epithelial-to-mesenchymal transition (EMT) . The maintenance of the epithelial phenotype in cells depends, at least in part, on the correct regulation of AJ that form the epithelial barrier. Thus, whenever an epithelial phenotype changes to a mesenchymal one, it has been observed that the E-cadherin expression level decreases while N-cadherin is upregulated in a process termed “cadherin switch” (Araki *et al.*, 2011). Metalloproteinases like ADAM10 have been the focus of

many studies relating EMT with their E-cadherin cleavage however, in some cases, it is not clear whether this is in fact because of a direct action of the protease on E-cadherin or as a consequence of the enhanced Notch signaling (Park *et al.*, 2015; Hou *et al.*, 2018; Liu *et al.*, 2018; Mueller *et al.*, 2021; Xie *et al.*, 2021).

Among the most important diseases where an important role has been attributed to ADAM10 is AD. This most common neurodegenerative disease is suffered by over 55 million people worldwide in 2020 and has an estimate of 139 million by 2050, according to Alzheimer's Disease International. It is characterized by memory loss and a progressive disability to perform routine functions. According to the amyloid cascade hypothesis of AD, the cause of the disease's progression is the formation of amyloid plaques in neurons. These plaques are generated after the C99 fragment from the β-secretase-processed amyloid precursor protein (APP) is processed by γ-secretases(O'Brien and Wong, 2011). Processing by α-secretases such as ADAM10 is under investigation as a possible future therapeutical option against AD because they generate a fragment that γ-secretases will not process (Nunan and Small, 2000). Additionally, ADAM10 has been extensively investigated for its roles in the inflammatory response, as well as in the progression of various immunological and autoimmune diseases. ADAM10's role in several inflammatory diseases has, therefore, also been a subject of research, e.g., in multiple sclerosis (MS), rheumatoid arthritis (RA) and atherosclerosis. It has been shown that an increased content of ADAM10 in synovial fluid of RA patients is correlated with joint degradation and that it plays significant pro-migratory roles in MS (Smith, Tharakan and Martin, 2020).

ADAM10 has been identified as a prominent target for certain diseases; therefore, efforts have been made to regulate its expression and activity more effectively. Several synthetic metalloproteinase inhibitors, such as batimastat and marimastat, have been developed. However, these inhibitors affect numerous metalloproteinases and lack selectivity among them (Parsons, Watson and Steele, 1997; Groves *et al.*, 2006). Other synthetic inhibitors capable of selectively targeting particular members have been produced since then. One example that is still frequently used in ADAM10 research is GI254023X (GI), which shows a 100-fold increased selectivity to ADAM10 in comparison to its closely related member ADAM17 (Hoettecke *et al.*, 2010). However, clinical trials involving this inhibitor were discontinued due to hepatic toxicity (Smith, Tharakan and Martin, 2020).

Consequently, new regulatory mechanisms of ADAM10 need to be investigated to achieve its modulation. For example, researchers have found the presence of a CaM binding domain in the C-terminus which plays important roles in the activation of the protease itself (Pan *et al.*, 2012; Reboud *et al.*, 2017). The entry of Ca^{2+} promotes the dissociation of CaM from its target molecules at a rate that depends on the affinities, sensitivities and concentrations of all proteins that bind CaM (Williams, 1992). Furthermore, it has been demonstrated that Ca^{2+} influx leads to an increase in the activity of ADAM10; however, the mechanism underlying this activation has only been hypothesized to date (Ito *et al.*, 1999). Since the discovery that stimulation with certain Ca^{2+} ionophores like ionomycin can act as ADAM10 agonists (Dethlefsen *et al.*, 1998), researchers have tried to elucidate the possible mode of action of such activation. Studies have shwon that Ca^{2+} entry into the cell releases CaM from the C-terminal tail of ADAM10 during its processing in the Golgi apparatus, leading to a stronger and faster surface translocation (Nagano *et al.*, 2004). While some other studies have shown that the C-terminal tail is dispensable for the active state exhibited by ADAM10 after stimulation with Ca^{2+} ionophores (Maretzky *et al.*, 2015). Furthermore, other investigations showed that the Ca^{2+} influx activates scramblases like Anoctamine-6 resulting in the translocation of phosphatidylserine (PS) from the inner leaflet of the plasmatic membrane to the outer one resulting in a binding of the negatively charged PS with a positively-charged stalk region of ADAM10 close to the surface, resulting in a conformational change to a more active state (Bleibaum *et al.*, 2019).

Aside from the work presented so far regarding the activation of ADAM10, little is known regarding the kinetics underlying this process. Ionomycin, a known Ca^{2+} ionophore, as well as CaM inhibitors, have been used for many years as a tool to augment the activity of ADAM10. Although different concentrations of ionomycin have been used throughout the years when researching ADAM10, different concentrations of ionomycin and the consequential increase of Ca^{2+} concentration reached in the cytosol when activating ADAM10 has not been tested, calculated nor measured. The kinetics of ADAM10 activation and its release in exosomes or as a soluble form are not well understood, nor are their effects on ADAM10 packaging or release. Further research is needed on Ca^{2+} entry points and their role in activating ADAM10, especially in conditions like bacterial infections. Targeting ADAM10 for therapy is challenging due to its essential housekeeping functions and role in Notch signaling, making it crucial to better understand its regulatory mechanisms for safer, organ-specific treatments.

2.2 Calcium Signaling

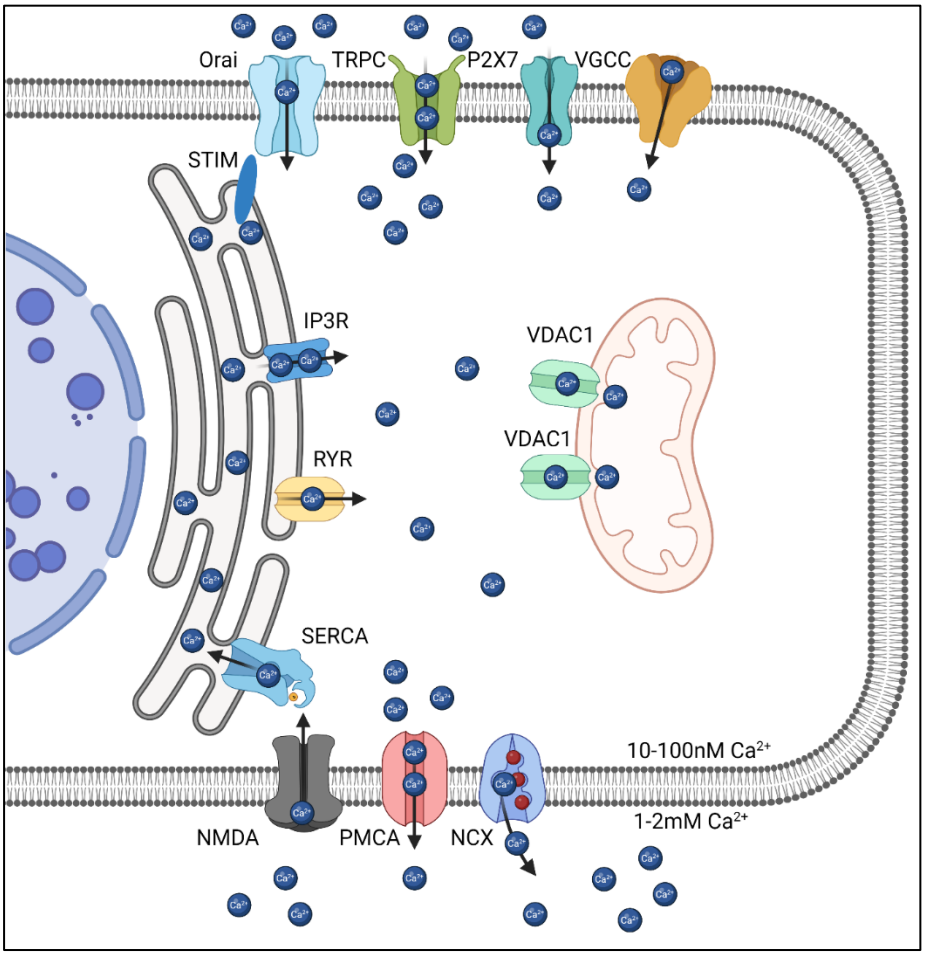

Figure 2.4. Calcium signalling associated pathways.

Schematic representation of distinct forms of Ca^{2+} signaling in a cell. Adapted from Patergnani *et al.*, 2020. TRPC, transient receptor potential canonical channel; VGCC, voltage-gated calcium channel; STIM, stromal interaction molecule; IP3R, IP3R, IP3 receptor; RYR, ryanodine receptor; SERCA, sarcoplasmic/endoplasmic reticulum Ca^{2+}-ATPase; VDAC, voltage-dependent anion channel; NMDA, N-methyl-D-aspartate receptor; PMCA, plasma membrane Ca^{2+}-ATPase; NCX, sodium-calcium exchanger.

Ca^{2+} plays an important role as a second messenger. Cytosolic concentration levels of Ca^{2+} ($[Ca^{2+}]_i$), as well as those of internal organelles such as the endoplasmic reticulum (ER), lysosomes, mitochondria and nucleus, are tightly controlled. While the normal physiological levels of extracellular Ca^{2+} revolves around 1-2 mM, $[Ca^{2+}]$i ranges between 10-100 nM. The concentration of proteins in mitochondria and

the nucleus is maintained at similar levels. On the other hand, the ER is considered the principal internal Ca^{2+} storage with a concentration of 100 to 800 µM (Raffaello *et al.*, 2016). To maintain strict control over Ca^{2+} entry and efflux, cells possess a diverse array of channels, pumps, transporters and Ca^{2+}-binding or buffering proteins, thereby ensuring that any change in Ca^{2+} levels is adequately detected as a signal and elicits the correct response.

The Ca^{2+} signaling machinery is composed by transporters such as the voltage-gated calcium channels (VGCC), which are mostly expressed in excitable cells like neurons (Catterall, 2011), receptor operated Ca^{2+} channels (McFadzean and Gibson, 2002), store-operated Ca^{2+} entry (SOCE) channels like Orais (Prakriya and Lewis, 2015) or several members of the transient receptor channels (TRPs) (Song and Yuan, 2010). Other members of the machinery that focus on the transport of Ca^{2+} ions through the ER are 1,4,5-triphosphate receptors (IP_3R), which are activated by IP_3 production from receptors on the plasma membrane, leading to an increase in $[Ca^{2+}]i$ (Foskett et al., 2007; Wu and Chen, 2023). Other members are represented in Fig. 2.5.

Calcium signaling is related to many physiological roles, with a prominent role in the progression during the cell cycle (Patergnani *et al.*, 2020). Ca^{2+} signaling also plays a role in apoptosis, a form of programmed cell death, acting as a trigger. (Pinton *et al.*, 2008). Thus, deregulation of the components of the calcium signaling machinery potentially leads to tumor development through promotion of the EMT or the overexpression of Ca^{2+} permeable mechanical channels PIEZO1 or PIEZO2, further promoting the tumor invasiveness. (Yu *et al.*, 2021)(Norgard *et al.*, 2021) (Dombroski *et al.*, 2021). The implication of Ca^{2+} signaling in these physiological roles and the activation of ADAM10 by Ca^{2+} would suggest that there is spatial control, coordinated by the neighboring localization of both the entry point of Ca^{2+} ions and the protease.

2.2.1 Store-operated calcium entry (SOCE) and Calcium Release-Activated Channels (CRACs)

An almost universal Ca^{2+} entry pathway into cells after phospholipid cleavage by phospholipase C (PLC) and the consequential production of diacylglycerol and IP3 will, in turn, activate IP_3R in the ER and promote $[Ca^{2+}]i$ rise (Wu and Chen, 2023). This led to the hypothesis that there is a capacitative entry of Ca^{2+} through the plasma membrane whenever internal stores are depleted. This pathway was, therefore, named capacitative calcium entry (CCE). Nevertheless, the nature of the entry, as well as the type of permeabilization that occurred in the membrane, was unknown. SOCE, distinct from other Ca^{2+} entry mechanisms like VGCCs (Prakriya and Lewis, 2015), was studied using tools such as SERCA inhibitors (e.g., thapsigargin) that induce ER Ca^{2+} leak without activating IP3 production. Fluorescent dyes (Fura2, Fluo-2) enabled live Ca^{2+} detection (Grynkiewicz, Poenie and Tsien, 1985). Thapsigargin in Ca^{2+}-free conditions helped measure ER leak and Ca^{2+} entry (Kang *et al.*, 2017). Key CRAC components, Orai1 and STIM1, were identified (Liou *et al.*, 2005; Feske *et al.*, 2006), and TRP channels were later linked to the CCE pathway, with some classified as CCE channels due to store depletion activation (Alexander, Mathie and Peters, 2009).

2.2.1.1 STIM proteins

SOCE is generally initiated with the activation of STIM proteins. These proteins are dimers of two single-pass type I proteins located in the membrane of the ER. Their primary role is the sensing of the Ca^{2+} depletion in the ER achieved by the presence of a canonical and a non-canonical EF-hand domains towards the ER-lumen (Kodakandla, Akimzhanov and Boehning, 2023). Store depletion sensing will ultimately lead to a conformational change in STIM1, enabling its interaction with Orai1. Additionally, whenever the stores are not depleted, STIM1 proteins are diffused throughout the ER membrane;

however, after depletion occurs, they oligomerize, interacting with Orai1 channels at ER-PM junctions. These junctions or "puncta" had been initially found in muscle cells but later on discovered together with STIM1 in several other non-excitable cells (Chang, Chen and Liou, 2017). An augment in STIM1 presence in coronary smooth cells and also prior to the development of atherosclerotic plaques (Wan *et al.*, 2022).

2.2.1.2 Orai channels

Orai channels are the primary point of entry in SOCE and are therefore considered CRACs, together with some TRP channels, from which some members are considered to be part of SOCE complexes. Higher vertebrates possess three different isoforms named Orai1, Orai2 and Orai3 all participating in SOCE though with different biophysical activation kinetics (Trebak and Putney, 2017).

The CRAC channels are typically formed by homomeric or heteromeric complexes of several individual Orai subunits (Prakriya, 2013). After store depletion and oligomerization of STIM into ER-PM junctions, STIM binds to both the N- and C-termini of the cytosolic domain of Orai, thereby promoting the opening of Orai1. The C-terminal domain of STIM has a key domain for such interaction termed STIM-Orai activating region (SOAR) and it has proven essential for the interaction with Orai (Bodnar *et al.*, 2017). It has been observed that Orai1-deficient patients suffer from persistent infections, leading to pneumonia, meningitis, or candidiasis. This is the product of a defect in T-, B- and NK- cell activation (Qu *et al.*, 2011; Emrich *et al.*, 2023). The development, progression and metastasis of several tumor forms have also been correlated with increased expressions of STIM and Orai. For example, the progression of the cell cycle and the migration of breast cancer cells are dependent on the

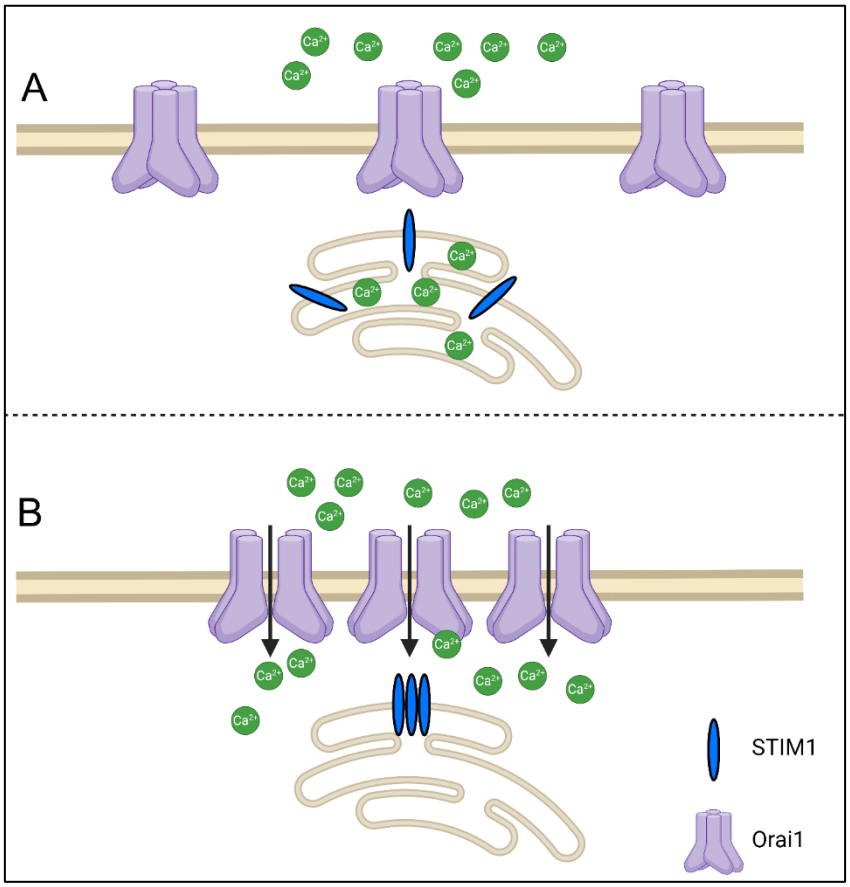

Figure 2.4. Store operated calcium entry.

Representation of the store operated calcium entry machinery. A: Close state where no multimerization of STIM1 is observed. B: After multimerization of STIM1 due to store depletion from ER, gating of Orai1 is promoted.

overexpression of Orai2 and Orai3. Also, an oncogenic switch has been revealed in prostatic cancer, the cause of the remodeling of channel-forming Orai (Xie *et al.*, 2016; Bruce and James, 2020).

2.2.2 Transient receptor potential (TRP) channels

Members of the TRP superfamily share the presence of six transmembrane segments, with the pore-forming region located between the fifth and sixth transmembrane segments. They possess a diverse homology among members due to the varied differences in the primary amino acid sequence, as well as a diverse permeability to cations. Furthermore, members of different subfamilies can be activated in the same manner; thus, this cannot be predicted based on their sequence similarity and, therefore, subfamily precedence. Functional channels are in reality formed by homo- or heteromers of mainly four subunits of TRP channels (Nilius and Owsianik, 2011). Their gating mechanisms involve a broad myriad of stimuli ranging from hot or cold temperature, stringent compounds like menthol or camphor, mechanical stimulation, or changes in the lipidic interphase (Minke, 2006).

The TRP superfamily is divided into two main groups based on their topological and sequence similarities. Group 1 has five subfamilies: canonical TRPs or TRPCs, TRPV (Vanilloid), TRPM (Melastatin), TRPA (Ankyrin) and TRPN, named after the NO-mechano-potential-C channel of *Caenorhabditis elegans*. TRPML (Mucolipin) and TRPP (Polycystic) are the members of group 2 (Minke, 2006; Nilius and Owsianik, 2011; Amrita, Hughes and Moiseenkova-Bell, 2018).

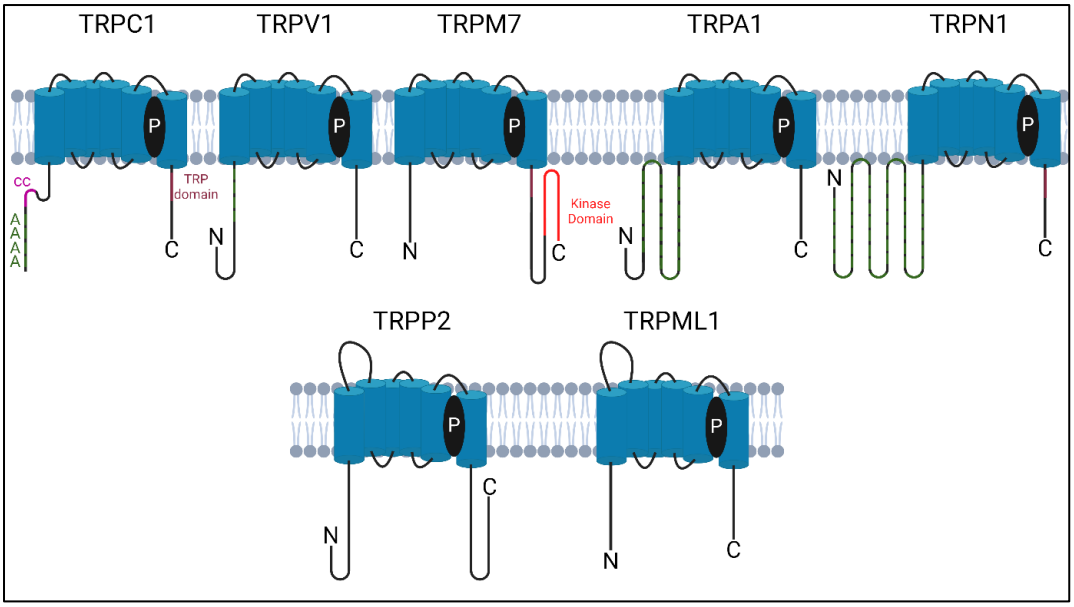

Figure 2.5. The transient receptor potential channels.

Examples of TRP subfamily members and scheme of their different topologies. Figure was adapted from Venkatachalam and Montell, 2007. Domains are indicated as: A, ankyrin repeats; cc, coiled-coil domain; protein kinase domain; TRP domain and transmembrane regions as vertical cylinders.

2.2.2.1 TRPC subfamily

The canonical TRP channels are the first studied subfamily among the TRP channels and are the closest related members to the original TRP channels that were cloned from *Drosophila*. Its members are divided into four groups based on their sequence homologies: 1) TRPC1, 2) TRPC2 which in humans is a pseudogene, 3) TRPC3/6/7 and 4) TRPC4/5 (Wang *et al.*, 2020). Mammalian TRPCs are all stimulated by PLC and in most cases, this effect is due to a DAG dependency, as it has been shown that the deletion of endogenous TRPC6/7 ablates the conductance produced by DAG (Itsuki *et al.*, 2014). Additionally, some of its members' activities are tightly controlled via membrane fusion from internal vesicles and exocytosis. For example, TRPC4/5 fusion into the plasma membrane seems to rely on EGF (Kim *et al.*,

2012), thus raising the possibility that some TRPs are constitutively active and depend on their membrane fusion to perform their function. Additionally, it has been shown that some members of TRPCs significantly contribute to SOCE activity, as observed after IP3 or thapsigargin stimulation. TRPC1 contributes to SOCE through modulation of Orai channels, despite lacking functional homomeric channel formation (Ambudkar, de Souza and Ong, 2017; Kim *et al.*, 2019). Complexes like STIM1-Orai1-TRPC1-TRPC4 are involved in cardiac remodeling and muscle physiology (Lopez *et al.*, 2020). TRPC4/5 channels are activated by Gq-coupled receptors and tyrosine kinases, with lanthanides enhancing their activity (Kim *et al.*, 2012; Bouron, Kiselyov and Oberwinkler, 2015). Englerin A is a selective agonist of TRPC4/5. TRPC3/6/7 are activated by diacylglycerol (Svobodova and Groschner, 2016).

TRPC1/4 upregulation disrupts Ca^{2+} homeostasis and signaling in heart disease (Collins et al., 2013; Sabourin et al., 2022). TRPC6 loss impairs kidney filtration, contributing to renal disease (Spires, Manis and Staruschenko, 2019). TRPC channels are also linked to tumor progression, apoptosis regulation, and drug resistance (Zeng et al., 2010; Bidaux et al., 2012; Cai et al., 2009; He et al., 2012; Ma et al., 2012).

2.2.2.2 TRPM subfamily

Characteristically, this family possesses an N-terminal TRPM homology domain among its members and lacks the N-terminal ankyrin repeats typically found in other subfamilies, although it does contain the typical C-terminal TRP box motif. Originally, TRPM channels were only found in cancerous tissues and were therefore only associated with cancer proliferation and differentiation (Venkatachalam and Montell, 2007). TRPM members play crucial roles in Mg^{2+} homeostasis, temperature sensation and taste (Kashio and Tominaga, 2022; Chubanov *et al.*, 2023). Structurally, they have been divided into three groups: TRPM1/3, TRPM4/5, TRPM2/6/7 and TRPM8. TRPM4/5 were shown to be permeable only to monovalent cations. TRPM4 is highly expressed in the intestine, while TRPM5 is located in the taste buds, where it is involved in sensing taste (Chubanov *et al.*, 2023). TRPM2/6/7 are bifunctional proteins. Not only do they perform their functions as cationic channels, but they also possess hydrolase functions (TRPM2) or kinase functions (TRPM6/7) due to their C-terminal catalytic domain (Chubanov *et al.*, 2005). TRPM8 is best known for its ability to sense cold temperatures and is the most Ca^{2+}-selective TRPM channel (Peier *et al.*, 2002). Finally, TRPM1, the first known member of this subfamily, has been identified as a tumor suppressor and a marker for melanomas, as it is present in non-metastatic melanomas (Varin *et al.*, 2020). It is physiologically found in the brain, macrophages and heart, though at very low levels. TRPM3, on the other hand, can form homotetramers or heterotetramers together with TRPM1. It plays a crucial role in the sensation of heat within the somatosensory system. Several activating conditions for TRPM3 have been identified, including sphingolipids, pregnenolone sulfate, cell swelling and possibly store depletion (Thiel *et al.*, 2017). To enable experimental conditions in which TRPM3 channel activity can be selectively induced, TRPM3 was chosen due to the possibility of specifically promoting its gating. This allows for controlled and traceable activation of TRPM3, facilitating experimental setups where its opening can be isolated and studied independently.

Mutations in TRPM proteins affect their ability to absorb magnesium in the intestine, which leads to hypomagnesemia. A mutation in the TRPM6 channel leads to both hypomagnesemia and hypocalcemia. Alteration on expression levels of TRPM4, TRPM5 and TRPM7 have also been linked to cancer in CD5+ B-cell lymphomas, prostate cancer proliferation, Wilms tumors, rhabdomyosarcomas and in the enhancement of proliferation potential from grade III breast tumor cells, among others. (Prawitt *et al.*, 2000; Singh *et al.*, 2006; Suguro *et al.*, 2006; Guilbert *et al.*, 2009). Furthermore, patients presenting atrial fibrillation possess an upregulation of both TRPM7 and TRPC3 in atrial fibroblasts

(Gwanyanya and Mubagwa, 2022). Polymorphisms detected in TRPM5 might associate this channel with an increased risk of developing diabetes mellitus type 2 because these patients present insulin insensitivity, hyperglycaemia and low glucagon-like peptide-1 levels in oral glucose tolerance test (Ketterer *et al.*, 2011).

The presence of both the SOCE and various members of the TRP channels in non-excitable mammalian cells raises the question of whether any of these Ca^{2+} entry pathways might influence the catalytic activity of ADAM10 when activated. Therefore, Ca^{2+} entry promotion through CRAC channels belonging to the SOCE system as well as through specific TRP channels like TRPC4, TRPC5 and TRPM3 in the context with ADAM10 activity increase will be tested.

To more closely approximate pathophysiological conditions, it becomes necessary to assess how these Ca^{2+} entry mechanisms respond to natural stimuli. One such relevant and clinically significant stimulus is infection by *Pseudomonas aeruginosa*, a bacterium capable of triggering strong host cell responses through a variety of virulence factors. Investigating calcium influx during *P. aeruginosa* infection may reveal how this effect integrates with ADAM10 activity.

2.3 Pseudomonas aeruginosa

The nosocomial pathogen *Pseudomonas aeruginosa* (*P. aeruginosa*) is considered by the World Health Organization to be in urgent need of alternative treatment because of its rising resistance to several antibiotics over the years (*WHO World Health Organization; 2024. Licence: CC BY-NC-SA 3.0 I*, 2024). It is a ubiquitous Gram-negative bacteria considered to be a commensal on the human body capable of transforming into an opportunistic pathogen whenever main body barriers are disrupted or in case of impairment of the immunological system (de Lorenzo, 2015). The pathogenicity of *P. aeruginosa* is governed by the expression of different virulence factors throughout their life cycle (Jurado-Martín, Sainz-Mejías and McClean, 2021). Notable examples include the formation of biofilms, which act as protective barriers against both antibiotic treatment and host immune clearance (Mulcahy, Isabella and Lewis, 2014); the secretion of pore-forming exotoxins that increase pathogenicity by inducing host cell death, compromising epithelial barriers, and facilitating further colonization (Reboud *et al.*, 2017); and the production of siderophores such as pyoverdine, which sequester host iron to support bacterial growth. Additionally, pyocyanin contributes to infection by promoting oxidative stress, thereby enhancing colonization (Abdallah, Pfestorf and Döring, 1989).

2.3.1 PQS Quorum Sensing System of *P. aeruginosa*

The expression of most of these virulence factors is regulated by a mechanism known as Quorum Sensing (QS). QS is a chemical communication system present in many bacteria, where a cellular density threshold serves as a trigger for the production of messengers that promote the synthesis of virulence factors. It was first discovered in *Aliivibrio fischeri,* where investigators observed that chemiluminescence occurred only after specific cellular densities were reached (Chong, Kimyon and Manefield, 2013). This mechanism has been shown to be crucial for the pathogenicity of several bacteria. Therefore, both synthetic and natural compounds are thoroughly being investigated as Quorum Quenchers or QS inhibitors because of their ability to impair this communication between bacterial cells and thus reduce their infectivity (Rather *et al.*, 2022).

P. aeruginosa possesses four interconnected QS systems, each with their characteristic signaling molecules and their related expressed virulence factors; these are: OdDHL, IQS, BHL and PQS system (Lee and Zhang, 2015). The latter is known to be involved in the expression of pyocyanin or the agglutinating protein Lectin A (LecA). Researchers have observed a positive synergistic effect of QS inhibitors (QSI) in combination with tobramycin treatment in the clearance of *P. aeruginosa* produced biofilm (Schütz *et al.*, 2021)

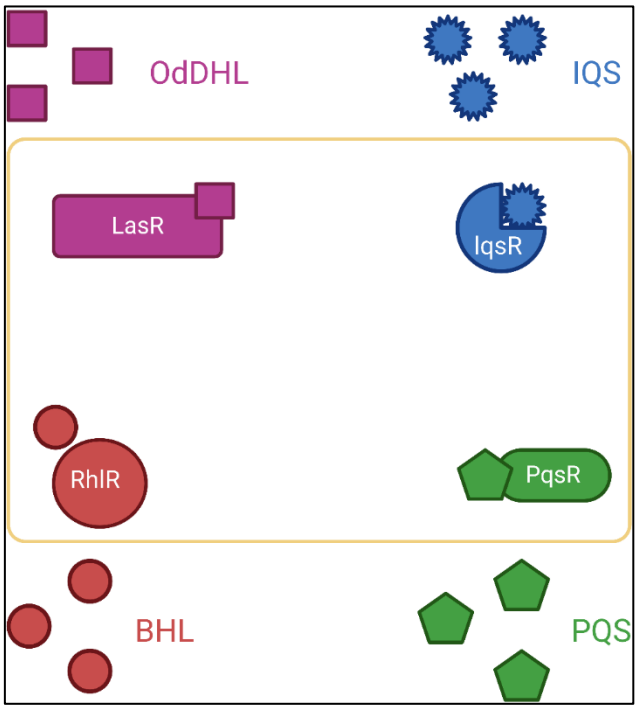

Figure 2.6. *P. aeruginosa* QS systems.
QS systems present in *P. aeruginosa*, their respective main signaling molecule is shown outside of the main square and main enzymes interacting with them are represented inside. Adapted from Schütz *et al.*, 2021.

ADAM10 is known to be activated during *P. aeruginosa* infection, and this process likely involves the production of virulence factors as well as an overtime Ca^{2+} entry (Reboud *et al.*, 2017; Aljohmani *et al.*, 2022). Since the activation of host proteases, particularly ADAM10, is used as a strategy for entry and colonization in P. aeruginosa infections, it is paramount to investigate further the mechanisms involved in this process.

2.4 Aim of the study

ADAM10 plays a key role in fundamental cellular pathways, such as Notch signaling. Therefore, its targeting for clinical purposes has proven challenging; therefore, further research is required regarding its regulation to facilitate the development of additional translational studies. Ca^{2+} influx is a known activator of ADAM10 activity, however, little is known regarding its kinetics, the actual concentration of Ca^{2+} required to elicit increased ADAM10 activity and specific entry points, such as TRP or Orai channels. ADAM10 is also of great importance in various pathophysiological processes, including pathogen entry and inflammation.

Aim 1 – Different times of stimulation or origins from the activating Ca^{2+} ions could be paramount for the consequent ADAM10 activation. Spatiotemporal regulation of ADAM10 by Ca^{2+}: Mechanistic studies using cell-based assays on lung epithelial cells should be conducted. These cells express the endogenous ADAM10 substrate, E-cadherin, allowing for the measurement of ADAM10 activity under various conditions. Pharmacological inhibition of ADAM10, as well as GI and shRNA (small hairpin RNA) knockdown (KD), allows for the assessment of ADAM10-specific processes.

After this, the activation of ADAM10 after Ca^{2+} influx should be investigated. For this, stimulation with different ADAM10 agonists, such as the ionophore ionomycin or CaM inhibitors like trifluoperazine or ophiobolin A, was performed under various time and concentration conditions and the Ca^{2+} response was monitored via Ca^{2+} imaging using the Ca^{2+} binding fluorophore Fura2-AM. Additionally, the release and activation of both soluble forms or exosome-contained ADAM10 were also assessed. The spatial control of specific Ca^{2+} entry points, such as TRPC or TRPM subfamily members, was investigated using HEK cell lines stably expressing TRP channels, along with further activity assays and Ca^{2+} imaging. To assess whether entry of Ca^{2+} through physiological means activates ADAM10.

Aim 2 – The activity from other proteases on the cleavage of E-cadherin could affect the interpretation of the results from one important read-out used for this work for ADAM10 activity. Therefore, the order of E-cadherin cleavage events: Additionally, the role of other protease types in generating different fragments of E-cadherin was investigated. The production of different fragments by ADAM10 was also investigated using HA-tag-labeled E-cadherin constructs, as well as the confirmation of the generation of a 36 Kilodalton (kDa) fragment by ADAM10.

Aim 3 – Having tested a more physiological manner of Ca^{2+} entry like some TRP channels, it was also important to assess the effect of a natural stimuli like a pathophysiological Ca^{2+}-dependent ADAM10 activation through natural stimuli. Therefore, infection with the opportunistic pathogen *P. aeruginosa* and its relation with Ca^{2+} entry will be used to test the Ca^{2+}-dependent activation of ADAM10. Ca^{2+}-dependent activation of ADAM10 using pathophysiology-relevant stimuli will be investigated through infection experiments on lung epithelial cells with the nosocomial pathogen *P. aeruginosa*. Given that pathogenicity is often regulated by the expression and release of quorum sensing-related virulence factors, the roles played by some of these factors and the inhibition of the PQS quorum sensing pathway will also be investigated.

3 Materials & Methods

3.1 Materials

3.1.1 Reagents

Reagents were obtained from Merck Millipore (Darmstadt, Germany) and Invitrogen by Thermo Fisher Scientific (Frankfurt, Germany) with a purity of at least 90% *pro analysis* (p.a.).

Table 1: Reagents utilized

Reagent	Company	Working Concentration
Ionomycin	Merck Millipore	0.1 µM-10 µM
Trifluoperazine	Merck Millipore	100 µM
Thapsigargin	Invitrogen by Thermo Fisher Scientific	1 µM
Ophiobolin A	Merck Millipore	10 µM
4Br-A23187	Merck Millipore	20 µM
GM6001	Merck Millipore	10 µM
Iodoacetamide	Invitrogen by Thermo Fisher Scientific	10 µM
GI	Merck Millipore	10 µM
BAPTA-AM	Invitrogen by Thermo Fisher Scientific	10 µM
EGTA	Merck Millipore	3 mM
Fura2-AM	Invitrogen by Thermo Fisher Scientific	5 µM
Magnetic Dynabeads Protein G	Invitrogen by Thermo Fisher Scientific	0.12 µg/µL
Polybrene Infection/Transfection agent	Merck Millipore	4 µg/mL

3.1.2 Antibodies

Antibodies were obtained either as a ready-to-use solution diluted in PBS with 0.1% sodium azide or in a powder form that was further resolved and diluted in PBS with 0.1% sodium azide. Their respective application and working concentrations are listed below (Table 2).

Table 2: Antibodies used

Antibody	Company	Working dilution or concentration	Application
Monoclonal E-cadherin C-terminal Antibody	BD Biosciences (Heidelberg, Germany)	0.25 µg/mL	Western blot
Monoclonal E-cadherin N-terminal Antibody	Santa Cruz Biotechnology (Dallas, Texas, USA)	0.20 µg/mL	Western blot
Polyclonal ADAM10 C-terminal Antibody	Invitrogen by Thermo Fisher Scientific	0.1 µg/mL	Western blot
ADAM10 Ectodomain Antibody	R&D System (Wiesbaden, Germany)	1 µg/mL	Flow Cytometry
HA Antibody	Invitrogen by Thermo Fisher Scientific	1 µg/mL	Western blot
V5 Antibody	Affinity Purification Antibody	0.5 µg/mL	Western blot
Allophycocyanin (APC)-conjugated Mouse Ly6G	Invitrogen by Thermo Fisher Scientific	0.8 µg/mL	Flow Cytometry
Amersham ECL HRP-conjugated anti-mouse secondary antibody	GE Healthcaren(Chicago, IL, USA).	0.005 µg/µL	Western blot
Amersham ECL HRP-conjugated anti-goat secondary antibody	GE Healthcare	0.005 µg/µL	Western blot
Amersham ECL HRP-conjugated anti-rabbit secondary antibody	GE Healthcare	0.0025 µg/µL	Western blot
Amersham ECL HRP-conjugated anti-rat secondary antibody	Cytiva Europe GmbH (Freiburg, Germany)	0.01 µg/µL	Western blot
IgG isotype control rabbit	Invitrogen by Thermo Fisher Scientific	0.02 µg/µL	Flow Cytometry Analysis
IgG2B isotype control mouse	R&D System	0.02 µg/µL	Flow Cytometry Analysis

3.1.3 Buffers and solutions

Table 3: Final composition of buffers and solutions utilized.

Buffer/Solution	Composition
ADAM10 lysis buffer	5 mM Tris-HCl; 1 mM EGTA, 250 mM Saccharose; 0.1% (w/v) SDS 1% TritonX-100; 1x Complete, 1 mM Na_3VO_4; 1 mM PMSF; 10 mM 1,10-Phenantrolin.
ADAM-IP lysis buffer	20 mM HEPES; 100 mM NaCl; 1 mM EDTA; 0,1% Triton X-100; Glycerol 5%; 1 mM Na_3VO_4; 1 mM phenylmethylsulfonyl fluoride (PMSF); 1 mM ditihiothreitol (DTT); 1X complete; pH 7.4
Stacking gel buffer	0.5 M Tris; 0.4% SDS; pH 6.8

Running gel buffer	1.5 M Tris; 0.4% SDS; pH 8.8
4% Stacking gel	25% Stacking gel buffer; 10% 40% Acrylamide solution 29:1; 0.75% 10% ammonium persulfate (APS) solution; 0.15% Tetramethyl ethylenediamine (TEMED)
10% Running gel	25% Running gel buffer; 25% 40% Acrylamide solution 29:1; 0,75% 10% APS solution; 0.15% TEMED
Laemmli Buffer	250 mM Tris HCl (pH 6.8); 50% glycerol; 10% SDS; 0.1% bromophenol blue; and 5 % β-mercaptoethanol
Fluorescence activated cell sorting (FACS) Buffer	136 mM NaCl; 2.7 mM KCl; KH_2PO_4; Na_2HPO_4; 0.2% BSA
Alkaline phosphatase assay lysis buffer	1% Triton-X100; 50 mM Tris; 0.15 M NaCl; 1x Complete; pH 7.5
Alkaline phosphatase assay activity buffer	40 mM Tris-HCl; 40 mM NaCl; 10 mM $MgCl_2$; pH 9.5
Ringer Solution	140 mM NaCl; 4 mM KCl; 1 mM $MgCl_2$; 10 mM HEPES and 10 mM D-Glucose
0Ca/EGTA saline solution	Ringer solution without $CaCl_2$, 10 mM EGTA
10Ca/EGTA saline solution	Ringer solution without $CaCl_2$, 10 mM EGTA; 10 mM $CaCl_2$; 20 µM 4Br-A23187
20Ca saline solution	Ringer solution without $CaCl_2$; 10 mM $CaCl_2$; 20 µM 4Br-A23187
ADAM10 FRET-based activity assay buffer	20 mM Tris; 0.0006% Brij-35; pH 8.0

3.1.4 Equipment

Table 4: Equipment utilized for preparation, processing and/or measurement of samples

Equipment	Company
Beckman rotor Type Ti50.2	Beckman Coulter GmbH, Krefeld, Germany.
Beckman TLA-55 rotor	Beckman Coulter GmbH, Krefeld, Germany.
Buffer Tank	Bio-Rad Laboratories, Inc., Hercules, USA.
Cell culture incubator CB170-E7	Binder GmbH, Tuttlingen, Germany.
Centrifugation device 5418 R	Eppendorf AG, Hamburg, Germany.

Cooled charge-coupled device (CCD) camera	Imago, TILL photonics.
Hemocytometer	Invitrogen, Frankfurt, Germany.
HLC Heating-ThermoMixer TH 21	DITABIS AG, Pforzheim, Germany.
Inverted Microscope	Axiovert S100, Carl Zeiss, Jena, Germany.
LAS3000 reader	Fujifilm, Tokyo, Japan.
Lionheart (FX) Automated Microscope system	Biotec, Highland Park, IL, USA.
M200 infinite TECAN reader	Tecan, Grödig, Austria.
Mini-PROTEAN® Casting Frame	Bio-Rad Laboratories, Inc., Hercules, USA.
Mini-PROTEAN® Casting Stand	Bio-Rad Laboratories, Inc., Hercules, USA.
Mini-PROTEAN® Tetra Electrode Assembly	Bio-Rad Laboratories, Inc., Hercules, USA.
PowerPac™ HC High-Current Power Supply	Bio-Rad Laboratories, Inc., Hercules, USA.
Sony SH800 FACS Device	Sony, Berlin, Germany.

3.1.5 Software

Table 5: Software utilized for managing devices, preparing figures and analysis of results.

Software	Company
AIDA Image Analysis Software 4.27.039	Elysia-raytest, Straubenhardt, Germany.
CorelDRAW X7 19.0.0.491	Corel Corporation, Alludo, Ottawa, Canada.
FlowJo 10.6.2 Software	Tree Star, Inc., Ashland, OR, USA.
Gen5 Software Version 3.05.11	BioTek, Highland Park, Winooski, VT, USA.
GraphPad PRISM 9.0	GraphPad Software, La Jollla, CA, USA.
TillVision Online Analysis Software	TILL Photonics, Kaufbeuren, Germany.

3.1.6 Consumables and miscellaneous material

Table 6: General cell culture consumables and other miscellaneous laboratory equipment utilized.

Material	Company
25mm thick Coverslips	Carl Roth GmbH + Co. KG, Karlsruhe, Germany
Columbia blood agar with sheep blood medium	Thermo Fisher, Karlsruhe, Germany.
Conical bottom polypropylene tube, 15, 50 ml	Greiner Bio-One GmbH, Frickenhausen, Germany.
Dulbecco's Phosphate Buffered Saline	Sigma-Aldrich, Taufkirchen, Germany.
Filtered pipettes tips, 10, 20, 200, 1000 µl	Thermo Fisher, Karlsruhe, Germany.
Microplate, 96 wells, flat bottom, black	SARSTEDT AG & Co. KG, Nümbrecht, Germany.
Microplate, 96 wells, flat bottom, transparent	SARSTEDT AG & Co. KG, Nümbrecht, Germany.
Microtube, 1.5 ml	SARSTEDT AG & Co. KG, Nümbrecht, Germany.
Microtube, 2 ml	SARSTEDT AG & Co. KG, Nümbrecht, Germany.
Pipette Tips, 10, 20, 200, 1000 µl	Thermo Fisher, Karlsruhe, Germany.
Pipettes, 2.5, 10, 20, 200, 1000 µl	BrandTech Scientific, Inc., NY, USA.

Serological pipettes, 2, 5, 10, 25 ml	SARSTEDT AG & Co. KG, Nümbrecht, Germany.
Tissue culture plate, 12 wells, flat bottom	SARSTEDT AG & Co. KG, Nümbrecht, Germany.
Tissue culture plate, 6 wells, flat bottom.	FALCON, corning incorporated, NY, USA.
Tissue culture plate, 96 wells, flat bottom	SARSTEDT AG & Co. KG, Nümbrecht, Germany.

3.2 Methodology

3.2.1 Cell culture

3.2.1.1 Cell lines

A549

Isolated from lung tissue of a 58-year-old caucasian male with lung cancer. It is an adenocarcinomic human alveolar basal epithelial cell line. This cell line is used as a model for studying lung cancer and other lung-related pathologies, as well as a testing and calibration platform in ISO 17025 laboratories to evaluate assay performance, linearity and specificity. It is commercially available (ATCC, CRM-CCL-185 ™).

A431

A431 cells are immortalized skin carcinoma carcinoma cells with an epidermal morphology. Given its high expression of epidermal growth factor receptor (EGFR), this cell line is used to study cell-cycle and cancer-related cell signaling pathways. They are commercially available (ATCC, CRL-1555 ™).

HEK-293

It was generated via the transfection of cultures from human embryonic kidney cells with sheared adenovirus 5 DNA. They present epithelial morphology. They have also shown other applications, including biomedical research, biotechnology and toxicological research. They are commercially available (ATCC, CRL-1573 ™).

μOR-TRPC4-HEK-293

This cell line was obtained through the stable transfection of HEK-293 cells with TRPC4 using Lipofectamine 2000. The μ-opioid receptor cDNA was placed in the pIREShygro2 vector (Clontech) and cell lines were selected in the medium containing 400 μg/ml G418 and 100 μg/ml hygromycin B (Miller et al., 2011).

HEK-293-CCE2(TRPC5)

The cell line was obtained from the stable transfection of HEK-293 cells with TRPC5 (previously known as TRP5 or CCE2). They were initially obtained by transfecting pdiCCE2 using lipofectamine on HEK-293 cells and stable transfected cells were selected with 400 μg/mL G418 (Philipp et al., 1998).

HEK-293-TRPM3α2

The cell line was obtained from the stable transfection of HEK-293 cells with TRPM3α2. They were transfected with TRPM3α2 cDNA using FUGENE (Roche Applied Science) and then selected in a medium containing 500 μg/mL G418 (Frühwald *et al.*, 2012).

3.2.1.2 Passaging and seeding

A549 and A431 cells were both cultured in Dulbecco's modified Eagle Medium (DMEM) supplemented with 10% fetal calf serum (FCS). HEK wild-type (WT) cells were cultured in Minimal Essential Medium (MEM) supplemented with 10% FCS. TRPM3 overexpressing HEK cells or HEK-TRPM3α2 (Becker *et al.*, 2020) cells were cultured in MEM supplemented with 10% FCS and 500 μg/mL G418. HEK-μOR TRPC4α

(Miller *et al.*, 2011) were cultured in DMEM supplemented with 10% FCS, 100 µg/mL Hygromycin B and 500 µg/mL G418. HEK-CCE2 (TRPC5) (Philipp *et al.*, 1998) cells were cultured in MEM supplemented with 10% FCS and 400 µg/mL G418. In all cases, cells were maintained in an atmosphere of 5% CO_2 at 37°C.

3.2.1.3 Cell stimulation, transfection and transduction

Prior to stimulation, cells were starved in their corresponding media supplemented with 0.5% FCS overnight, followed by one hour incubation with the corresponding media without FCS. For transfection, cells were always treated with Lipofectamine 3000 reagent and the corresponding plasmid according to the manufacturer's protocol. Transductions were performed with a lentiviral strategy. A short hairpin ADAM10 RNA sequence was introduced into the lentiviral vector pLVTHM (Addgene plasmid 12247), targeting both ADAM10 mRNA sequences gacatttcaacctacgaat and acagtgcagtccaagtcaa. A sequence ccgtcacatcaattgccgt introduced in the same lentiviral vector was used as a scramble control for experiments. Maria Rieseweber regularly produced lentiviral vectors as previously described in Aljohmani *et al.*, 2022. For transduction, cells were seeded with a density of $2*10^5$ cells in a 6-well plate, followed by addition of lentiviral particles after 24 h in polybrene-supplemented medium (4 µg/mL, increase of transduction efficiency). Transduced cells were used for experiments for a maximum of seven days after transduction to prevent a compensation of the knockdown or loss of integrated viral sequences. Transduction efficiency was analyzed using fluorescence microscopy to determine the number of GFP-positive cells. The KD was confirmed by Western blot.

3.2.2 Molecular biology

3.2.2.1 Cloning and production of E-cadherin constructs

cDNA from the E-cadherin (CDH1) sequence was obtained from A549 cell isolates by RT-PCR using a cDNA synthesis kit (Microsynth Seqlab GmbH, Göttingen, Germany) according to the manufacturer's protocol. Tagged constructs of E-cadherin were generated by subcloning the CDH1-201 sequence into the pMax-IRES-GFP plasmid, which contains a built-in kanamycin resistance. N-terminal HA-tagged proteins were obtained by introducing the HA sequence (YPYDVPDYA) between amino acid numbers 24 and 25 of QE-PE. The C-terminal V5 construct was obtained by introducing a V5 sequence (GKPIPNPLLGLDST) at the end of the E-cadherin sequence. HA-tagged constructs in the extracellular domain were obtained by introducing the HA sequence between the cadherin repeats and after the Ca^{2+} binding domains, in positions between amino acids 266-267, 379-380, 490-491 and 599-600 for each respective construct. All tags were introduced using a muta-PCR approach with a Q5 mutagenesis kit (Qiagen, Hilden, Germany) according to the manufacturer's protocol. The obtained constructs were used to transform competent E. coli cells, which were then streaked on kanamycin-containing LB agar plates. The resulting DNA of interest was purified with a NucleoSpin Tissue, Mini Kit (Macherey-Nagel, Düren, Germany). After confirmation of the sequence (Microsynth Seqlab GmbH, Gleiswerk 36, 37081 Göttingen, Germany), the plasmids were further purified using a PureYield™ Plasmid Maxiprep System (Promega, Madison, USA) according to the manufacturer's protocol. Final plasmids were prepared to an approximate concentration of 0.5 µg/µL per aliquot. A mapping of the final constructs is shown in Fig. 3.1.

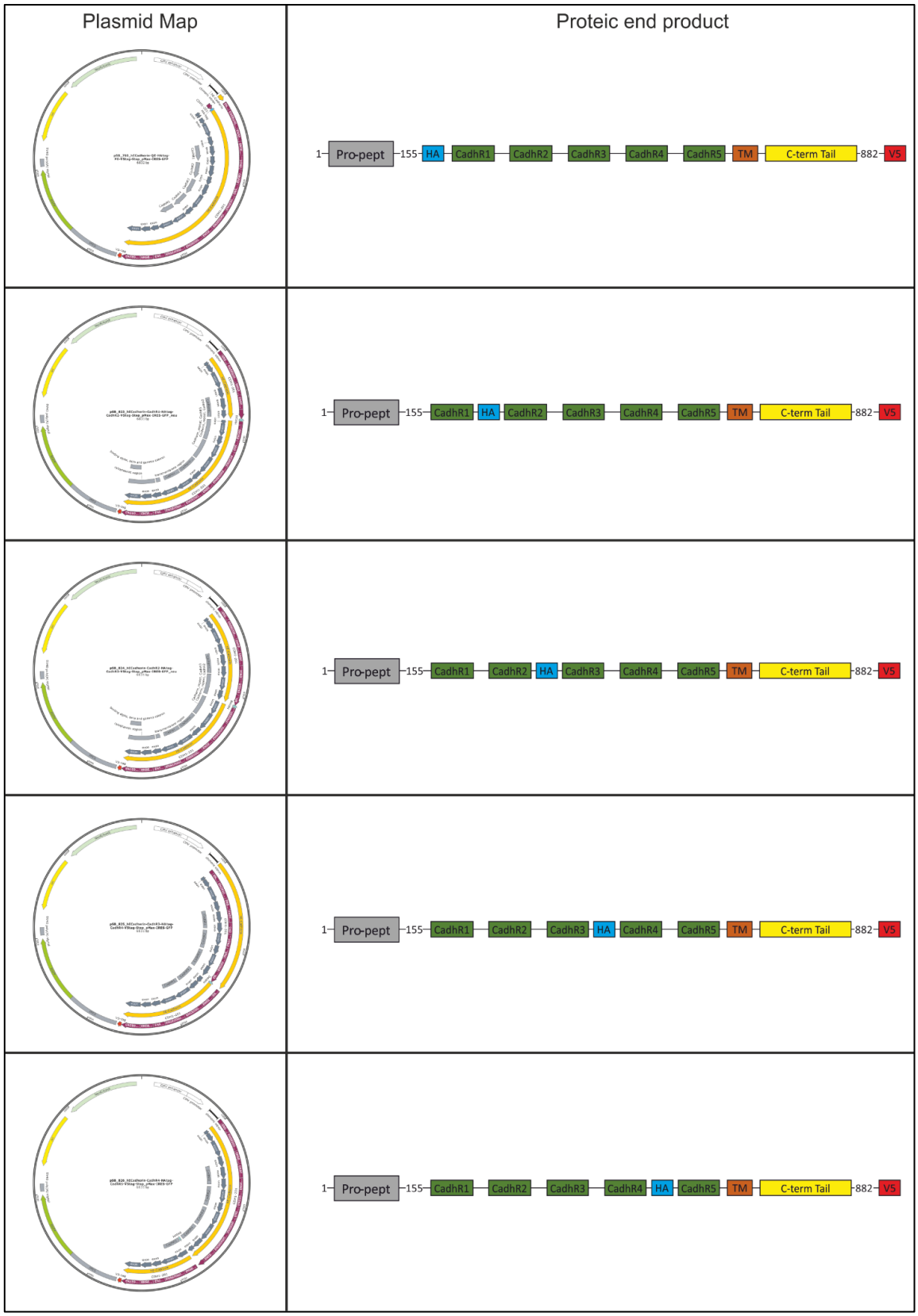

Figure 3.1. Plasmid maps and their corresponding E-cadherin end product. CadhR: Cadherin repeat; TM: transmembrane; C-term: C-terminal.

3.2.3 Biochemical Methods

3.2.3.1 Protein content determination

The protein content of cell lysates was quantified using a Bicinchoninic acid assay kit (Thermo Fisher, Karlsruhe, Germany) according to the manufacturer's protocol. A 1:100 and 1:200 dilution of samples was transferred to a 96-well plate together with a standard concentration series of 0 µg/µL, 0.01 µg/µL, 0.02 µg/µL, 0.04 µg/µL, 0.06 µg/µL, 0.08 µg/µL and 0.1 µg/µL provided with the kit and diluted with H_20. Both sample and standard series were added in technical duplicates. Meanwhile, reagent solutions A and B were prepared in a 50:1 ratio (A:B), added to the samples and standard series in a 8:1 ratio and then incubated at 37°C for 30 min. Finally, absorbance at 540 nm was measured with a TECAN plate reader. The mean values of the duplicates were calculated, and the protein concentration was interpolated from the calibration line obtained by the standard series.

3.2.3.2 Sodium dodecyl sulfate polyacrylamide gel electrophoresis (SDS-PAGE)

Equal protein content for each sample was prepared by adding 1x SDS buffer and denaturing at 60°C for 30 min. Samples were then loaded onto polyacrylamide 4%/10% gels and subjected to electrophoresis (SDS-PAGE). The gel containing the loaded samples was subjected to an electrical field of 80 V for 20 min to concentrate the samples at the start of the run. Then, the voltage was increased to 160 V. The samples were left to run until the bromophenol blue from the SDS buffer, visualized as the running front, reached the bottom of the gel.

3.2.3.3 Western blot Analysis

The separated proteins were transferred onto nitrocellulose membranes (Amersham Protran Premium 0.45 NC, GE Healthcare Life Sciences, Freiburg, Germany) by subjecting the gel to an electroblotting process in close contact with the membrane. Afterwards, membranes were blocked with 5% (w/v) non-fat milk in 0.05% TBS for 1 h, followed by incubation with a primary antibody of interest overnight. Membranes were incubated with the corresponding secondary antibody for 1 h and washed three times before adding chemiluminescence substrate (PerkinElmer, Waltham, MA, USA). Chemiluminescence was detected in a LAS3000 device (Fujifilm, Tokyo, Japan). Densitometry analysis and image acquisition were performed using AIDA Image Analysis software version 4.27.039 (Elysia-raytest, Angleur, Belgium), and further image preparation was carried out with CorelDraw X7 (Ontario, Canada). A representative blot from the experiment was chosen, and relevant lanes were shown, neither contrast nor intensity on images was changed. Densitometry was performed after background subtraction and utilizing equally sized squares for band acquisitions. E-cadherin cleavage, used as a readout for ADAM10 activity, was obtained by calculating the ratio of the 36 kDa fragment to the 120 kDa full-length fragment, since ADAM10 proteolytic activity is known to release these two fragments (Maretzky *et al.*, 2005).

3.2.3.4 Immunoprecipitation

Cells were lysed with an appropriate amount of ADAM-IP lysis buffer. The lysates were sheared and then incubated on a shaker for 30 min at 4°C to ensure proper lysis. 20 µL of each lysate were removed and denaturated with SDS buffer (input). The lysates were centrifuged at 100.000g for 45 min at 4°C. Afterward, 60 µL of magnetic beads were washed twice with ADAM-IP lysis buffer on a magnetic stand and then incubated for 1 h with 10 µg of antibody against the protein of interest or its corresponding IgG control in 500 µL ADAM-IP lysis buffer on a shaker. After this, the beads were washed five times to remove any unbound antibodies and were further incubated with the cell lysates overnight at 4°C. On the following day, the beads were washed five times with ADAM-IP lysis buffer and denaturated with SDS buffer at 60°C for 30 min. Input (lysate before bead preparation), output (bead preparation with lysate) and IgG control samples were then analyzed by SDS-Page and Western blot analysis.

3.2.3.5 Antibody surface staining and flow cytometry analysis

At the end of the experiment, cells were detached using Accutase (Merck Milipore, Darmstadt, Germany), centrifuged at 300g for 10 min and resuspended in FACS buffer. A431 cells were gently scraped off after a 10-min incubation with Accutase using cell scrapers. Afterwards, cells were washed three times with FACS buffer before incubating with an ectodomain ADAM10 antibody, an IgG isotype control, or FACS buffer for 1 h. Consequently, cells were washed three times with FACS buffer, followed by incubation with a secondary Alexa Fluor 647-conjugated anti-mouse antibody in the dark for 45 min. Cells were then washed three times with FACS buffer, fixed with 1% paraformaldehyde (PFA) for 5 min and resuspended in FACS buffer before being assigned for flow cytometry analysis and fluorescence signal measurement (Sony SH800, Sony, Berlin, Germany). Cell detachment and antibody staining and incubation were done on ice. The end of data recording was set to 500,000 cells per sample per forward and side scatter channel. Data were further processed using forward and side scatter analysis to discard cells with decreased viability or cell debris, as determined by FlowJo 10.6.2 software (Tree Star, Inc., Ashland, OR, USA). IgG isotype control measurements were discounted before comparison between conditions.

3.2.4 Functional assays

3.2.4.1 Alkaline phosphatase assay

Cells were transfected with a plasmid containing an N-terminally tagged alkaline phosphatase-betacellulin (AP-BTC) for 24 h using a Lipofectamine 3000 kit (Thermo Fisher, Karlsruhe, Germany) according to the manufacturer's protocol. Consequently, $3*10^5$ cells were seeded in a 12-well plate, left to grow until the next day and treated as stated in the figure legends. At the end of the experiment, 100 µL of supernatant was transferred to a 96-well measuring plate, while cells were lysed with AP assay lysis buffer, of which 100 µL were transferred to the measuring plate. Afterwards, the plate was supplemented with 100 µL of a 2 mg/mL solution of AP substrate 4-nitrophenyl phosphate (Merck Millipore, Darmstadt, Germany) (in AP-assay activity buffer). Proteolytic activity was quantified by measuring absorption at 405 nm for 2.5 h, every 1.5 min, at 37 °C in an M200 Infinite Tecan reader (Tecan, Grödig, Austria). Final results were obtained by quantifying slopes of linear regions and normalization against the experimental control.

3.2.4.2 FRET assay

Cells were seeded in DMSO and phenol-red free DMEM media. After cell treatment, supernatants were removed and transferred to a 96-well measurement plate in technical duplicates. Consequently, the supernatants were supplemented with 10 µM ADAM10 FRET-based fluorogenic substrate PEPDAB063A (Biozyme Inc., North Carolina, USA). GI was also supplemented to the plate to a final concentration of 100 µM before fluorescence measurement. The plate was then transferred to an M200 infinite Tecan reader (Tecan, Grödig, Austria) to measure fluorescence every 2 min for 4 h; measurement was performed with the gain function of the device activated with an excitation wavelength of 485 nm and an emission wavelength of 530 nm. The final results are represented as means + SD of slope from the linear region of the measurement.

3.2.4.3 Calcium imaging

$2{,}5*10^5$ cells were seeded on previously poly-L-Lysine (PLL) -coated 25 mm coverslips until cells reached a 70% confluence on the next day. Before the experiment, cells were incubated with 4 µM Fura2-AM for 30 min. Then, coverslips were transferred to an open-bottom camera and washed three times with ringer solution before supplementing with 300µL ringer solution and then placed onto stage of an inverted microscope (Axivert S100, Carl Zeisss, Jena, Germany) or onto stage of an iMIC inverted microscope (TILL Photonics, Planegg/Martinsried, Germany) both attached to a charge-coupled device (CCD) camera and a monochromator (Polychrome V, TILL Photonics, Planegg/Martinsried, Germany)

at room temperature for imaging. At least 20 cells per measurement were selected as regions of interest (ROIs) and background regions for subtraction. Images were taken every 2 seconds, and fluorescence was captured by alternately exciting (0.5 Hz) at 340 and 380 nm every 20 ms for 20 minutes. Reagents were applied online during baseline measurement. The ratio of captured fluorescence at 340/380 nm was automatically plotted by an online analysis software program (TILL Photonics, Germany). Individual cells with substantial independent deviations were considered outliers and discarded from the final analysis. The area under the curve using the trapezoidal method, as well as the difference between the maximum and minimum baseline numbers (amplitude), were also calculated.

3.2.4.4 Fura2-AM calibration and intracellular calcium calculation

To calibrate Fura2-AM and calculate intracellular calcium, cells were seeded on PLL-coated coverslips, loaded with Fura2-AM and washed three times before being transferred to an open-bottom chamber and mounted to an inverted microscope. Cells and background were selected as ROIs, as in the calcium imaging protocol, but supplemented with 160 µL 0 Ca/EGTA saline solution. After the plateau of measurement was reached, the ratio of Rmin and Sf2 (the excitation intensity of individual λ2 ((380 nm) channel representing unbound Fura2) values were extracted and 240 µL of 10Ca/EGTA saline solution was added online, accounting for a final concentration of Ca^{2+} of 260 nM as calculated in webmaxc standard webpage: https://somapp.ucdmc.ucdavis.edu/pharmacology/bers/maxchelator/webmaxc/webmaxcS.htm.
After the plateau was reached, the ratio named R260 nM was extracted. Finally, 400 µL of 20 Ca saline solution was added online and the ratios named Rmax and Sb2 were extracted (excitation intensity of the individual λ2 (380 nm) channel representing bound Fura2). Then, the following formula was applied to calculate the effective dissociation constant from Fura2:

$$Kd_{eff} = 260nM/(\frac{R_{260\,nM} - R_{min}}{R_{max} - R_{260\,nM}} * \left(\frac{Sf2}{Sb2}\right))$$

Afterwards, following equation from (Grynkiewicz, Poenie and Tsien, 1985) was used to calculate experimental Ca^{2+} concentrations:

$$[Ca^{2+}]i = Kd_{eff} * \frac{R_{exp} - R_{\min}}{R_{max} - R_{exp}} * (\frac{Sf2}{Sb2})$$

The last term, Sf2/Sb2, representing the ratio of the 380 nm in Ca^{2+} free and Ca^{2+} bound conditions is also known as b in some articles (Padar *et al.*, 2004).

3.2.5 Exosome preparation

Cells were seeded in collagen G pre-coated 150 mm dishes. When confluent, cells were stimulated with correspondent stimulants. Afterwards, the supernatants were collected and subjected to sequential centrifugation steps (300g for 10 min, 1000g for 20 min and 10,000 g for 30 min) at 4°C. The final supernatant was filtered through a 0.45 µm filter and transferred to ultracentrifuge tubes, which were subsequently centrifuged for 1 h at 100,000 g and 4°C. The supernatant was then discarded, and the pellet was washed with ice-cold PBS and further centrifuged at 100,000g for 1 h at 4°C. The final pellet was lysed in SDS buffer and denatured at 60°C for 30 minutes and then subjected to Western blot analysis.

3.2.6 Bacteria preparation

P. aeruginosa and its quorum-sensing strains were taken from stock at -80°C and plated on THY-agar plates overnight in an incubator at 37 °C. Afterwards, bacterial colonies were inoculated in Todd-Hewitt-Bouillon broth supplemented with 2% yeast extract (THY) in a liquid culture flask and allowed

to grow overnight in an incubator at 37°C with shaking at 150 rpm, in the presence or absence of quorum sensing inhibitors. The next day, a new culture was initiated with an initial OD600 of 0.05 at 37°C and 150 rpm shaking for 3 h. After this time, a 1 mL culture with an OD600 of 1 was prepared and used for infection experiments.

3.2.7 Statistical methodology

Data were analyzed using the program GraphPad Prism 9.0 (GraphPad Software, La Jolla, CA, USA). Quantitative data were represented as means + SD, and a p value > 0.05 was considered statistically significant. The analysis of the non-normalized E-cadherin cleavage experiments was performed using one way ANOVA followed by a Tukey's post – hoc test for multiple comparisons between groups. Significant differences in AP-BTC cleavage (normalized data) were analyzed with a one-sample t-test followed by a false discovery rate (FDR) analysis. All experiments were performed in at least three independent biological replicates unless stated otherwise. Statistical tests used for the other experiments are indicated in the corresponding figure legends.

4 Results

4.1 Calcium-dependent regulation of ADAM10

4.1.1 Ca^{2+} influx and calmodulin inhibition but not SERCA blockage promote ADAM10 activity

The influence of different sources on the ADAM10-activating intracellular calcium increase was tested using ionomycin as a calcium ionophore, thapsigargin as a SERCA inhibitor promoting calcium release from the ER and trifluoperazine as a CaM inhibitor. The cleavage of E-cadherin, an endogenous substrate of ADAM10, resulted in a 36 kDa fragment in addition to the 120 kDa full-length protein, serving as a readout for activation. Both calcium entry, due to the action of ionomycin, as well as stimulation with trifluoperazine, increased the activity of ADAM10, which could be prevented by GI pretreatment. Thapsigargin did not elicit an increase in E-cadherin cleavage (Fig. 4. 1B).

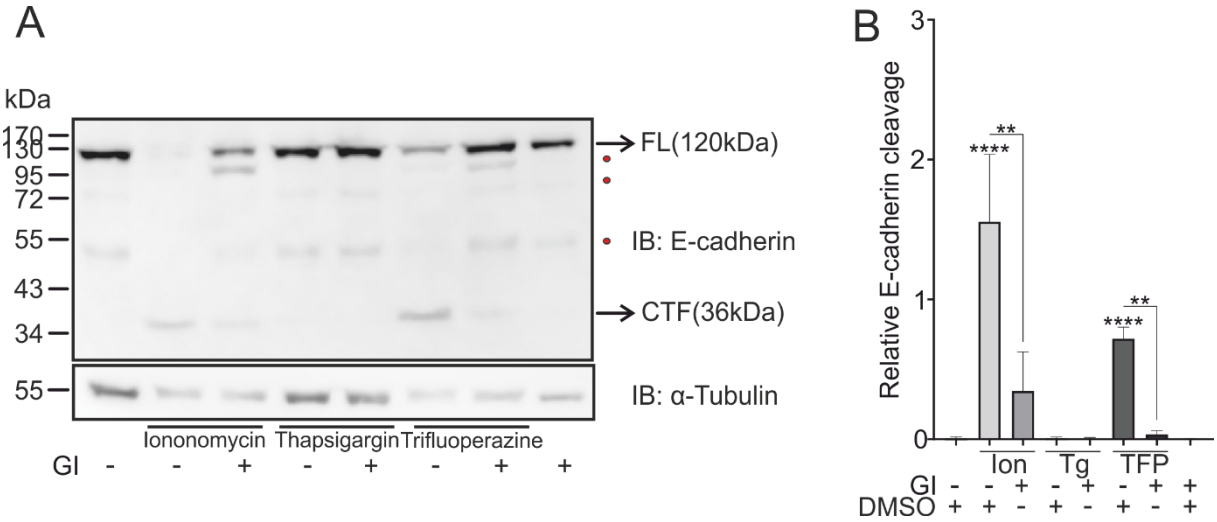

Figure 4.1. Activation of ADAM10 by after ionomycin and trifluoperazine stimulations

A: A, B: A549 cells were seeded on 6-well plates, grown until confluence, and starved overnight in medium containing 0.5% FCS. Prior to stimulation, cells were incubated in medium without FCS for 1 h, followed by incubation with 10 µM GI or 0.1% DMSO (vehicle control) for 30 min. Cells were stimulated with 10 µM ionomycin, 1 µM thapsigargin, 100 µM trifluoperazine or 0.1% DMSO as vehicle control for 1 h. Subsequently, cells were lysed, and cleavage was assessed by Western blot analysis using a C-terminal antibody against E-cadherin. α-tubulin served as loading control. Bands were quantified via densitometry and graphed as ratio of C-terminal fragment (CTF) to full-length (FL). A representative blot is given in A. Additional bands marked with red dots are products from cleavage activity of other proteases and are addressed later on. B: Quantitative data are shown as mean + SD. Statistical analysis was performed with a one sample t-test. Asterisks with no connecting line represent differences with control and those with lines represent differences among groups (* $p < 0.05$, ** $p < 0.01$, *** $p < 0.001$, **** $p < 0.0001$).

To gain further insight into the influence of CaM inhibition on ADAM10 activation, ophiobolin A, a natural product derived from Aspergillus, was used as a more specific CaM inhibitor. Similar effects were observed as previously described for trifluoperazine.

To test whether this effect was substrate-specific, the experiments were repeated with another readout based on the cleavage of an Alkaline Phosphatase-BTC substrate by ADAM10 (referred to as ADAM10 activity). As observed previously, both ionomycin and trifluoperazine promoted ADAM10 activity, whereas thapsigargin did not (Fig 4.2B).

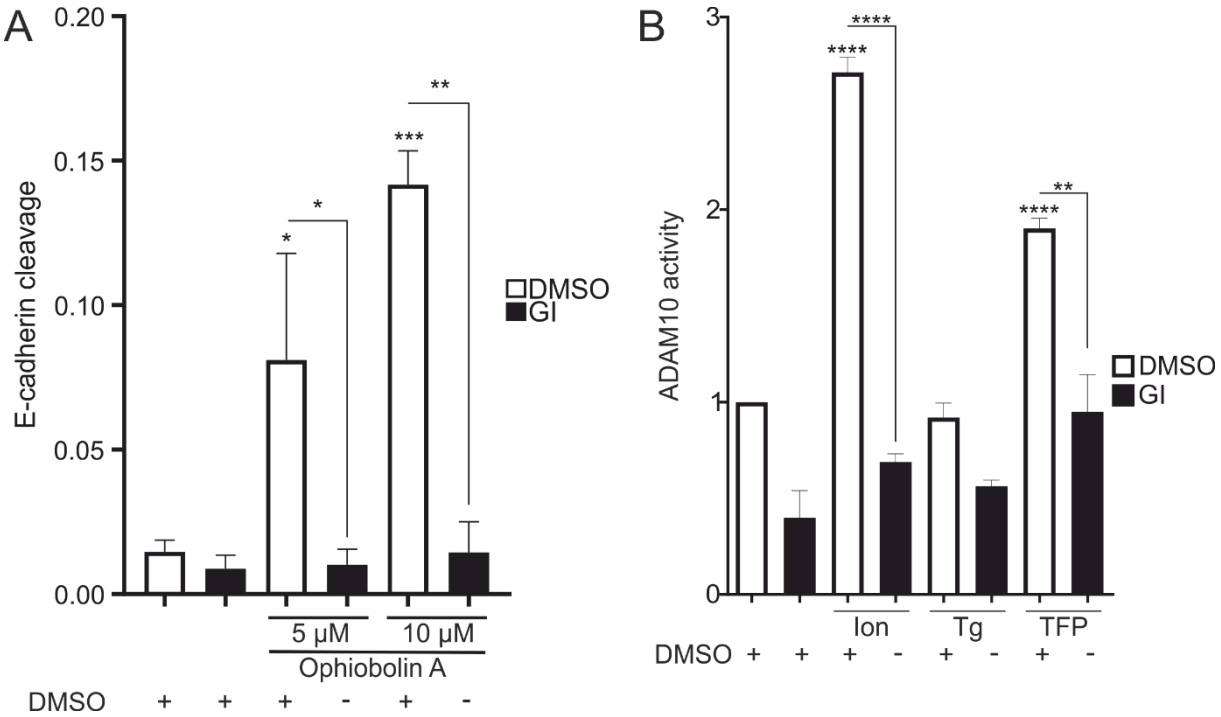

Figure 4.2. Activation of ADAM10 mediated by CaM inhibition.

A: A549 cells were seeded on 6-well plates, grown until confluence and starved with medium containing 0.5% FCS overnight. Afterwards, cells were further starved with medium containing 0% FCS for 1 h before incubating with 10 µM GI or 0.1% DMSO (vehicle control) for 30 min. Then, cells were stimulated with 5 µM or 10 µM ophiobolin A or 0.1% DMSO for 1 h. Cells were then lysed and lysates were afterwards subjected to a Western blot against a C-terminal E-cadherin antibody and α-tubulin as a loading control. Bands were quantified via densitometry and graphed as ratio of C-terminal fragment (CTF) to full-length (FL). B: A549 cells were transfected with AP-BTC overnight. Then, cells were seeded on 12-well plates, grown until confluence and starved with medium containing 0.5% FCS overnight. Afterwards, cells were further starved with medium containing 0% FCS for 1 h before incubating with 10 µM GI or 0.1% DMSO (vehicle control) for 30 min. Consequently, cells were stimulated with 10 µM ionomycin, 1 µM thapsigargin, 100 µM trifluoperazine or 0.1% DMSO for 1 h. Subsequently AP activity from supernatant and cell lysates was measured. Quantitative data are shown as mean + SD. Data from B were normalized to first lane. Statistical analysis was performed with a one sample t-test. Asterisks with no connecting line represent differences with control and those with lines represent differences among groups (* $p < 0.05$, ** $p < 0.01$, *** $p < 0.001$). Quantitative data are shown as mean + SD. Statistical analysis was performed with a one sample t-test. Asterisks with no connecting line represent differences with control and those with lines represent differences among groups (* $p < 0.05$, ** $p < 0.01$).

Different activation patterns may result from varying intensities or durations of calcium transients. Calcium imaging experiments revealed a biphasic, fast and constant increase in intracellular Ca^{2+}, which is abolished when the experiment is repeated in the presence of EGTA. The two phases observed are characteristic of an internal release from stores and a subsequent influx from extracellular space (Morgan and Jacob, 1994). The peak observed in the presence of EGTA can only be attributed to the release from internal stores. Thapsigargin caused a transient increase of intracellular Ca^{2+} levels without significantly affecting the area under the curve (AUC) or peak amplitude. A 3.4-fold lower amplitude is observed under stimulation with trifluoperazine, which leads to a stable and significant increase in intracellular Ca^{2+} levels, as shown in the AUC and is not affected by EGTA.

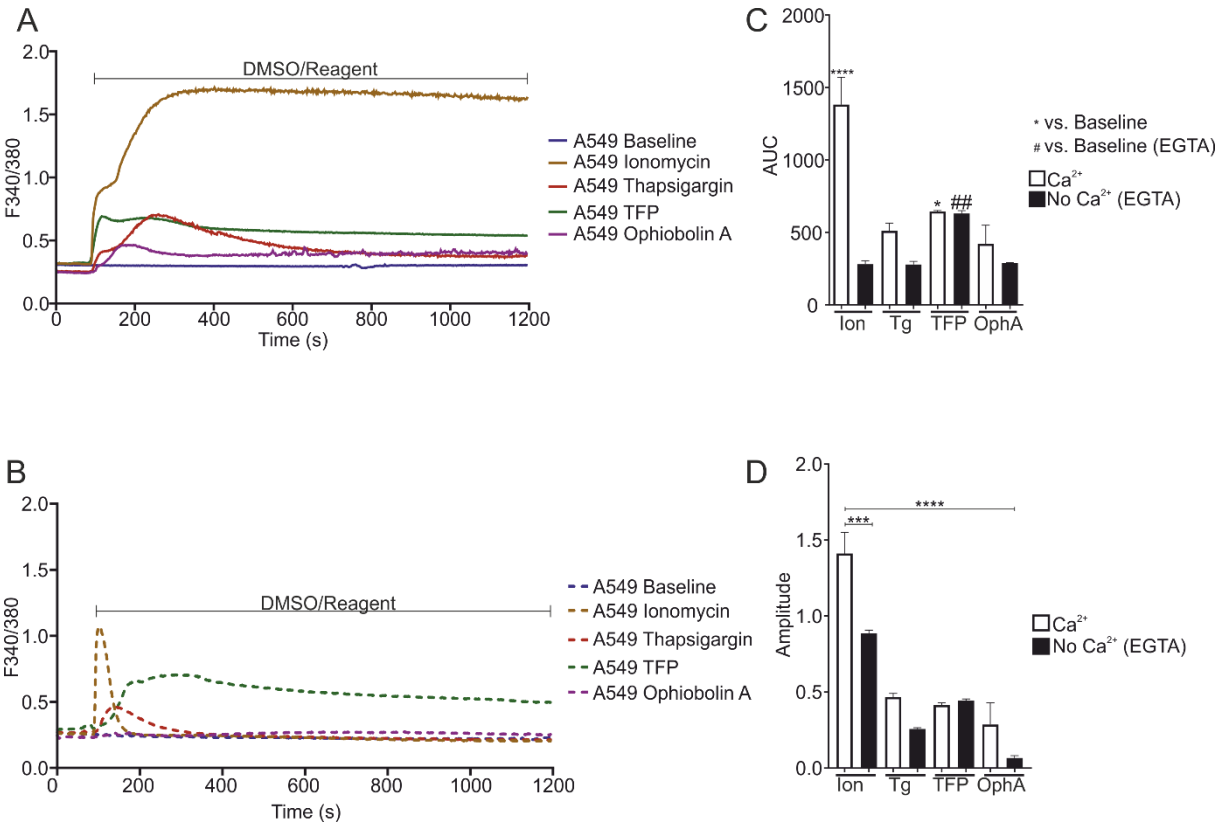

Figure 4.3. Intracellular Ca^{2+} increase mediated by ionomycin, thapsigargin, trifluoperazine and ophiobolin A treatment.

A549 cells were seeded and grown to a 70% confluence on 6-well plates containing previously poly-L-Lysine coated coverslips. Cells were then loaded with 4 µM Fura2-AM for 30 min. Calcium imaging experiments were performed with addition of 10 µM ionomycin, 1 µM thapsigargin, 100 µM trifluoperazine, 10 µM ophiobolin A or 0.1% DMSO after 1.5 min of baseline reading either in the presence of Ca^{2+} (A) or in the absence of it given by the use of EGTA-containing Ringer solution (B): Area under the curve (C) using the trapezoid method and amplitude (D) as difference between peak and lowest value were calculated and plotted. Quantitative data are shown as mean + SD. Statistical analysis was performed with a one sample t-test. Asterisks or numerals with no connecting line represent differences with control and those with lines represent differences among groups (* $p < 0.05$, ** $p < 0.01$).

The amplitude given by the difference between the peak value and the baseline value and the area under the curve were calculated. As observed by the amplitude calculation, ionomycin promotes the highest Ca^{2+} entry, caused by an influx from the extracellular into the intracellular milieu (Fig. 4. 3C, D).

4.1.2 Activation of ADAM10 under ionomycin stimulation shows external Ca^{2+} dependency

To further assess the activation of ADAM10 elicited by these sources of Ca^{2+} increase, ionomycin and trifluoperazine stimulations were repeated this time in the nominal absence of extracellular Ca^{2+} (the lack of Ca^{2+} in extracellular media) and in the presence of two different Ca^{2+} chelators. Ethylene glycol-bis (β-aminoethyl ether)-N, N, N', N'-tetraacetic acid (EGTA) was used as external chelator which has proven to be more specific towards Ca^{2+} in comparison to Zn^{2+} to buffer extracellular Ca^{2+}(Raaflaub, 1956). On the other hand, BAPTA-AM, a potent Ca^{2+}-selective chelator capable of chelating intracellular Ca^{2+} due to the presence of the acetoxymethyl (AM) ether, was used to buffer intracellular Ca^{2+} (Wang and Augustine, 2015). BAPTA-AM chelates Ca^{2+} only after the removal of the AM ether after intracellular esterase action.

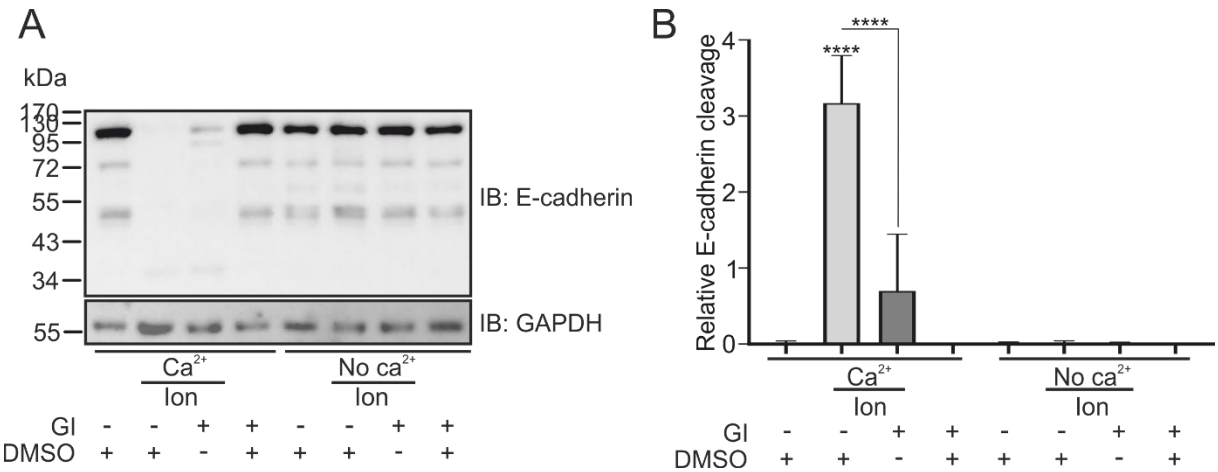

Figure 4.4. Ionomycin-mediated activation of ADAM10 is abrogated under nominal absence of extracellular Ca^{2+}.

A: Representative blot from quantitative data shown in B. B: A549 cells were seeded on 6-well plates, grown until confluence and starved with medium containing 0.5% FCS overnight. Afterwards, cells were further starved with medium containing 0% FCS for 1 h before incubating with 10 µM GI or 0.1% DMSO (vehicle control) for 30 min. Then, cells were stimulated with 10 µM ionomycin or 0.1% DMSO as vehicle control for 1 h in the presence/absence of 2 mM $CaCl_2$. Cells were lysed and lysates were afterwards subjected to a Western blot against a C-terminal E-cadherin antibody and α-tubulin as a loading control. Bands were quantified via densitometry and graphed as ratio of C-terminal fragment (CTF) to full-length (FL) in B. Quantitative data are shown as mean + SD. Statistical analysis was performed with a one sample t-test. Asterisks with no connecting line represent differences with control and those with lines represent differences among groups (* $p < 0.05$, ** $p < 0.01$, *** $p < 0.001$).

The nominal absence of Ca^{2+} showed a complete abrogation of E-cadherin cleavage induced by 10 µM ionomycin (Fig. 4.4B)

As confirmation of this experiment, a chelation of Ca^{2+} to achieve a Ca^{2+}-free condition was also tested. In this scenario, the ablation of the E-cadherin cleavage occurred as well (Fig. 4.5B). However, it is important to note that, although EGTA has shown a higher selectivity towards Ca^{2+} chelation, it is also capable of sequestering the Zn ion important for the catalytic activity of ADAMs and therefore, such an inhibitory effect cannot be discarded (Radford and Lippard, 2013).

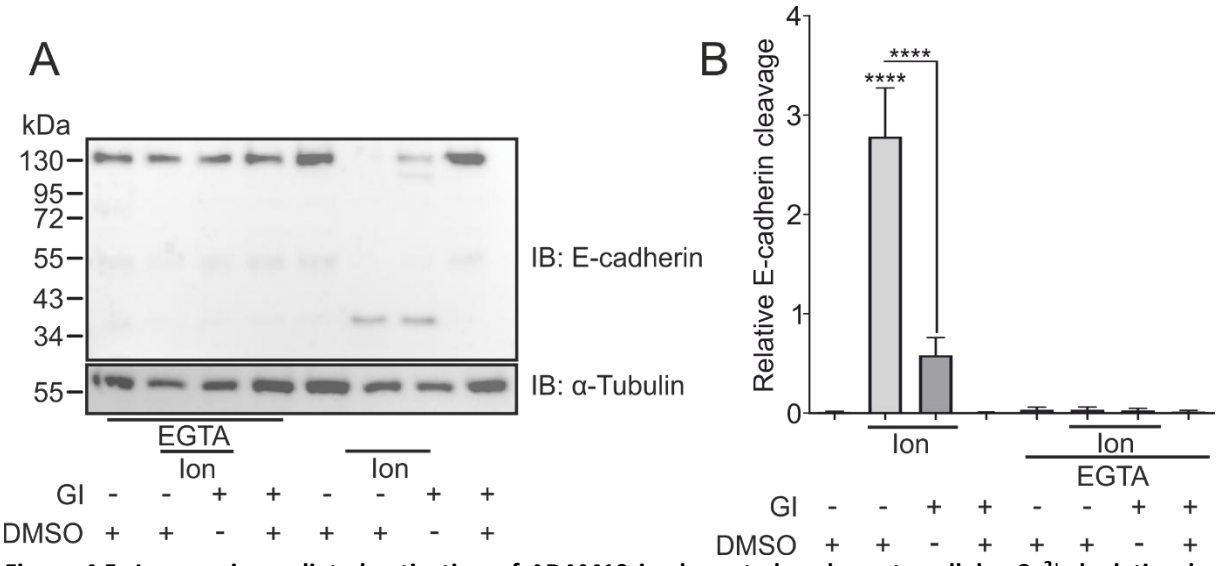

Figure 4.5. Ionomycin-mediated activation of ADAM10 is abrogated under extracellular Ca^{2+} depletion by EGTA.

A549 cells were seeded on 6-well plates, grown until confluence and starved with medium containing 0.5% FCS overnight. Afterwards, cells were further starved with medium containing 0% FCS for 1 h before incubating with 10 µM GI254023X or 0.1% DMSO (vehicle control) for 30 min. Then, cells were stimulated with 10 µM ionomycin or 0.1% DMSO for 1 h in the presence of $CaCl_2$ or the absence of it given by the chelation of extracellular Ca^{2+} with 3 mM EGTA. Cells were lysed and lysates were afterwards subjected to a Western blot against a C-terminal E-cadherin antibody and α-tubulin as a loading control. Bands were quantified via densitometry and graphed as ratio of c-terminal fragment (CTF) to full-length (FL) in B. Quantitative data are shown as mean + SD. Statistical analysis was performed with a one sample t-test. Asterisks with no connecting line represent differences with control and those with lines represent differences among groups (* $p < 0.05$, ** $p < 0.01$, *** $p < 0.001$).

Subsequently, to investigate the role played by intracellular Ca^{2+} ions, the nominal absence of Ca^{2+} condition was also combined with the sequestration of intracellular Ca^{2+} with BAPTA-AM.

Once again, the E-cadherin cleavage did not occur whenever there is no extracellular Ca^{2+} present, in this case even when intracellular Ca^{2+} has been chelated through the action of BAPTA, this would mean that the origin of the Ca^{2+} ions for the activity promotion of ADAM10 during the 10 µM ionomycin stimulation is most likely extracellular (Fig. 4.6B).These experiments were also performed under trifluoperazine stimulation to assess the importance of Ca^{2+} ions and their origins in the cleavage of E-cadherin by ADAM10.

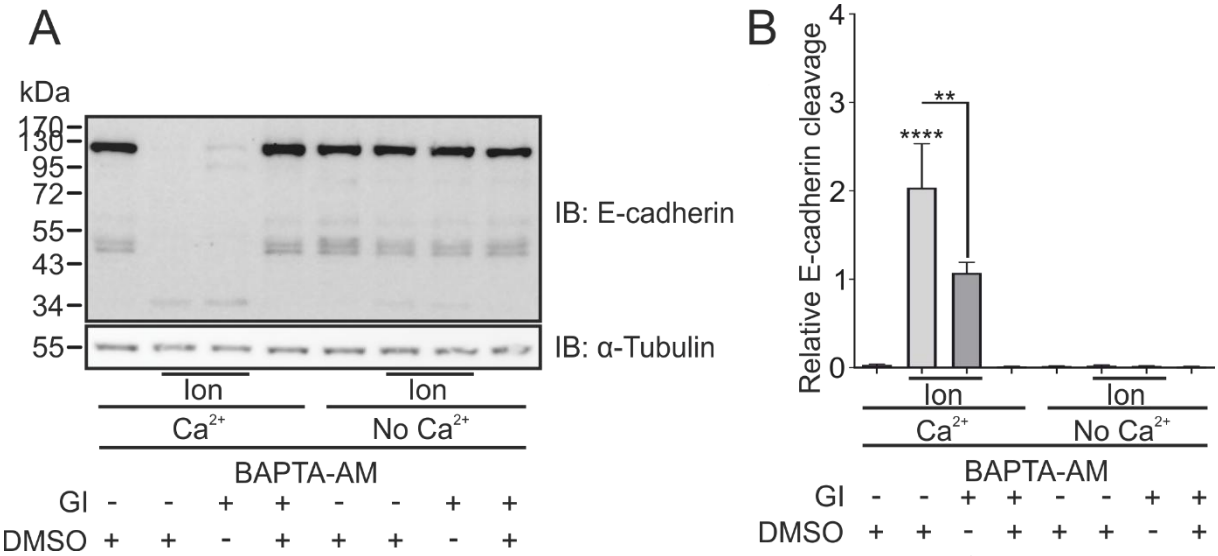

Figure 4.6. Ionomycin-mediated activation of ADAM10 is not affected by intracellular Ca^{2+} depletion by BAPTA-AM.

A549 cells were seeded on 6-well plates, grown until confluence and starved with medium containing 0.5% FCS overnight. Afterwards, cells were further starved with medium containing0% FCS for 1 h and preincubated with 10 µM BAPTA-AM before incubating with 10 µM GI or 0.1% DMSO (vehicle control) for 30 min. Then, cells were stimulated with 10 µM ionomycin or 0.1% DMSO for 1 h in the presence/absence of 2 mM $CaCl_2$. Cells were then lysed and lysates were afterwards subjected to a Western blot against a C-terminal E-cadherin antibody and α-tubulin as a loading control. Bands were quantified via densitometry and graphed as ratio of C-terminal fragment (CTF) to full-length (FL) in B. Quantitative data are shown as mean + SD. Statistical analysis was performed with a one sample t-test. Asterisks with no connecting line represent differences with control and those with lines represent differences among groups (* $p < 0.05$, ** $p < 0.01$, *** $p < 0.001$, **** $p < 0.0001$).

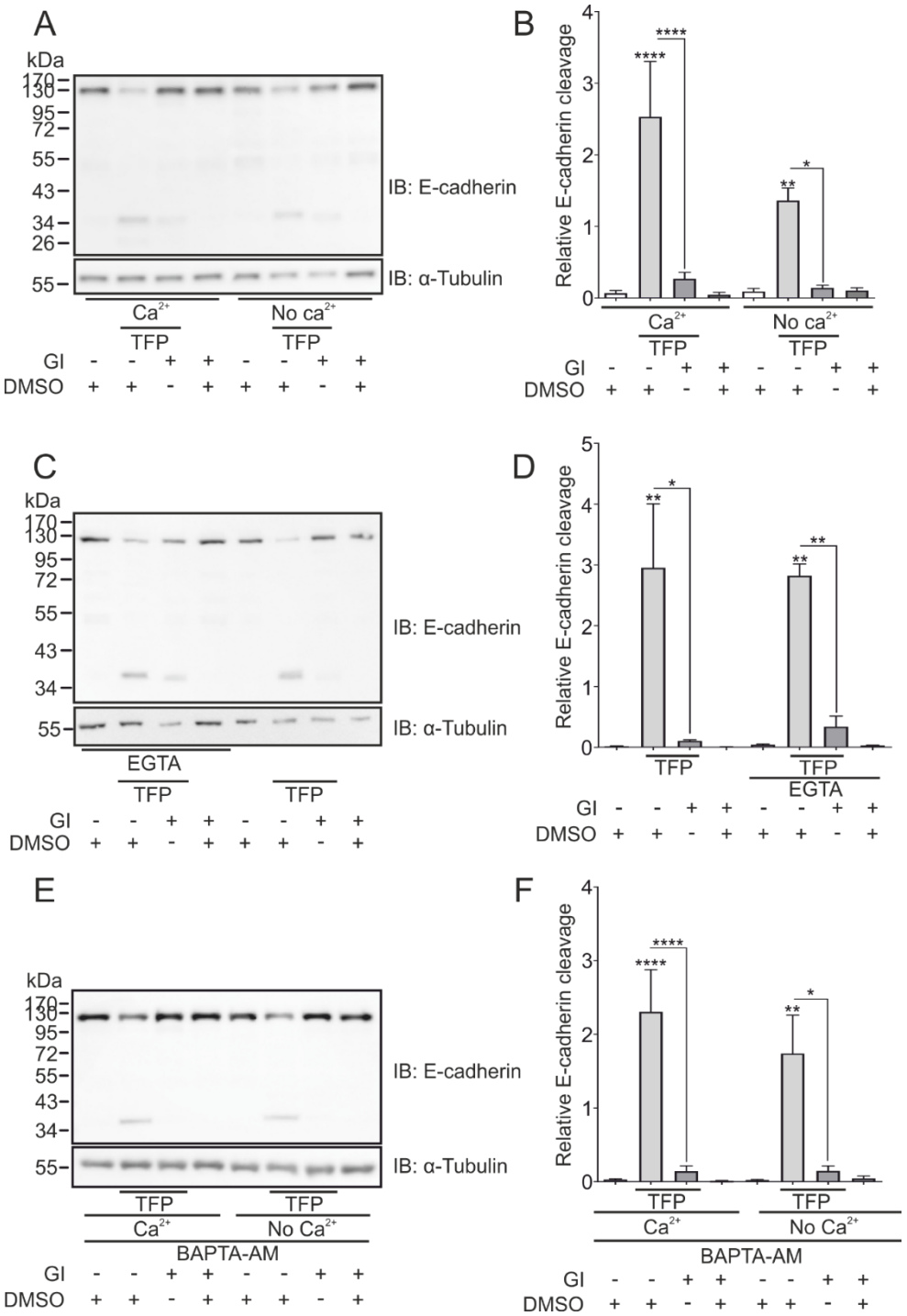

Figure 4.7. Trifluoperazine-mediated activation of ADAM10 is not affected by nominal absence of Ca^{2+}, extracellular depletion of Ca^{2+} by EGTA or intracellular depletion of Ca^{2+} by BAPTA-AM.

A549 cells were seeded on 6-well plates, grown until confluence and starved with medium containing 0.5% FCS overnight. Afterwards, cells were further starved with 0% FCS media before incubating with 10 µM GI or 0.1% DMSO (vehicle control) for 30 min. Then, cells were stimulated with 10 µM ionomycin or 0,1% DMSO for 1 h in the presence/absence of 2 mM $CaCl_2$ (A and B); in the presence Ca^{2+} or its absence given by its sequestration with 3 mM EGTA (C and D) or preincubating with 10 µM BAPTA-AM and the presence/absence of 2 mM $CaCl_2$ (E and F). Cells were then lysed and lysates were afterwards subjected to a Western blot against a c-terminal E-cadherin antibody and α-tubulin as a loading control. Bands were quantified via densitometry and graphed as ratio of c-terminal fragment (CTF) to full-length (FL) in B. Quantitative data are shown as mean + SD. Statistical analysis was performed with a one sample t-test. Asterisks with no connecting line represent differences with control and those with lines represent differences among groups (* $p < 0.05$, ** $p < 0.01$, *** $p < 0.001$, **** $p < 0,0001$).

In this scenario, an activity promotion after TFP stimulation is still observed in the absence of extracellular Ca^{2+} (Fig. 4.7A, B). This is also observed when Ca^{2+} is chelated by EGTA and under the chelation of intracellular Ca^{2+} with BAPTA (Fig 4.7 E, F). This contrasts with the results observed under 10 µM ionomycin stimulation. Either intracellular Ca^{2+} plays a more significant role in the cleavage of E-cadherin by ADAM10 when stimulated with trifluoperazine, or Ca^{2+} is completely inconsequential for this effect, which might occur as a result of CaM inhibition. Since a slight increase of E-cadherin cleavage is observed under chelation of intracellular Ca^{2+} by BAPTA when extracellular Ca^{2+} is present in comparison to the nominal absence of it (Fig. 4.7F), a partial contribution from both phenomena is therefore most likely.

BAPTA chelation of intracellular Ca^{2+} was controlled using Ca^{2+} imaging measurements on cells previously incubated with BAPTA-AM, followed by further measurement of Ca^{2+} in the absence of extracellular Ca^{2+}. The BAPTA chelation performance is assessed by the lack of Ca^{2+} increase due to efflux from intracellular stores after stimulation with ionomycin as observed when cells were not treated with the chelator (Fig. 4. 8B).

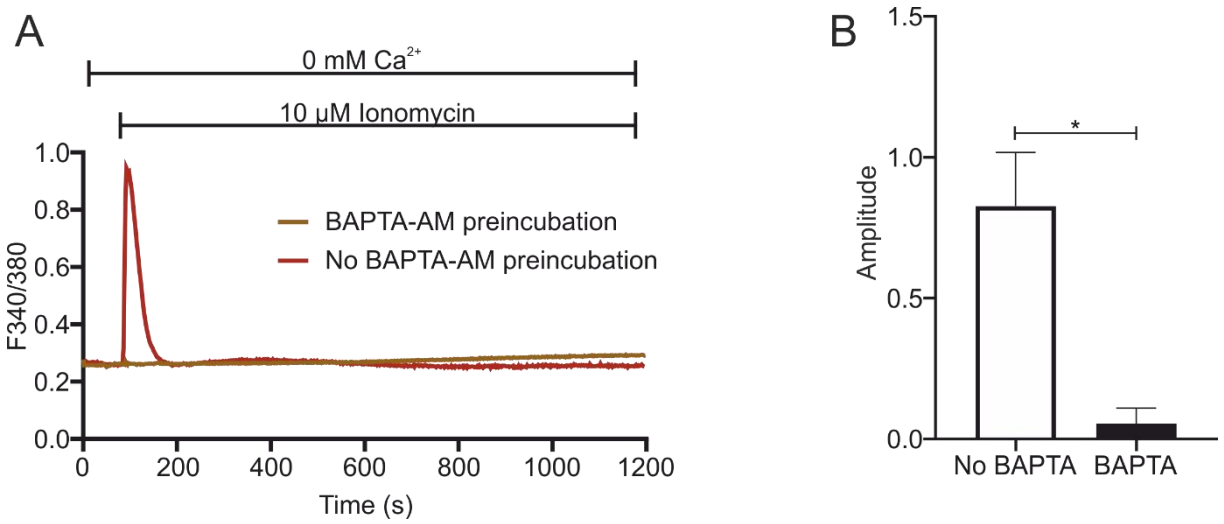

Figure 4.8. Intracellular Ca^{2+} is chelated by BAPTA-AM.

A549 cells were seeded and grown to a 70% confluence on previously poly-L-Lysine coated coverslips. Cells were then treated with 10 µM BAPTA-AM or 0.1% DMSO and loaded with 4 µM Fura2-AM for 30 min. Calcium imaging experiments were performed with addition of 10 µM ionomycin or 0.1% DMSO after 1.5 min of baseline reading in the absence of extracellular Ca^{2+}. Amplitude (B) as difference between peak and lowest value was calculated and plotted. Quantitative data are shown as mean + SD. Statistical analysis was performed with a one sample t-test. Asterisks with lines represent differences among groups (* $p < 0.05$).

Lastly, these conditions were further confirmed using the AP-BTC substrate, where a similar trend to that observed before was also noted. However, ionomycin in the absence of extracellular Ca^{2+} still shows some residual activity, which might be due to an increased sensitivity of ADAM10 towards exogenous BTC or might be an artifact given by the overexpression of the substrate (Fig. 4. 9A, B).

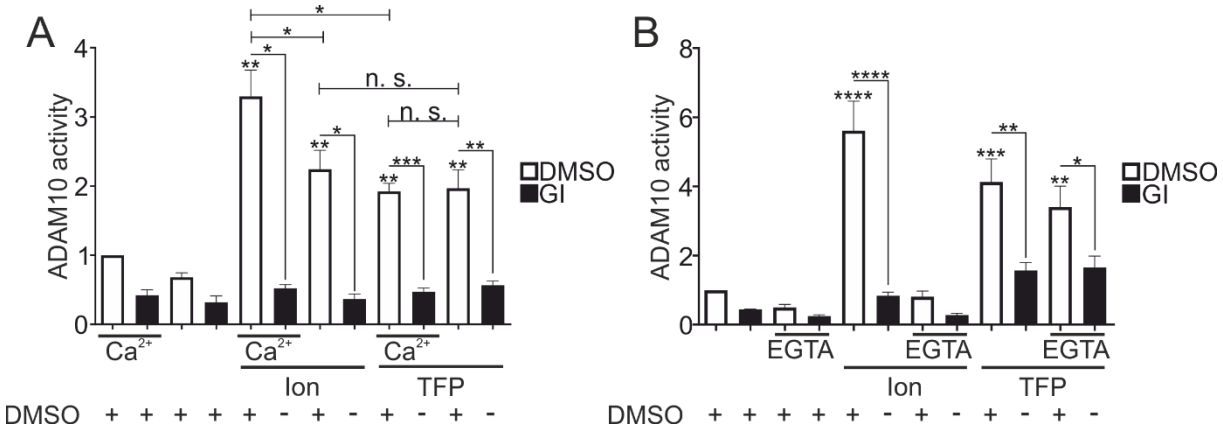

Figure 4.9. AP-BTC cleavage by ADAM10 is promoted by Ca^{2+} influx under ionomycin treatment and by CaM inhibition under trifluoperazine treatment.

A549 cells were transfected with AP-BTC overnight. Then, cells were seeded on 12-well plates, grown until confluence and starved with medium containing 0.5% FCS overnight. Afterwards, cells were further starved with medium containing 0% FCS for 1 h before incubating with 10 µM GI or 0.1% DMSO (vehicle control) for 30 min. Then, cells were stimulated with 10 µM ionomycin, 100 µM trifluoperazine or 0.1% DMSO for 1 h in the presence/absence of 2 mM $CaCl_2$ or in the presence/absence of Ca^{2+} given by the chelation of extracellular Ca^{2+} with 3 mM EGTA. Subsequently, AP activity from supernatant and cell lysates was measured. Quantitative data are shown as mean + SD. Data were normalized to control. Statistical analysis was performed with a one sample t-test. Asterisks with no connecting line represent differences with control and those with lines represent differences among groups (* $p < 0.05$, ** $p < 0.01$, *** $p < 0.001$, **** $p < 0,0001$).

4.1.3 Ca^{2+} entry-dependent ADAM10 activation is kinetically controlled

Consequently, the ADAM10 activation kinetics after calcium influx, induced by ionomycin or CaM inhibition under TFP treatment, were assessed. Therefore, both stimulations were repeated within a timeframe of 1 minute to 60 minutes (graphed as e.g., 1') to test for cleavage against both E-cadherin and AP-BTC.

Surprisingly, the activation of ADAM10 under the stimulation of 10 µM ionomycin shows a rapid strong activation after only 1 min of incubation (Fig. 4. 10A, B). This effect will remain continuous in time until the 60-minute mark, where the cleavage loses strength, likely due to a cytotoxic effect caused by prolonged stimulation.

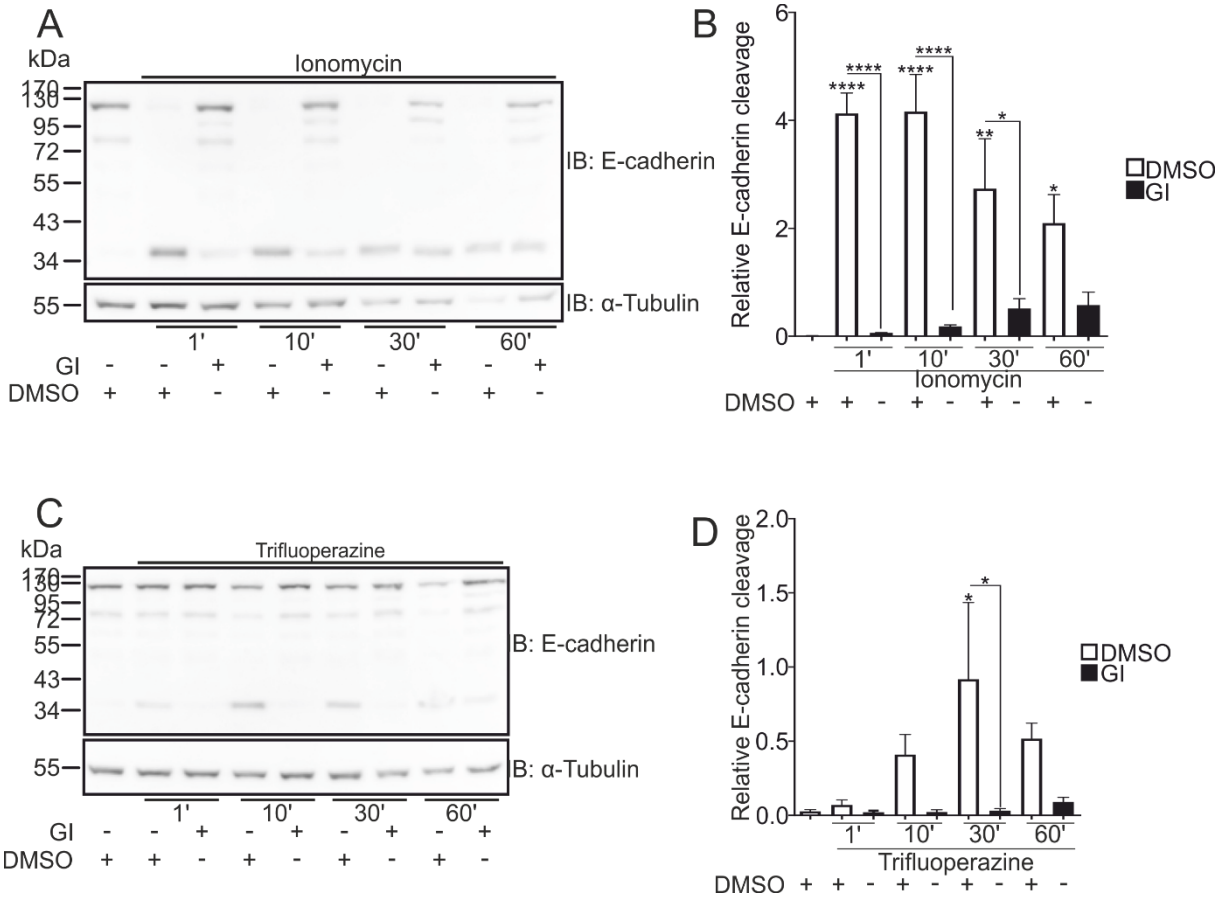

Figure 4.10. Ionomycin-mediated E-cadherin cleavage by ADAM10 shows time independency while trifluoperazine mediation is time-dependent.

A549 cells were seeded on 6-well plates, grown until confluence and starved with medium containing 0.5% FCS overnight. Afterwards, cells were further starved with medium containing 0% FCS for 1 h before incubating with 10 µM GI or 0.1% DMSO (vehicle control) for 30 min. Then, cells were stimulated with 10 µM ionomycin (A, B), 100 µM trifluoperazine (C, D) or 0.1% DMSO for different time points. Cells were then lysed, and lysates were afterwards subjected to a Western blot against a C-terminal E-cadherin antibody and α-tubulin as a loading control. Bands were quantified via densitometry and graphed as ratio of C-terminal fragment (CTF) to full-length (FL) in B and D. Quantitative data are shown as mean + SD. Statistical analysis was performed with a one sample t-test. Asterisks with no connecting line represent differences with control and those with lines represent differences among groups (* $p < 0.05$, ** $p < 0.01$, *** $p < 0.001$, **** $p < 0,0001$).

On the other hand, the cleavage of E-cadherin induced by ADAM10 stimulation with trifluoperazine required longer times, showing significance at the 10 min mark and full activity at 30 min. As with 10 µM ionomycin, this effect would also lose strength at the 60 min mark (Fig. 4. 10C, D).

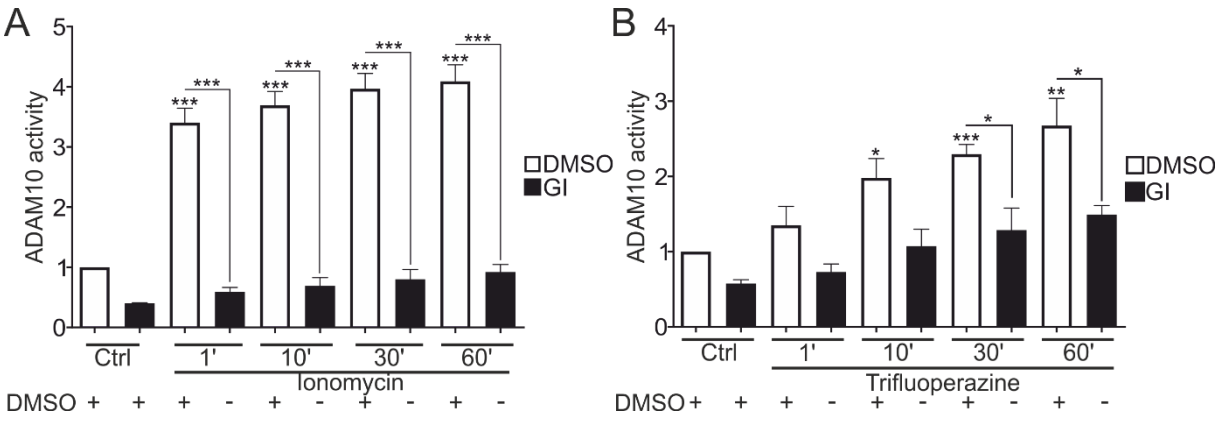

Figure 4.11. Ionomycin-mediated AP-BTC cleavage by ADAM10 shows time independency and trifluoperazine mediation shows time-dependency.

A549 cells were transfected with AP-BTC overnight, seeded on 12-well plates and grown until confluence. Then, cells were seeded starved with medium containing 0.5% FCS overnight. Afterwards, cells were further starved with medium containing 0% FCS for 1 h before incubating with 10 µM GI or 0.1% DMSO (vehicle control) for 30 min. Then, cells were stimulated with 10 µM ionomycin (A), 100 µM trifluoperazine (B) or 0.1% DMSO for different time points. Subsequently AP activity from supernatant and cell lysates was measured. Quantitative data are shown as mean + SD. Data were normalized to first lane. Statistical analysis was performed with a one sample t-test. Asterisks with no connecting line represent differences with control and those with lines represent differences among groups (* $p < 0.05$, ** $p < 0.01$, *** $p < 0.001$).

The AP-BTC cleavage after ionomycin stimulation also showed a fast, strong activation of ADAM10 that was continuous in time until 60 min (Fig. 4. 11A). On the other hand, the cleavage of the AP-BTC substrate when stimulating with trifluoperazine showed similar tendencies as with its action towards E-cadherin with the difference that longer times of 60 min showed no decreased activity but a slightly higher one (Fig. 4. 11B).

Furthermore, an additional experiment with the second CaM inhibitor was performed, this time assessing different time points as well. As with trifluoperazine in the cleavage of E-cadherin, a time-dependent augment of the activity of ADAM10 is also observed. However, it requires longer times to reach statistical significance.

When the experiment was performed to assess the cleavage of AP-BTC by ADAM10, a similar trend was observed, with a statistically significant cleavage after 30 min of stimulation (Fig. 4. 12).

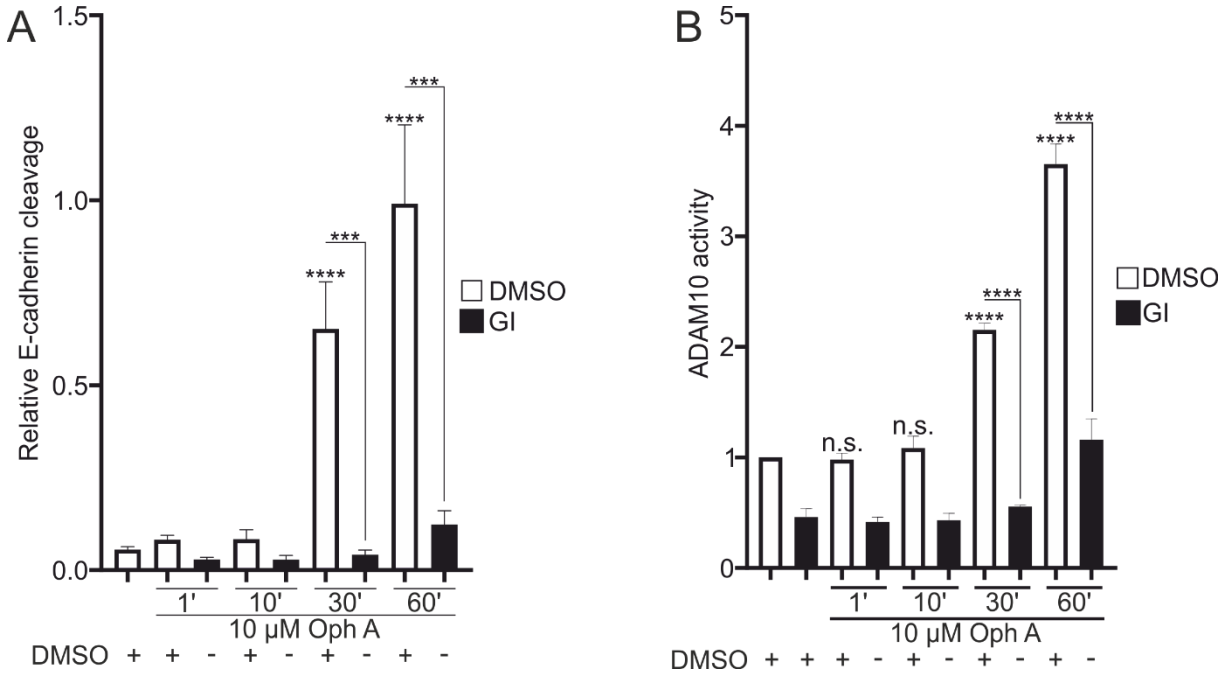

Figure 4.12. CaM inhibition by ophiobolin A shows time-dependency on E-cadherin and AP-BTC cleavage.

A: A549 cells were seeded on 6-well plates, grown until confluence and starved with medium containing 0.5% FCS overnight. Afterwards, cells were further starved with medium containing 0% FCS for 1 h before incubating with 10 µM GI or 0.1% DMSO (vehicle control) for 30 min. Then, cells were stimulated with 10 µM ophiobolin A or 0.1% DMSO for different time points. Cells were then lysed and lysates were afterwards subjected to a Western blot against a C-terminal E-cadherin antibody and α-tubulin as a loading control. Bands were quantified via densitometry and graphed as ratio of C-terminal fragment (CTF) to full-length (FL). B: A549 cells were transfected with AP-BTC overnight, seeded on 12-well plates and grown until confluence. Then, cells were starved with medium containing 0.5% FCS overnight. Afterwards, cells were further starved with medium containing 0% FCS for 1 h before incubating with 10 µM GI or 0.1%DMSO (vehicle control) for 30 min. Then, cells were stimulated with 10 µM ophiobolin A or 0.1% DMSO for different time points. Subsequently AP activity from supernatant and cell lysates was measured. Quantitative data are shown as mean + SD. Data from B were normalized to first lane. Statistical analysis was performed with a one sample t-test. Asterisks with no connecting line represent differences with control and those with lines represent differences among groups (* $p < 0.05$, ** $p < 0.01$, *** $p < 0.001$, **** $p < 0,0001$).

4.1.4 Ca^{2+} entry-activation of ADAM10 has a threshold dependency of $[Ca^{2+}]$

Due to the rapid activation of ADAM10 following stimulation with 10 µM ionomycin, it was then questioned whether there was a specific minimal concentration of Ca^{2+} promoted by ionomycin treatment that represented a threshold necessary for ADAM10 activation. For this reason, a calibration was performed using different concentrations of ionomycin. This was followed by calcium imaging measurements to investigate which range of ionomycin would promote an increase in intracellular Ca^{2+}.

A first approach was to test whether the investigated substrates, E-cadherin and AP-BTC, would exhibit any activity increase after 30 min of stimulation using lower concentrations of ionomycin. It was observed that the E-cadherin cleavage shows the first mild significance when stimulating with 0.4 µM ionomycin, reaching higher cleaving activities at 0.8 µM and 1 µM ionomycin (Fig. 4. 13). Although 0.6 µM ionomycin was not tested, an increase in activity under this condition is also feasible.When investigating the AP-BTC cleavage under different ionomycin concentrations, it was observed that 0.2 µM already elicited a statistically significant difference compared to the control. Each concentration also exhibited potent inhibition of activity with GI. Additionally, a stronger cleavage with lower concentrations might be due to the overexpression of the AP-BTC substrate or a higher sensitivity of this substate (Fig. 4. 14A).

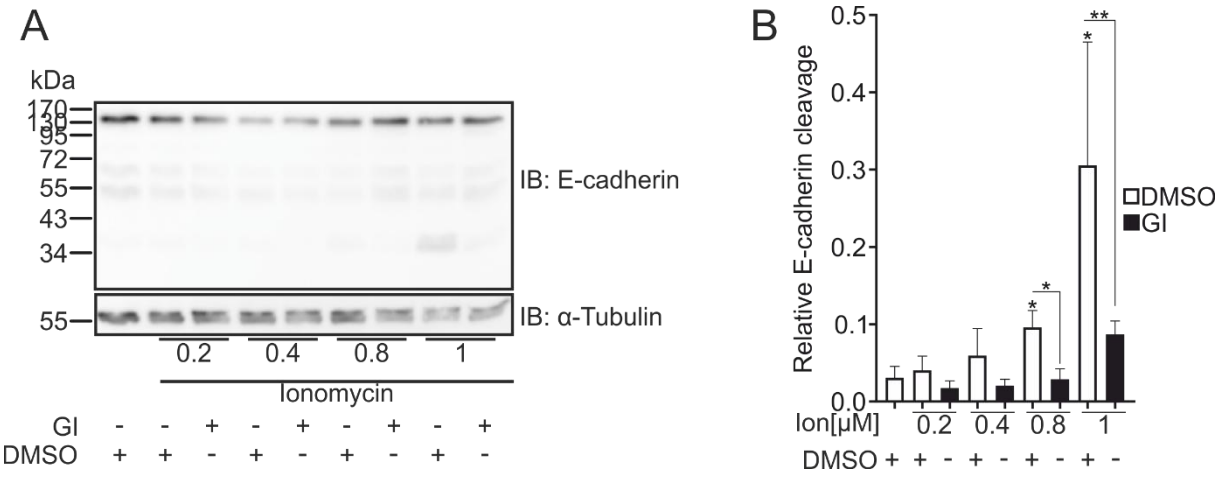

Figure 4.13. Ionomycin-mediated E-cadherin cleavage by ADAM10 shows ionomycin concentration-dependency.

A549 cells were seeded on 6-well plates, grown until confluence and starved with medium containing 0.5% FCS overnight. Afterwards, cells were further starved with medium containing 0% FCS for 1 h before incubating with 10 µM GI or 0.1% DMSO (vehicle control) for 30 min. Then, cells were stimulated with different concentrations of ionomycin or 0.1% DMSO for 30 min. Cells were then lysed and lysates were afterwards subjected to a Western blot against a C-terminal E-cadherin antibody and α-tubulin as a loading control. Bands were quantified via densitometry and graphed as ratio of C-terminal fragment (CTF) to full-length (FL) in B. Quantitative data are shown as mean + SD. Statistical analysis was performed with a one sample t-test. Asterisks with no connecting line represent differences with control and those with lines represent differences among groups (* $p < 0.05$, ** $p < 0.01$, *** $p < 0.001$, **** $p < 0,0001$).

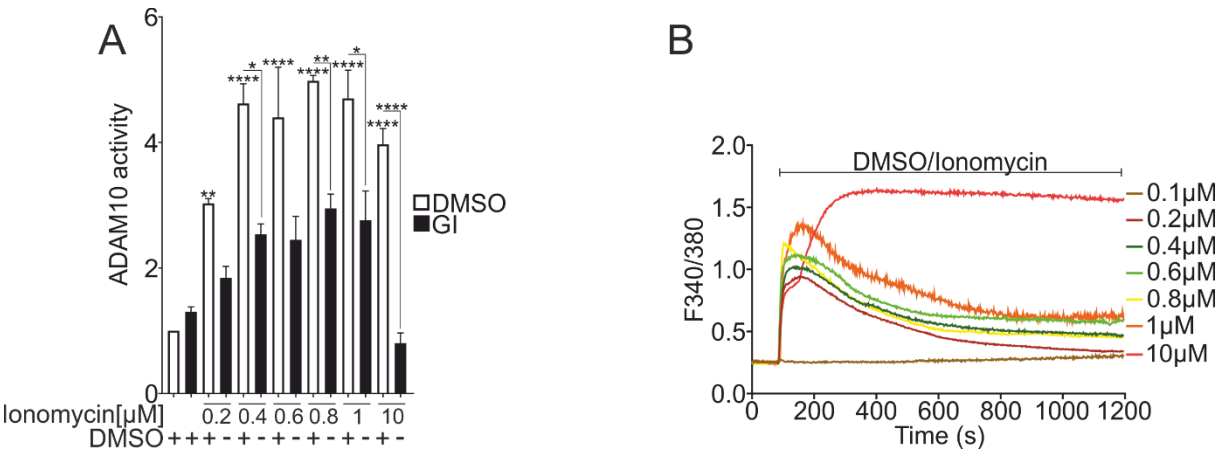

Figure 4.14. Ionomycin-mediated AP-BTC cleavage by ADAM10 shows ionomycin concentration-dependency.

A: A549 cells were transfected with AP-BTC overnight. Then, cells were seeded on 12-well plates, grown until confluence and starved with medium containing 0.5% FCS media overnight. Afterwards, cells were further starved with medium containing 0% FCS before incubating with 10 µM GI or 0.1% DMSO (vehicle control) for 30 min. Then, cells were stimulated with different concentrations ionomycin or 0.1% DMSO for 30 min. Subsequently AP activity from supernatant and cell lysates was measured. B: A549 cells were seeded and grown to a 70% confluence on previously poly-L-Lysine coated coverslips. Cells were then loaded with 4 µM Fura2-AM for 30 min. Calcium imaging experiments were performed with different concentrations of ionomycin after 1.5 min of baseline reading. Datasets were transformed to the same baseline as 0.1 µM since no difference was observed after ionomycin application. Quantitative data are shown as mean + SD. Data were normalized control. Statistical analysis was performed with a one sample t-test. Asterisks with no connecting line represent differences with control and those with lines represent differences among groups (* $p < 0.05$, ** $p < 0.01$, *** $p < 0.001$).

Some of these and further ionomycin concentrations were also used to perform Ca^{2+} measurements to observe whether there was a noticeable increase either in AUC or amplitude given by these stimulations (Fig. 4. 14B).

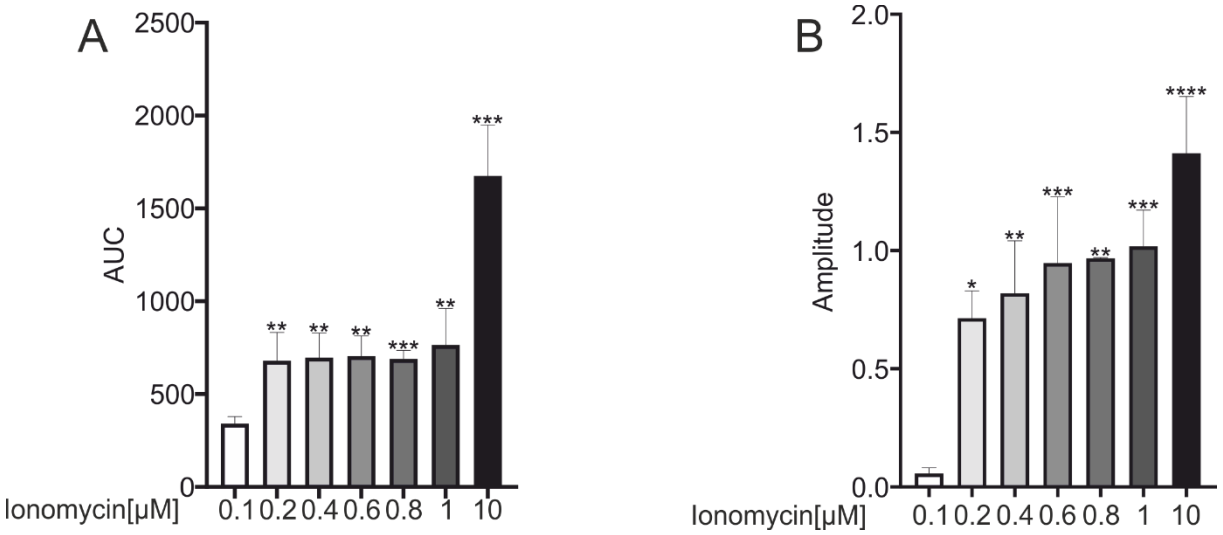

Figure 4.15. Ionomycin stimulation shows a concentration-dependent Ca^{2+} influx.

Area under the curve and amplitude were calculated from Ca^{2+} imaging experiments performed on the different ionomycin concentrations. Quantitative data are shown as mean + SD. Statistical analysis was performed with a one sample t-test. Asterisks with no connecting line represent differences with 0.1 µM ionomycin group (* $p < 0.05$, ** $p < 0.01$, *** $p < 0.001$).

Although no statistical difference is observed in either the area under the curve or amplitude for concentrations between 0.2 µM and 1 µM, amplitudes tend to show a slight, steady increase. Additionally, 0.1 µM did not promote any noticeable Ca^{2+} entry and was, therefore, considered the baseline of this experiment (Fig. 4. 15A, B). Using this concentration as a baseline, cells were stimulated over varying time points to determine whether a specific duration was required to detect increased ADAM10 activity. Based on the hypothesis that activation may occur rapidly, shorter stimulation times were prioritized.

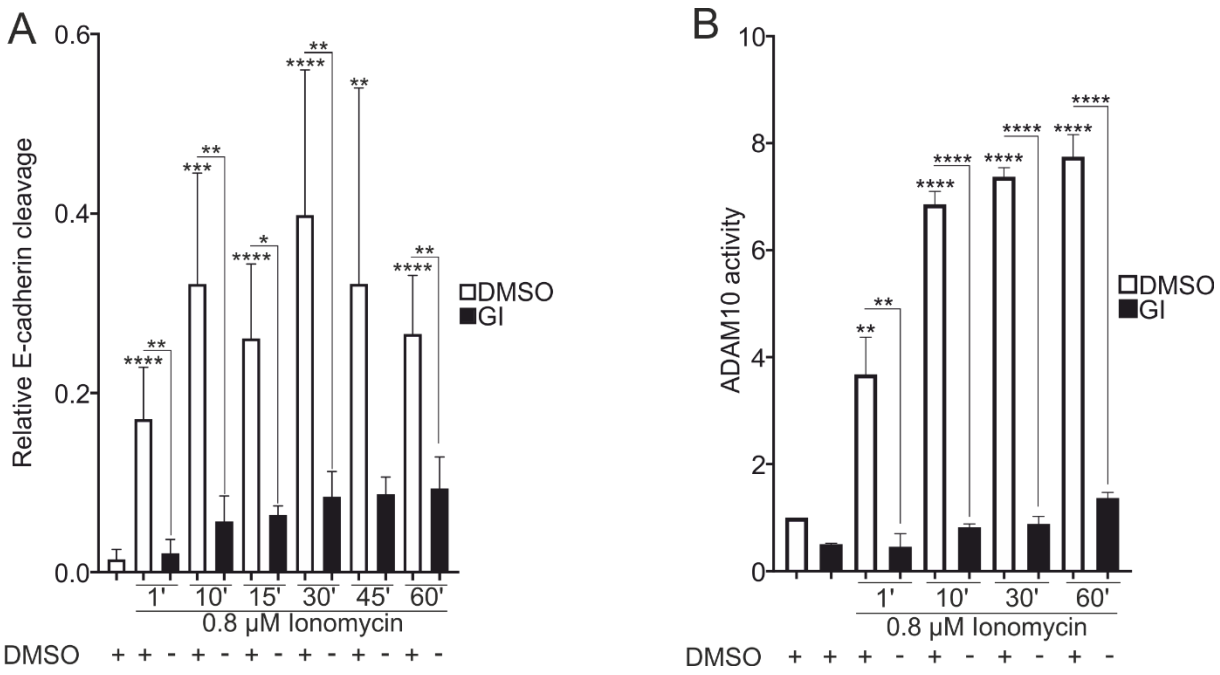

Figure 4.16. 0.8 µM ionomycin-mediated stimulation of ADAM10 shows a rapid activity increase.

A: A549 cells were seeded on 6-well plates, grown until confluence and starved with medium containing 0.5% FCS overnight. Afterwards, cells were further starved with medium containing 0% FCS for 1 h before incubating with 10 µM GI or 0.1% DMSO (vehicle control) for 30 min and then stimulated with 0.8 µM ionomycin or 0.1% DMSO for different time points. Cells were then lysed and lysates were afterwards subjected to a Western blot against a C-terminal E-cadherin antibody and α-tubulin as a loading control. Bands were quantified via densitometry and graphed as ratio of C-terminal fragment (CTF) to full-length (FL). B: A549 cells were transfected with AP-BTC overnight. Then, cells were seeded on 12-well plates, grown until confluence and starved with medium containing 0.5% FCS overnight. Afterwards, cells were further starved with medium containing 0% FCS for 1 h before incubating with 10 µM GI or 0.1% DMSO (vehicle control) for 30 min. Then, cells were stimulated with different concentrations of ionomycin or 0.1% DMSO for 30 min. Subsequently AP activity from supernatant and cell lysates was measured. Quantitative data are shown as mean + SD. Data from B were normalized control. Statistical analysis was performed with a one sample t-test. Asterisks with no connecting line represent differences with 0,1 µM ionomycin group (* $p < 0.05$, ** $p < 0.01$, *** $p < 0.001$, **** $p < 0,0001$).

It is observed that after 1 min of 0.8 µM ionomycin stimulation, an increase of activity is observed, though longer times promote even higher increases (Fig. 4. 16A). When testing the cleavage of the AP-BTC substrate, 1 min in the case of AP-BTC was also sufficient to promote ADAM10 activity (Fig. 4. 16B).

Finally, a Fura-2 AM calibration was performed to calculate the concentration of Ca^{2+} that would enter the cell when stimulated with these concentrations of ionomycin. Considering that it has already been demonstrated that the majority of the calcium increase promoted by ionomycin stimulation originates from the extracellular milieu, it can be concluded that most of the Ca^{2+} rise resulted from a Ca^{2+} influx. First, a Fura2-AM calibration was performed to calculate an experimental dissociation constant, which was used later to determine the concentration of Ca^{2+} as described in the Materials and Methods section. Afterwards, formulas and the last ionomycin concentrations Ca^{2+} measurements were used to calculate the peak concentrations of Ca^{2+} that influx into the cell as a product of the correspondent ionomycin stimulation. From these calculations, the correspondent concentration of Ca^{2+} was calculated that would elicit into the cell after each ionomycin concentration tested (Fig. 4. 17A). These concentrations were further used to construct a dose-response curve to calculate a half-maximal effective concentration (EC50) for Ca^{2+} entry in response to ionomycin. Since a maximal response was observed with 10 µM ionomycin, this concentration was used as a maximal value for Ca^{2+} entry.

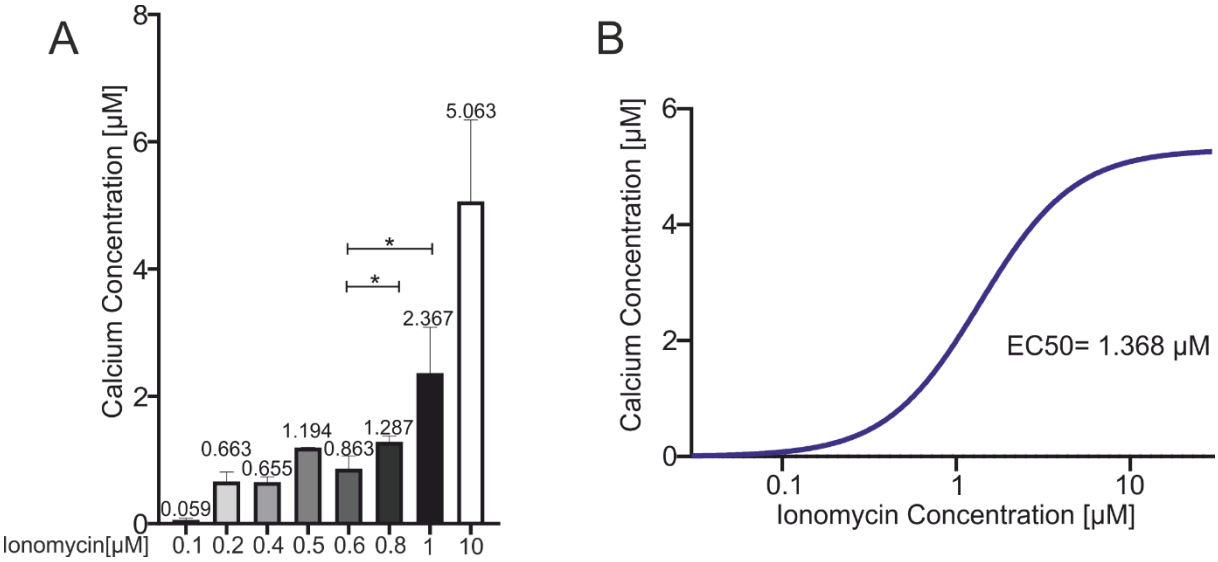

Figure 4.17. Ionomycin concentration and intracellular Ca^{2+} increase dosis response curve.

A: Data taken from the calcium imaging results using different ionomycin concentrations regarding peak values of fluorescence were used to calculate the Ca^{2+} concentration elicited after each respective stimulation. B: This data was used to build a dosis response curve from where a half maximal effective concentration was calculated. Quantitative data are shown as mean + SD. Data were normalized to first lane. Statistical analysis was performed with a one sample t-test. Asterisks with no connecting line represent differences with 0.1 µM ionomycin group (* $p < 0.05$, ** $p < 0.01$, *** $p < 0.001$).

The EC50 of Ca^{2+} entry promotion by different ionomycin concentrations was calculated to be 1.368 µM using a fit curve. Additionally, when interpolating from the curve, it was observed that an approximate extracellular [Ca^{2+}] of 1,287 µM ± 0,089 µM rise will subsequently activate ADAM10 after 0.8 µM ionomycin stimulation. However, given that a slight significance is achieved in E-cadherin cleavage by 0.4 µM ionomycin, it is likely that a 0.6 µM concentration would serve as the first-lowest concentration to show an activity promotion of ADAM10. Thus, a Ca^{2+} concentration threshold for such concentration would be 0.838 µM ± 0.2037 µM (Fig. 4. 17B) as given by interpolation from the dose-response curve. Activity measurements using both substrates and the influence of time on these effects were performed to confirm whether 0.6 µM ionomycin also promotes the activity of ADAM10.

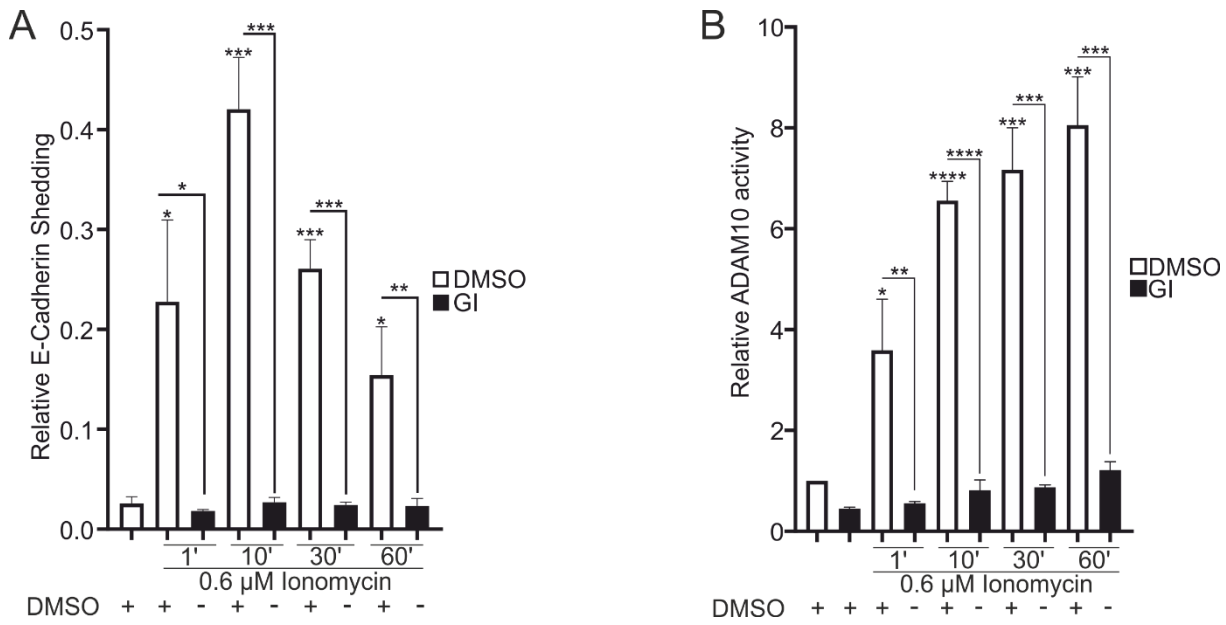

Figure 4.18. 0.6 µM ionomycin-mediated stimulation of ADAM10 shows a rapid activity increase.

A: A549 cells were seeded on 6-well plates, grown until confluence and starved with medium containing 0.5% FCS overnight. Afterwards, cells were further starved with medium containing 0% FCS for 1 h before incubating with 10 µM GI or 0.1% DMSO (vehicle control) for 30 min and then stimulated with 0.6 µM ionomycin or 0.1% DMSO as vehicle control for different time points. Cells were then lysed and lysates were afterwards subjected to a Western blot against a C-terminal E-cadherin antibody and α-tubulin as a loading control. Bands were quantified via densitometry and graphed as ratio of C-terminal fragment (CTF) to full-length (FL). B: A549 cells were transfected with AP-BTC overnight. Then, cells were seeded on 12-well plates, grown until confluence and starved with medium containing 0.5% FCS overnight. Afterwards, cells were further starved with medium containing 0% FCS for 1 h before incubating with 10 µM GI or 0.1% DMSO (vehicle control) for 30 min and then stimulated with different concentrations ionomycin or 0.1% DMSO for 30 min. Subsequently AP activity from supernatant and cell lysates was measured. Quantitative data are shown as mean + SD. Data from B were normalized to first lane. Statistical analysis was performed with a one sample t-test. Asterisks with no connecting line represent differences with 0.1 µM ionomycin group (* $p < 0.05$, ** $p < 0.01$, *** $p < 0.001$, **** $p < 0,0001$).

In this scenario, cleavage of both substrates E-cadherin as well as AP-BTC were significantly cleaved by ADAM10 after only 1 min of treatment (Fig. 4. 18A, B), although longer times promoted higher activity augments. This suggests a time-independent threshold-coupled increase in ADAM10 activity. Furthermore, Ca^{2+} measurements were performed on calcium imaging experiments in the absence of extracellular Ca^{2+} with 1 µM and 10 µM ionomycin to confirm that the concentration in intracellular stores is not sufficient to promote ADAM10 activity (Fig. 4. 19A).

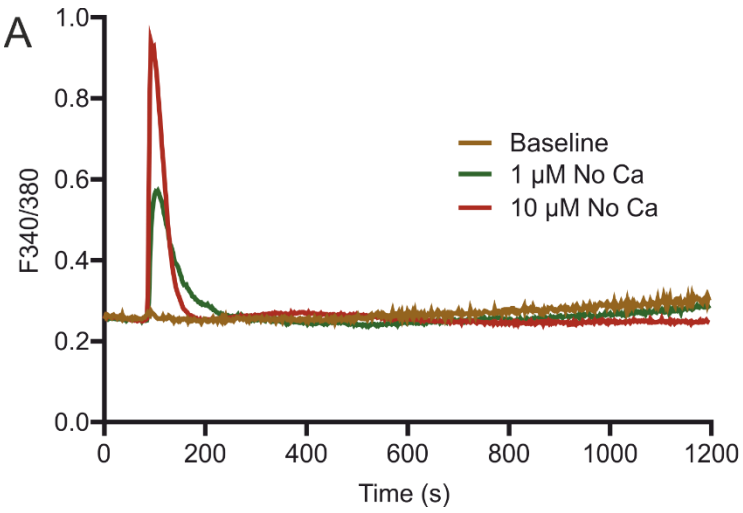

B

[Ionomycin]	[Ca^{2+}]
1 µM No Ca^{2+}	0.204±0.144 µM
10 µM No Ca^{2+}	0.336±0.300 µM

Figure 4.19. Intracellular Ca^{2+} efflux promoted by 1 µM or 10 µM ionomycin will not reach Ca^{2+} threshold necessary to activate ADAM10.

A: A549 cells were seeded and grown to a 70% confluence on previously poly-L-Lysine coated coverslips. Cells were then loaded with 4 µM Fura2-AM for 30 min. Calcium imaging experiments were performed with 1 µM, 10 µM ionomycin or 0.1% DMSO (vehicle control) after 1.5 min of baseline reading. Dataset was normalized to baseline. B: Table with calculated Ca^{2+} concentration values for each ionomycin application.

Ca^{2+} calculations after 1 µM and 10 µM ionomycin, both in the absence of extracellular Ca^{2+}, elicited an increase of up to 0.204 ± 0.144 µM and 0.336 ± 0.3 µM, respectively (Fig. 4. 19B). This would not be enough to reach the threshold calculated before for 0.6 µM ionomycin, thus explaining why no E-cadherin cleavage was observed under these conditions.

4.1.5 Ca^{2+} influx and calmodulin inhibition control extracellular ADAM10 activity

To further differentiate and identify which of the different forms of ADAM10 is executing its cleavage functions on AP-BTC and E-cadherin, a series of experiments was performed to isolate and detect soluble or exosome-related forms of ADAM10.

Firstly, exosomes from A549 cells, stimulated with ionomycin and trifluoperazine in the presence or absence of Ca^{2+}, were isolated as described in the Materials and Methods section. Samples were then subjected to Western blot analysis using an antibody raised against the C-terminal region of ADAM10 since the C-terminus is once packaged in extracellular vesicles facing the extracellular space.

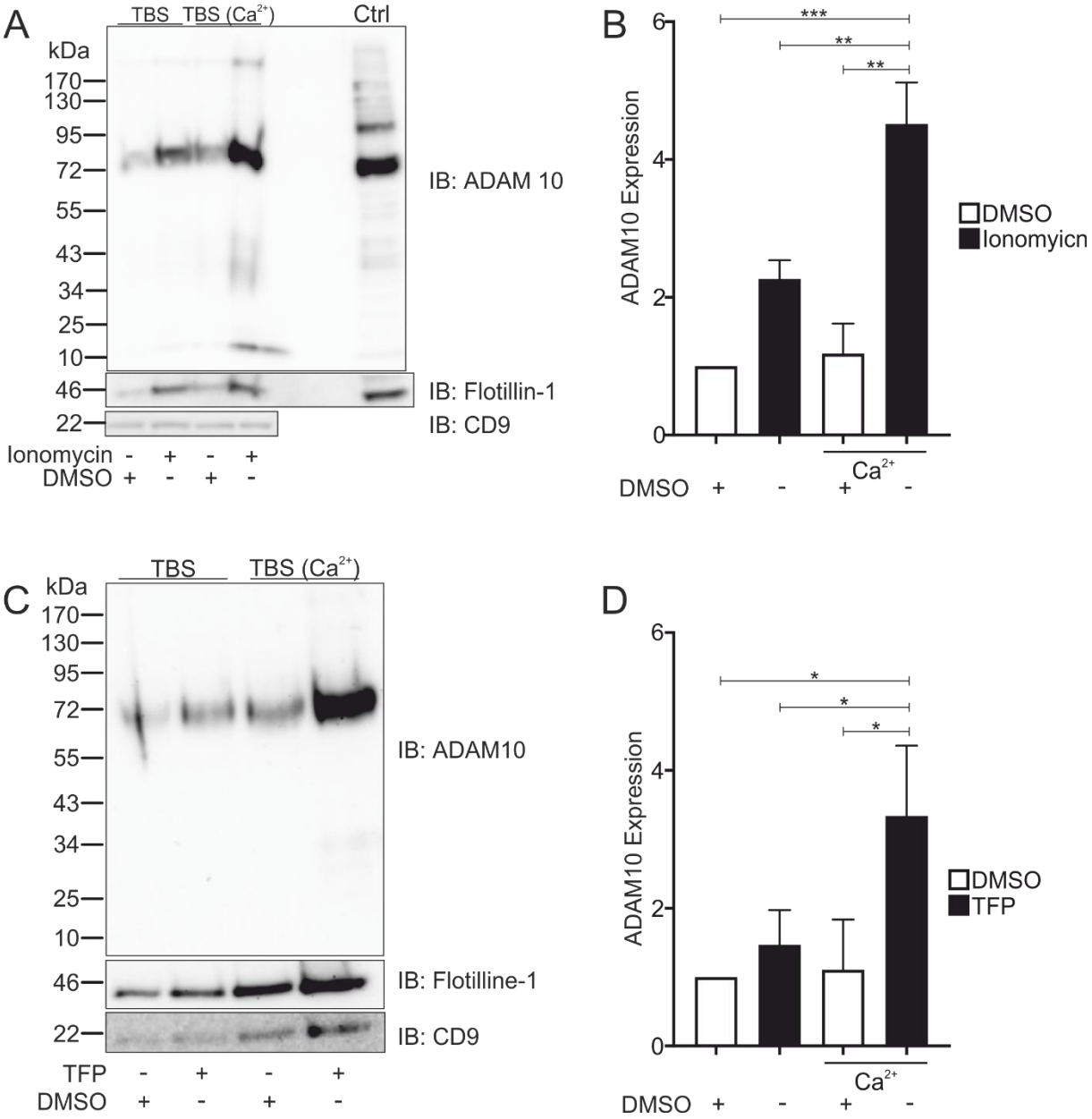

Figure 4.20. Mature form of ADAM10 is increased under ionomycin or trifluoperazine treatment when extracellular Ca^{2+} is present.

A, C: A549 cells were seeded on 6-well plates, grown until confluence and starved with medium containing 0.5% FCS overnight. Afterwards, cells were further starved with TBS in the presence/absence of 2 mM Ca^{2+} for 1 h before incubating with 10 µM ionomycin (A) or 100 µM trifluoperazine (B) for 1 h. Afterwards, supernatants were removed and assigned for exosome purification as stated in materials & methods. Samples were subsequently subjected to Western blot analysis probing against a C-terminal ADAM10 antibody, a flotiline-1 antibody as an exosome marker and CD9 as exosome marker and tetraspanin ADAM10-binding protein. Densitometry analysis for ionomycin (B) and trifluoperazine (D) was performed and plotted. Quantitative data are shown as mean + SD. Data were normalized to control. Statistical analysis was performed with a one sample t-test. Asterisks represent differences among between groups (* $p < 0.05$, ** $p < 0.01$, *** $p < 0.001$).

In both cases, the release of mature ADAM10 in exosomes was augmented only in the presence of extracellular Ca^{2+} (Fig. 4. 20). However, it is worth mentioning that under ionomycin treatment, a slight increase in ADAM10 was also observed in exosomes. Therefore, the activity elicited on the substrates may be at least partly derived from the released forms of ADAM10, either as soluble, active proteases or as cargo in exosomes. To compare with the relative regular expression of ADAM10 in cells, some membranes previously developed against E-cadherin were also incubated with the ADAM10 antibody.

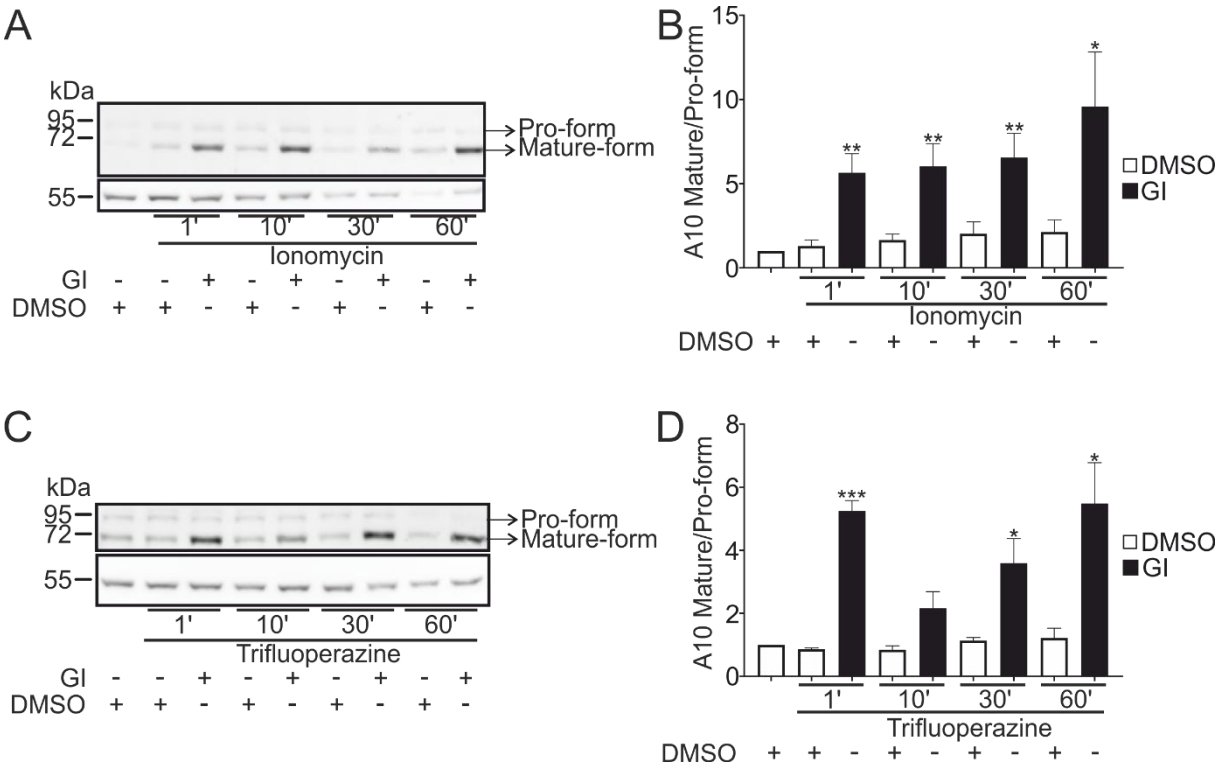

Figure 4.21. Ionomycin or trifluoperazine-mediated activity increase is not modulated by an increased ADAM10 expression.

A: Previous results from the ionomycin (A) and trifluoperazine (C) time points experiments shown in Figure 4.10 were stripped and re-blotted against ADAM10 using an antibody directed to its C-terminus. Maturation graphed as ratio of mature to pro-form was quantified and plotted in both ionomycin (B) and trifluoperazine (D). Quantitative data are shown as mean + SD. Data were normalized to first lane. Statistical analysis was performed with a one sample t-test. Asterisks with no connecting line represent differences with 0.1 µM ionomycin group (* $p < 0.05$, ** $p < 0.01$, *** $p < 0.001$).

Comparatively, no statistical difference in ADAM10 mature to pro-form ratio could be observed after either ionomycin or trifluoperazine stimulation. Although there was a significant ratio of mature to pro-form whenever cells were inhibited with GI, this effect has been described earlier and could be correlated with an internalization and de novo production as a form of compensation for the inactive ADAM10 (Seifert et al., 2021) (Fig. 4.21). Additionally, staining of surface ADAM10 and subsequent flow cytometry analysis were performed to determine the extent to which the total expression of ADAM10 observed in the previous experiment was localized to the plasma membrane after treatment with ionomycin, trifluoperazine, or thapsigargin. Kinetically, a faster translocation to the cell surface was observed under trifluoperazine stimulation (Fig. 4. 22A). Meanwhile, ionomycin required longer times to be translocated (Fig. 4. 22B).

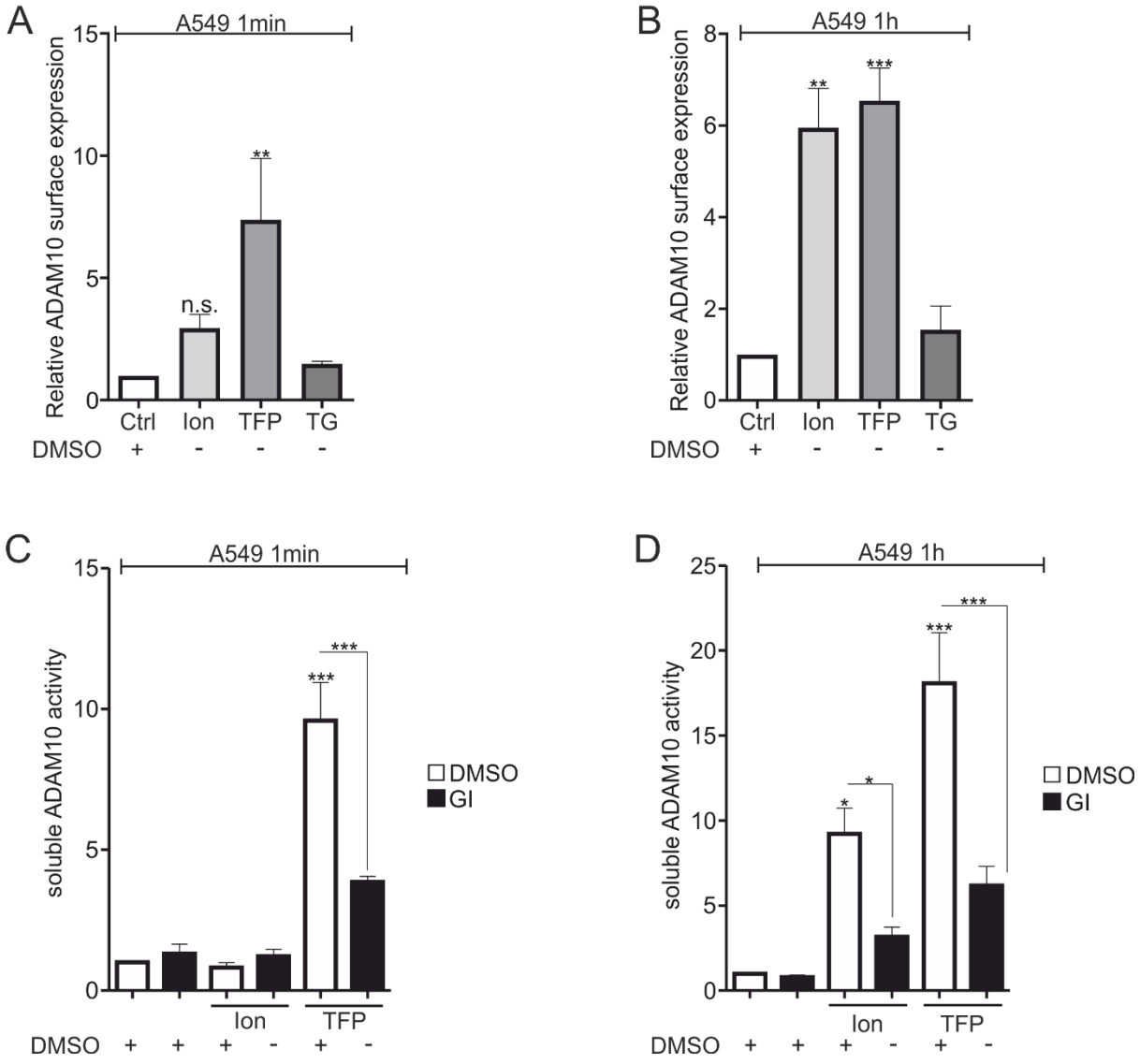

Figure 4.22. Trifluoperazine shows a faster surface translocation and activity increase of membrane unbound form of ADAM10 in A549 cells.

A, B: A549 cells were seeded on 6-well plates, grown until confluence and starved with medium containing 0.5% FCS overnight. Afterwards, cells were further starved with medium containing 0% FCS for 1 h before incubating with 10 µM ionomycin, 100 µM trifluoperazine, 1 µM thapsigargin or 0.1% DMSO for 1 min or 1 h. Cells were then detached with Accutase and incubated with an N-terminal ADAM10 antibody. After washing and incubating against a fluorescent secondary antibody, samples were assigned for flow cytometry analysis. Graphed is the median of the fluorescence intensity for each sample. C, D: A549 cells were seeded on 12-well plates, grown until confluence and starved with medium containing 0.5% FCS overnight. Afterwards, cells were further starved with medium containing 0% FCS for 1 h before incubating with 10 µM ionomycin, 100 µM trifluoperazine, 1 µM thapsigargin or 0.1% DMSO for 1 min or 1 h. Supernatants were then extracted, centrifuged and assigned for fluorescence measurement using a FRET-based ADAM10 substrate. Quantitative data are shown as mean + SD. Data were normalized to first lane. Statistical analysis was performed with a one sample t-test. Asterisks with no connecting line represent differences control (* $p < 0.05$, ** $p < 0.01$, *** $p < 0.001$).

To test whether these forms have any cleavage activity, supernatants from A549 cells stimulated with ionomycin, thapsigargin and trifluoperazine were incubated with a FRET-based substrate relatively more sensitive to ADAM10 (Caescu, Jeschke and Turk, 2009). Conditions were also further controlled using GI, not only during stimulations before removing the supernatants but also through additional supplementation on the plate during fluorescence measurements. To test whether there would be a difference in time regarding activity, these experiments were performed after 1 min of stimulation and after 1 h. It was observed that trifluoperazine significantly promotes the activity of ADAM10 at a faster rate than ionomycin since a difference can be observed after only 1 min of incubation (Fig 4. 22C). In contrast, ionomycin requires 1 h to significantly increase the activity of released forms of ADAM10 (Fig 4. 22D). These results correlate with the surface expression results under the treatment with the same reagents. As observed in the first cleavage assays, thapsigargin elicits no effect whatsoever at any time of stimulation.

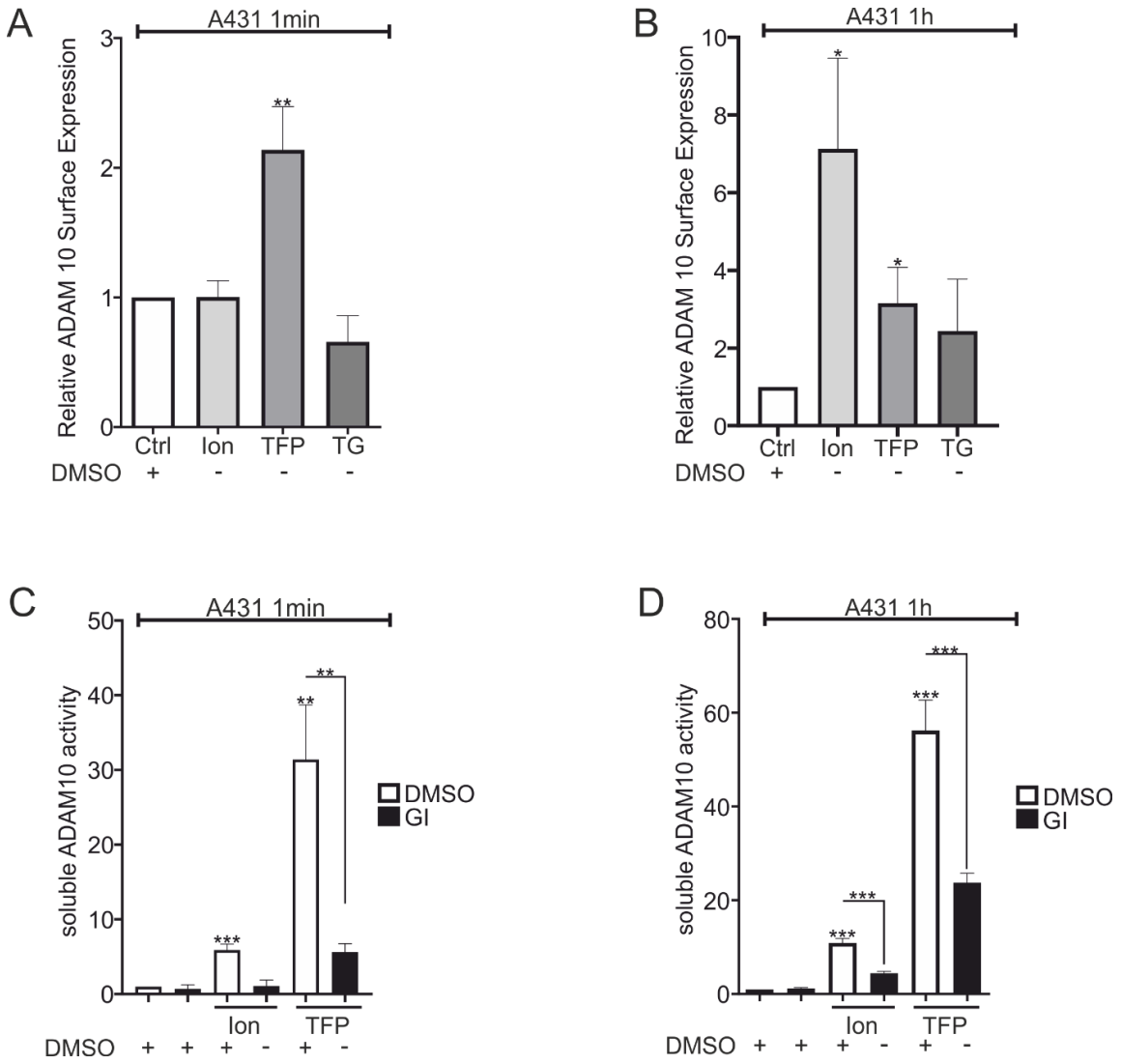

Figure 4.23. Trifluoperazine shows a faster surface translocation and activity increase of membrane unbound form of ADAM10 in A431 cells.

A, B: A431 cells were seeded on 6-well plates, grown until confluence and starved with medium containing 0.5% FCS overnight. Afterwards, cells were further starved with medium containing 0% FCS for 1 h before incubating with 10 µM ionomycin, 100 µM trifluoperazine, 1 µM thapsigargin or 0.1% DMSO for 1 min or 1 h. Cells were then detached with Accutase and incubated with an N-terminal ADAM10 antibody. After washing and incubating against a fluorescent secondary antibody, samples were assigned for flow cytometry analysis. Graphed is the median of the fluorescence intensity for each sample. C, D: A431 cells were seeded on 12-well plates, grown until confluence and starved with medium containing 0.5% FCS overnight. Afterwards, cells were further starved with medium containing 0% FCS for 1 h before incubating with 10 µM ionomycin, 100 µM trifluoperazine, 1 µM thapsigargin or 0.1% DMSO for 1 min or 1 h. Supernatants were then extracted, centrifuged and assigned for fluorescence measurement using a FRET-based ADAM10 substrate. Quantitative data are shown as mean + SD. Data were normalized to first lane. Statistical analysis was performed with a one sample t-test. Asterisks with no connecting line represent differences with control group (* $p < 0.05$, ** $p < 0.01$, *** $p < 0.001$).

To ensure that these effects where not delimited to a single cell line, experiments were repeated with a different one of epithelial origin such as A431 and it was observable that results exhibited the same trends, though it could be argued, that at later time points, activity promoted by trifluoperazine loses potency in comparison to A549 cells which can be caused by an increased cytotoxic effect of the reagent on this cell line (Fig. 4. 23).

4.1.6 ADAM10 exhibits a spatiotemporal dependency of its activity

To overcome the nonspecific nature of ionomycin as a Ca^{2+} ionophore, stably transfected HEK cell lines expressing Ca^{2+}-permeable TRP channels were stimulated with their respective agonists to specifically induce channel-mediated Ca^{2+} influx and assess ADAM10 activity. Corresponding Ca^{2+} imaging experiments were conducted under identical stimulation conditions to quantify intracellular Ca^{2+} elevation. Wild-type (WT) HEK cells served as controls in all experiments. ADAM10 activity was evaluated exclusively via cleavage of the AP-BTC substrate, given the low endogenous expression of E-cadherin in HEK cells.

As a first test, HEK cells containing a stable transfection of TRPC4 were tested after incubation with 60 nM englerin A, a specific agonist for the channeling of this channel (Akbulut et al., 2015) (Fig. 4. 24A, B). Cleavage of AP-BTC was found to be approximately twice as high after stimulation with englerin A compared to WT-HEK cells. Interestingly, however, ionomycin stimulation on TRPC4-transfected cells showed a tendentially lower ADAM10 activity than in WT-HEK cells. To test a different channel, TRPM3 was considered due to the existence of a specific agonist for its channeling, such as pregnenolone sulphate. Surprisingly, channeling of TRPM3 by pregnenolone sulphate, a known TRPM3 agonist (Thiel et al., 2017) did not elicit any activity augment of ADAM10 when compared with WT-HEK cells (Fig. 4. 24C, D).

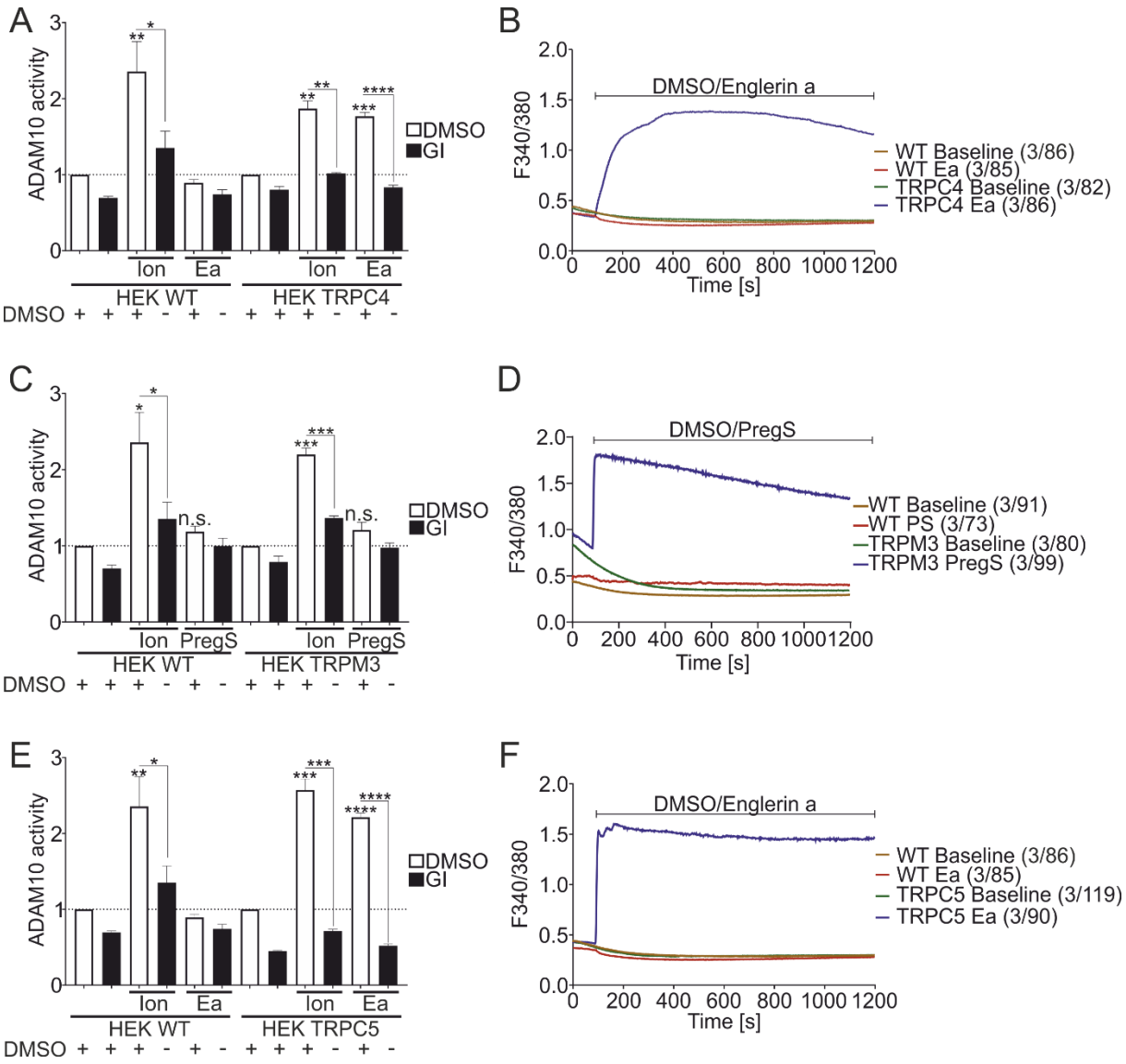

Figure 4.24. Ca^{2+} entry through canonical members of TRP channels mediates activation of ADAM10.

A, C, E: HEK wild type cells, µOR-TRPC4-HEK-293 cells and HEK-293-TRPM3α2 were transfected with AP-BTC overnight. Then, cells were seeded on 12-well plates, grown until confluence and starved with medium containing 0.5% FCS overnight. Afterwards, cells were further starved with medium containing 0% FCS for 1 h before incubating with 10 µM GI or 0.1% DMSO (vehicle control) for 30 min. Then, cells were stimulated with 60 nM englerin A, 100 µM pregnenolone sulphate or 0.1% DMSO for 30 min. Subsequently AP activity from supernatant and cell lysates was measured. B, D, F: cells were seeded and grown to a 70% confluence on previously poly-L-Lysine coated coverslips. HEK wild type cells, µOR-TRPC4-HEK-293 cells and HEK-293-TRPM3α2 cells were then loaded with 4 µM Fura2-AM for 30 min. Calcium imaging experiments were performed with addition of 60 nM englerin A, 100 µM pregnenolone sulphate or 0.1% DMSO after 1.5 min of baseline reading. Quantitative data are shown as mean + SD. Data were normalized to first lane. Statistical analysis was performed with a one sample t-test. Asterisks with no connecting line represent differences with 0.1 µM ionomycin group (* $p < 0.05$, ** $p < 0.01$, *** $p < 0.001$, **** $p < 0,0001$).

To elucidate whether this differential effect was specific to a specific subfamily of the TRP channels, the experiment was repeated with the closest phylogenetically related member of TRPC4, TRPC5, also using englerin A as an agonist. In this case, as with TRPC4, the activity of ADAM10 was significantly increased when stimulating with englerin A (Fig. 4. 24E, F).

Finally, to assess whether differences in activity were due to a differential Ca^{2+} influx, as indicated by Ca^{2+} imaging, the amplitude of peaks and the area under the curve of the measurements were calculated.

Figure 4.25. Slight increase in AUC after opening of TRPC4 and TRPC5 by englerin A and Ca^{2+} influx.

A, B: Area under the curve using the trapezoid method and amplitude as difference between peak and lowest value from previous experiment were calculated and plotted. Quantitative data are shown as mean + SD. Statistical analysis was performed with a one sample t-test. Asterisks or numerals with no connecting line represent differences with control and those with lines represent differences among groups (* $p < 0.05$, ** $p < 0.01$, *** $p < 0{,}001$).

Although there was no statistical difference among the amplitudes between peaks in the different stimulations, the area under the curve for TRPC4 and TRPC5 was 25% and 50% percent higher, respectively (Fig. 4. 25A, B). However, the slight differences in the area under the curve are likely not sufficient to provide a feasible cause for the lack of ADAM10 activity in TRPM3-containing HEK cells. Therefore, the interaction or colocalization of ADAM10 and canonical members of the TRP family might be related. An overexpression of these channels on the HEK-293 cell line platform might be considered an artifact for said activity promotion of ADAM10, however, if this were the case, this effect would be observable throughout all overexpressed channels and this is not the case for TRPM3. Therefore, co-immunoprecipitation experiments were performed to allocate TRPC4 and TRPC5 close to ADAM10. However, the results revealed no co-precipitation and it is, therefore, feasible that this effect depended on a microdomain where the interaction between these proteins occurs transiently.

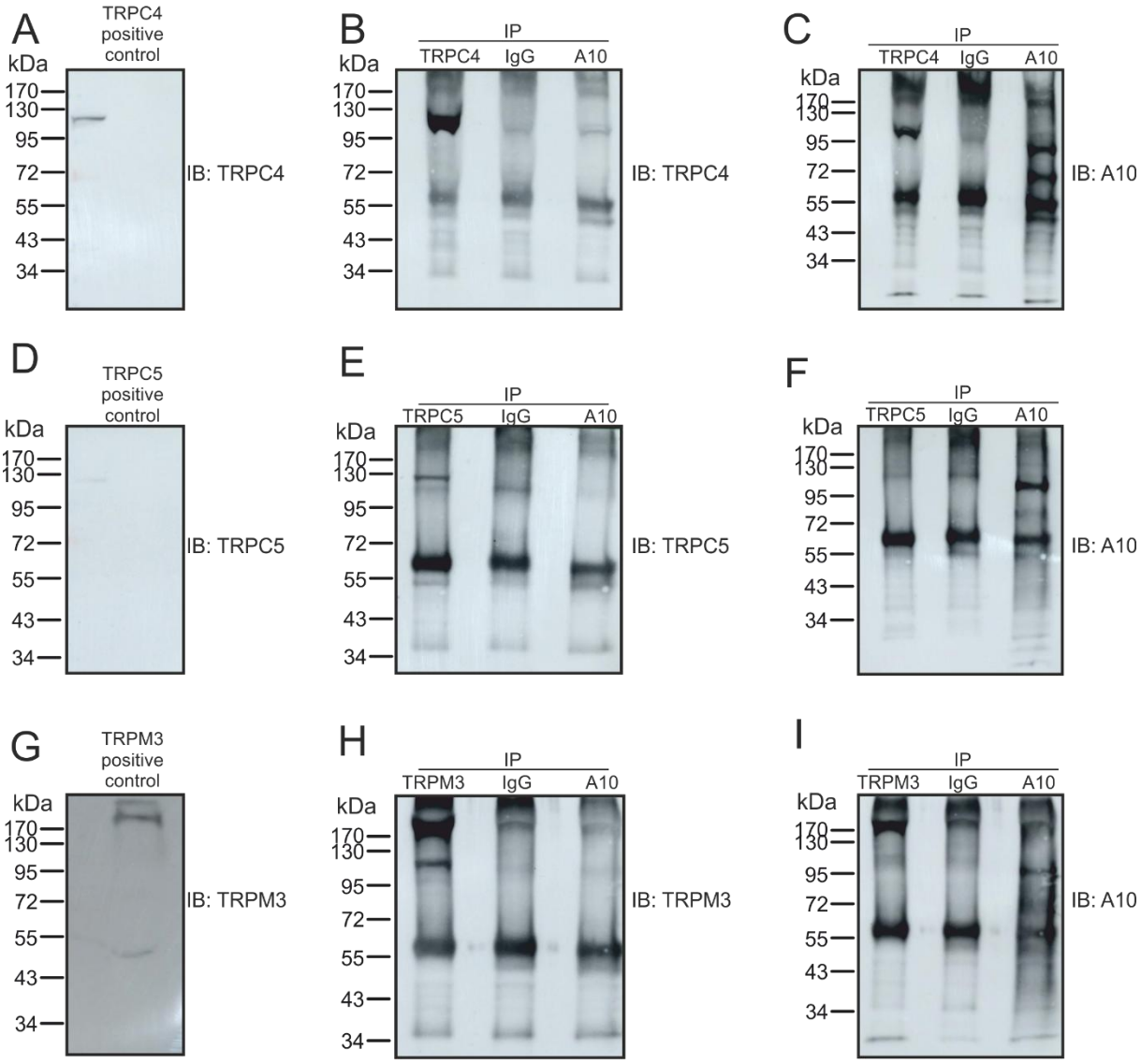

Figure 4.26. Co-immunoprecipitation of investigated TRP channels and ADAM10.

A-I. HEK wild type cells, μOR-TRPC4-HEK-293 cells and HEK-293-TRPM3α2 were seeded in T175 culture flasks, grown to confluence and then subjected to co-immunoprecipitation against TRPC4, TRPC5, TRPM3 and ADAM10, respectively, and subjected to Western blot analysis. For confirmation of TRP channel size, positive controls were generated by overexpression, and added as positive controls. Blots were splitted after development due to presence of three empty lanes between positive control and immunoprecipitation samples, and requirement for contrasting of the positive controls due to much weaker protein load.

An additional possibility was the assessment of ADAM10's activity in promoting the gating of endogenous Ca^{2+}-permeable channels. Because of this, E-cadherin cleavage was assessed after the gating of CRAC channels elicited by the depletion of intracellular stores.

Although a Ca^{2+} increase is observed after the readdition of Ca^{2+} to store-depleted cells treated with thapsigargin, no cleavage of E-cadherin was detected. Thus, it is probable that microdomains associated with ADAM10s' activity did not contain CRAC channels or that a certain co-localization is required for the transfer of activity promotion towards ADAM10 (Fig. 4. 27).

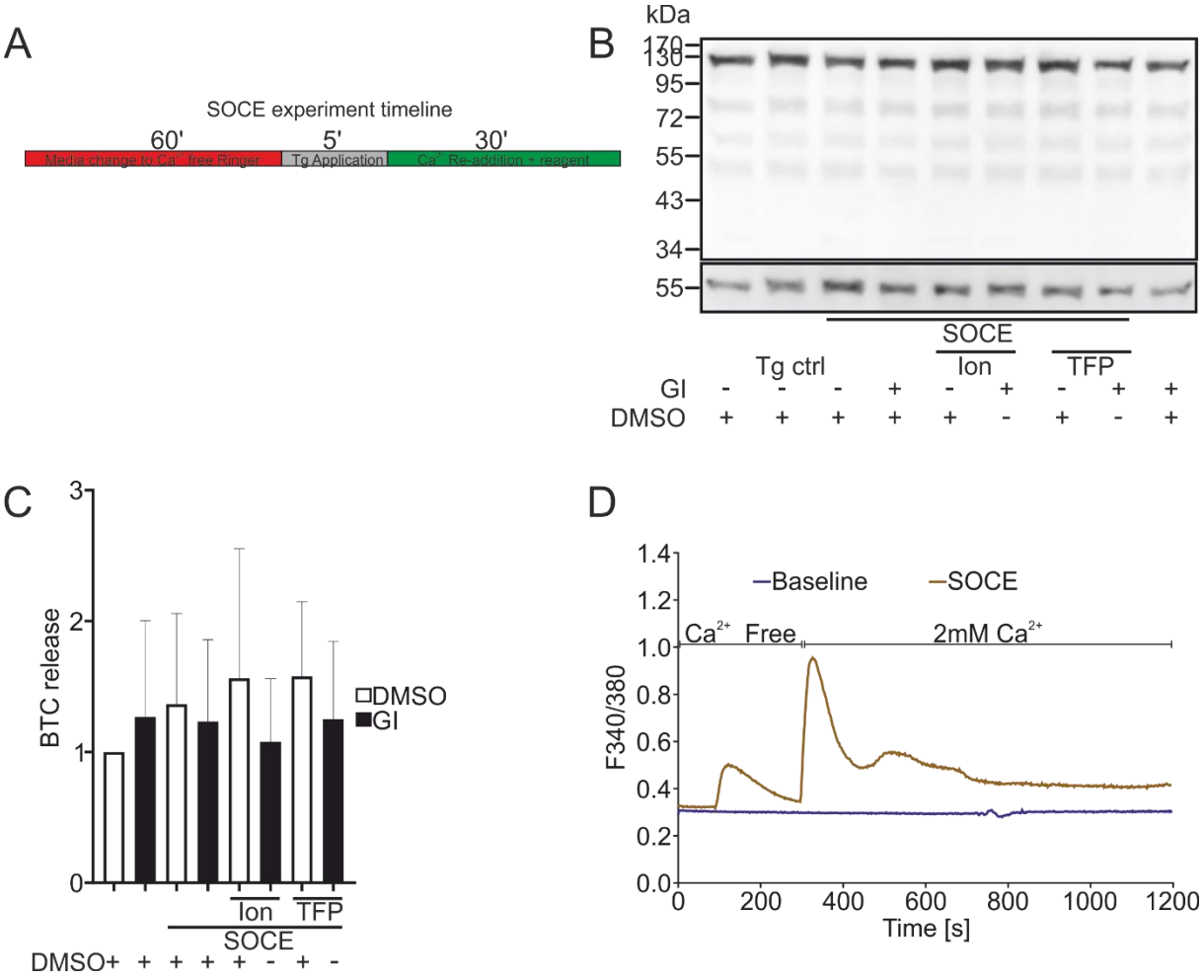

Figure 4.27. Ca^{2+} influx through SOCE does not mediate an activation of ADAM10.

A: Timeline of the store operated calcium entry experiment. B: A549 cells were seeded on 6-well plates, grown until confluence and starved with medium containing 0.5% FCS overnight. Afterwards, cells were further starved with Ca^{2+} free ringer solution for 1 h before incubating with 10 µM GI or 0.1% DMSO (vehicle control) for 30 min and then adding 1 µM thapsigargin to deplete intracellular stores. Readdition of Ca^{2+} was then performed to a final concentration of 2 mM together with 10 µM ionomycin, 100 µM trifluoperazine or 0,1% DMSO for 30 min. Cells were then lysed and lysates were afterwards subjected to a Western blot against a C-terminal E-cadherin antibody and α-tubulin as a loading control. C: A549 cells were transfected with AP-BTC overnight. Then, cells were seeded on 12-well plates, grown until confluence and starved with medium containing 0.5% FCS overnight. Afterwards, cells were further starved with Ca^{2+} free ringer solution for 1 h before incubating with 10 µM GI or 0.1% DMSO for 30 min and then adding 1 µM thapsigargin to deplete intracellular stores. Readdition of Ca^{2+} was then performed to a final concentration of 2 mM together with 10 µM ionomycin, 100 µM trifluoperazine or 0.1% DMSO as vehicle control for 30 min. Subsequently AP activity from supernatant and cell lysates was measured. D: A549 cells were seeded and grown to a 70% confluence on previously poly-L-Lysine coated coverslips. Cells were then loaded with 4 µM Fura2-AM for 30 min. Calcium imaging experiments were performed with a depletion of intracellular stores with 1 µM thapsigargin after 1.5min of baseline measurement in the absence of extracellular Ca^{2+}. After 5 min ringer containing Ca^{2+} was added to a final Ca^{2+} concentration of 2 mM. Quantitative data are shown as mean + SD. Data were normalized to first lane.

4.2 ADAM10-mediated processing of E-cadherin

4.2.1 ADAM10 participates in the cleavage of E-cadherin

As further confirmation of the cleavage of E-cadherin by ADAM10, KD of the protease mediated by a lentiviral vector containing a shRNA sequence targeting ADAM10 were performed during stimulation with ionomycin, thapsigargin and trifluoperazine. It is essential to note that a residual activity was expected, as under KD conditions, the expression of ADAM10 is reduced but not completely ablated. On the other hand, the involvement of different proteases in the cleavage of E-cadherin cannot be ruled out. Therefore, experiments using inhibitors targeting other proteases were also performed.

It can be observed that the previous activity augments under ionomycin or trifluperazine are significantly reduced when ADAM10 expression is downregulated (Fig. 4. 28B, D).

4.2.2 Participation of other proteases on the E-cadherin cleavage

Inhibition experiments showed the occurrence of an additional band of E-cadherin at 100 kDa. To investigate if this is directly related to the missing cleavage event by ADAM10, experiments were repeated with ADAM10 KD cells. Interestingly, while the cleavage of E-cadherin and the formation of the 36 kDa fragment were inhibited after ADAM10 KD, no change was observed in the 100 kDa fragment. Therefore, we hypothesized that another protease could be activated under these conditions. The inhibition of MMPs using the broad-spectrum inhibitor GM6001 revealed that the presence of the 100 kDa fragment is not affected. On the other hand, treatment with iodoacetamide results in the inhibition of the production of this fragment, indicating a role played by cysteine proteases in this processing step (Fig. 4. 29A, B). Thus, it is possible that other proteases, such as those from the cysteine protease group, also participate in the production of this fragment and are simultaneously activated by Ca^{2+} influx.

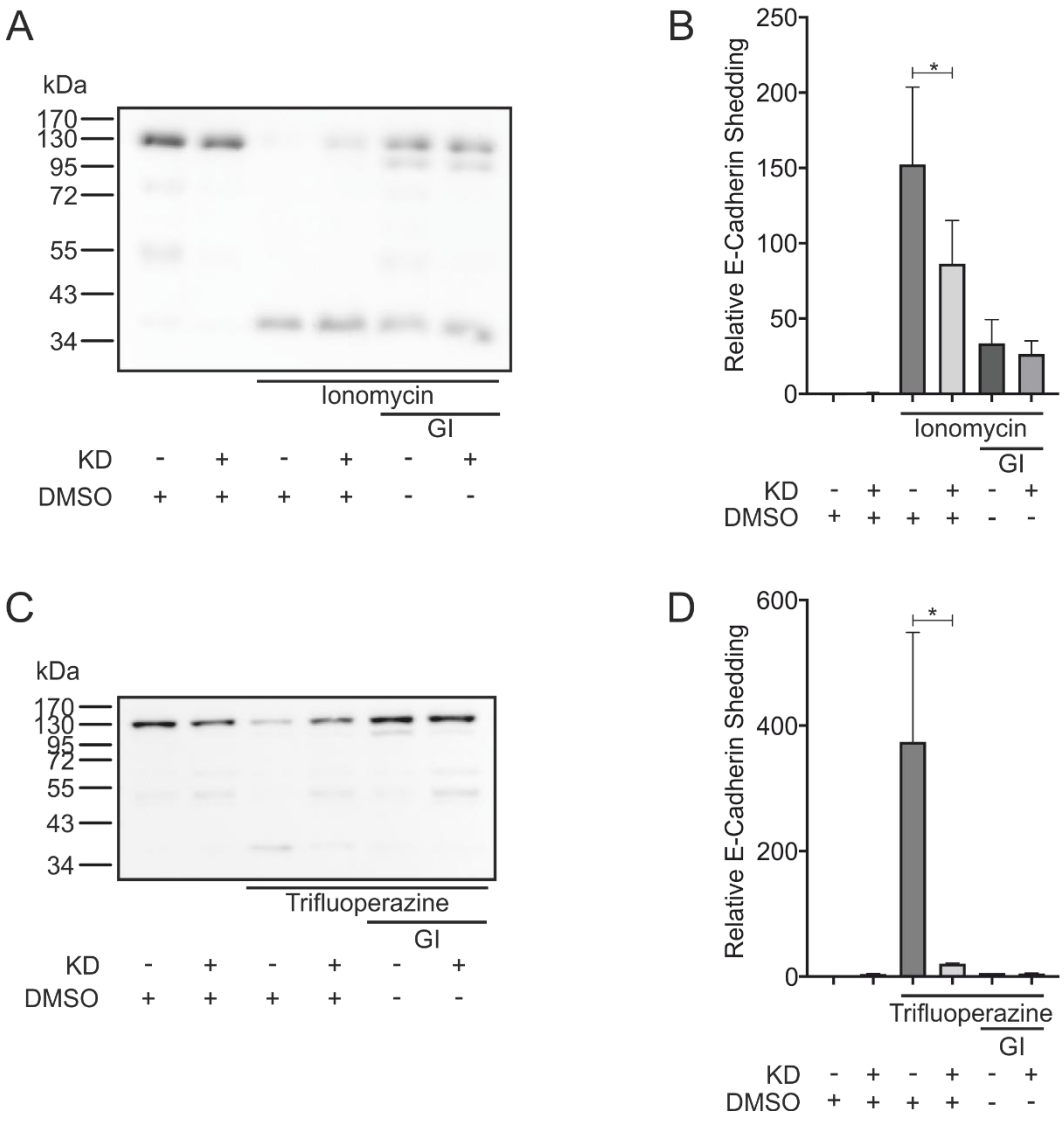

Figure 4.28. Ionomycin and trifluoperazine-mediated E-cadherin cleavage shows participation of ADAM10.

A, C: A549 cells were transduced with lentiviral particles expressing shRNA against ADAM10 or scramble shRNA as control. Transduced cells were seeded on 6 well plates and grown until confluence, starved overnight with medium containing 0.5% FCS followed by further starving in medium containing 0%FCS for 1 h. 30 min before stimulation, cells were incubated with 10 µM GI or 0.1% DMSO (vehicle control), followed by stimulation with 10 µM ionomycin, 100 µM trifluoperazine or 0,1% DMSO as vehicle control for 1 h. Subsequently, cells were lysed and lysates were afterwards subjected to a Western blot against a c-terminal E-cadherin antibody and α-tubulin as a loading control. Bands were quantified via densitometry and graphed as ratio of CTF to FL in B and D. Quantitative data are shown as mean + SD. Statistical analysis was performed with a one sample t-test. Asterisks with no connecting line represent differences with control group (* $p < 0.05$).

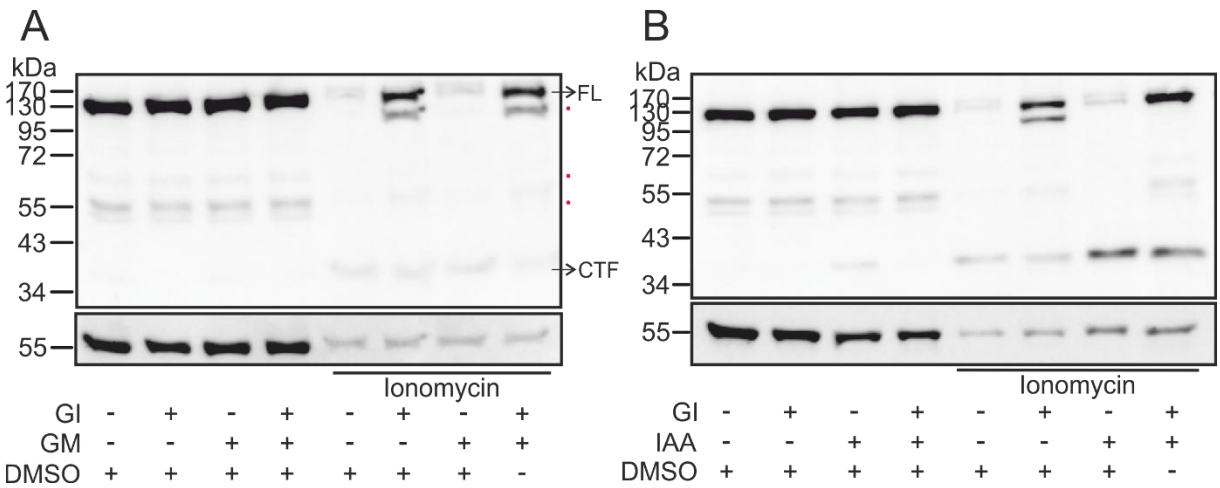

Figure 4.29. Generation of 100 kDa fragment is dependent on cysteine proteases.

A549 cells were seeded on 6-well plates, grown until confluence and starved with medium containing 0,5% FCS. Afterwards, cells were further starved with medium containing 0% FCS media for 1 h before incubating with 10 µM GI, GM6001 (GM) (A) or iodoacetamide (IAA) (B) or 0.1% DMSO (vehicle control) for 30 min and then stimulated with 10 µM ionomycin or 0,1% DMSO for 1 h. Subsequently, cells were lysed and lysates were afterwards subjected to a Western blot against a C-terminal E-cadherin antibody and α-tubulin as a loading control.

4.2.3 ADAM10 generates a 36 KDa fragment from E-cadherin

To verify the generation of the described fragments, a tagged version of E-cadherin was constructed with an HA epitope at the N-terminus (positioned C-terminal to the pro-peptide to prevent tag loss during signal peptide cleavage) and a V5 epitope at the C-terminal tail. This construct was inserted into a plasmid containing an IRES-GFP cassette using a muta-PCR approach. Subsequently, A549 cells were transfected with this construct and stimulated with ionomycin, thapsigargin and trifluoperazine to confirm the C-terminal cleavage of E-cadherin by ADAM10.

As observed on the blot after incubating with a V5 antibody, the 36kDa fragment observed in previous experiments can be observed in this tagged construct as well, confirming the C-terminal processing of E-cadherin by ADAM10 (Fig. 4. 30). However, a possible sequential processing step preceding the generation of the C-terminal fragment was questioned. Therefore, constructs containing an HA epitope tag between the N-terminal cadherin repeats of E-cadherin were generated and transfected into A549 cells. After inhibiting ADAM10's activity with GI, basal activity of ADAM10 on the N-terminus of E-cadherin was measured by quantifying the HA bands generated.

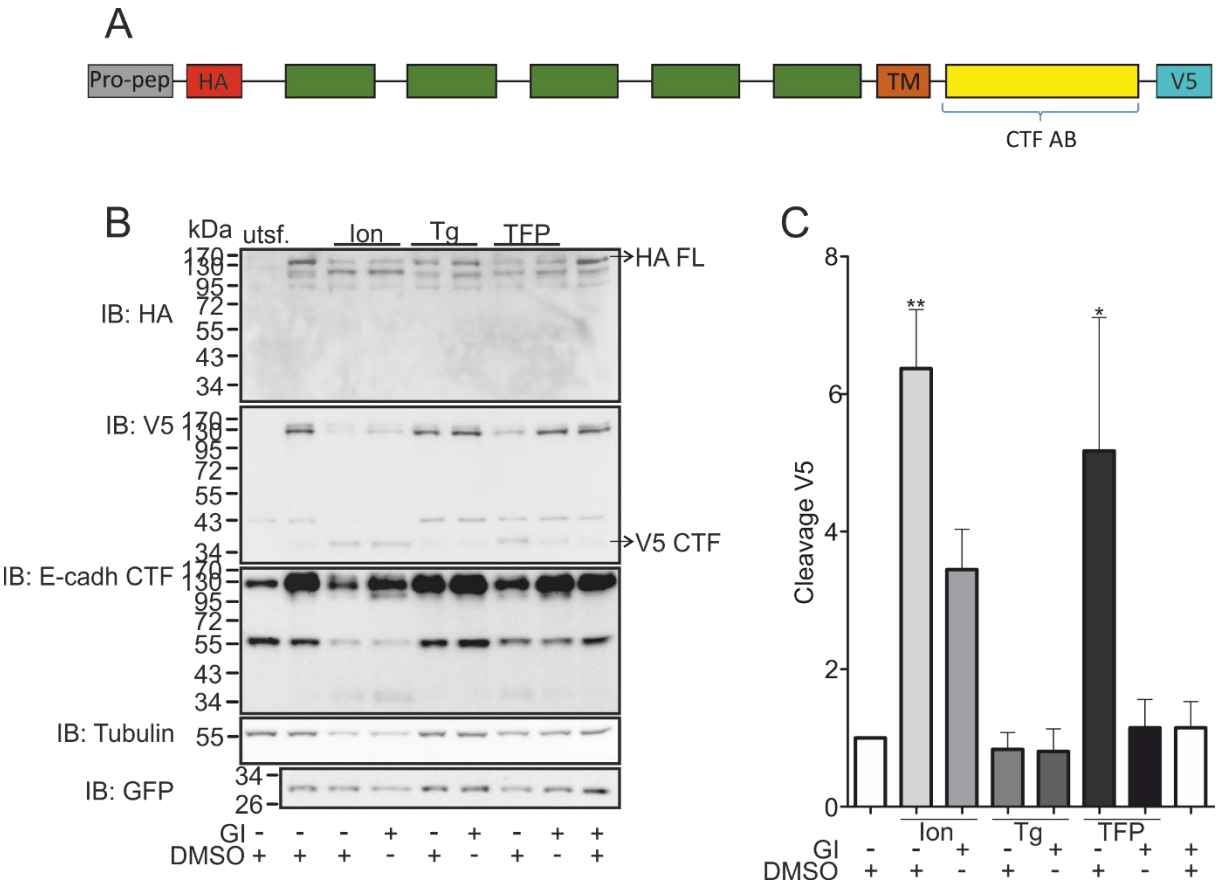

Figure 4.30. 36 kDa fragment corresponds to C-terminal fragment of E-cadherin and is mediated by ADAM10.

A: Scheme of the end product for the transfected tagged version of E-cadherin. Pro-pep: pro-peptide; TM: transmembrane domain. B: A549 cells were seeded on 6-well plates, grown until confluence and starved with medium containing 0.5% FCS and transfected with a tagged version of E-cadherin overnight. Afterwards, cells were further starved with medium containing 0% FCS for 1 h before incubating with 10 µM GI or 0.1% DMSO (vehicle control) for 30 min, followed by a stimulation with 10 µM ionomycin, 1 µM thapsigargin, 100 µM trifluoperazine or 0.1% DMSO for 30 min. Subsequently, cells were lysed and lysates were afterwards subjected to a Western blot against a C-terminal E-cadherin antibody, an α-tubulin as a loading control, an HA antibody, a V5 antibody and a GFP antibody as a control for transfection. Bands were quantified via densitometry and graphed as ratio of V5 CTF to HA full-length in after normalization to loading control C. Quantitative data are shown as mean + SD. Data were normalized to first transfected lane and to GFP. Statistical analysis was performed with a one sample t-test. Asterisks with no connecting line represent differences with control group (* $p < 0.05$, ** $p < 0.01$).

A comparison of the constitutive generation of the HA-tagged fragment with and without the usage of the ADAM10 inhibitor revealed that there is no significant change among constructs in the generation of the 90kDa fragment. Therefore, an N-terminal processing of E-cadherin by ADAM10 seemed unlikely under these conditions (Fig. 4. 31).

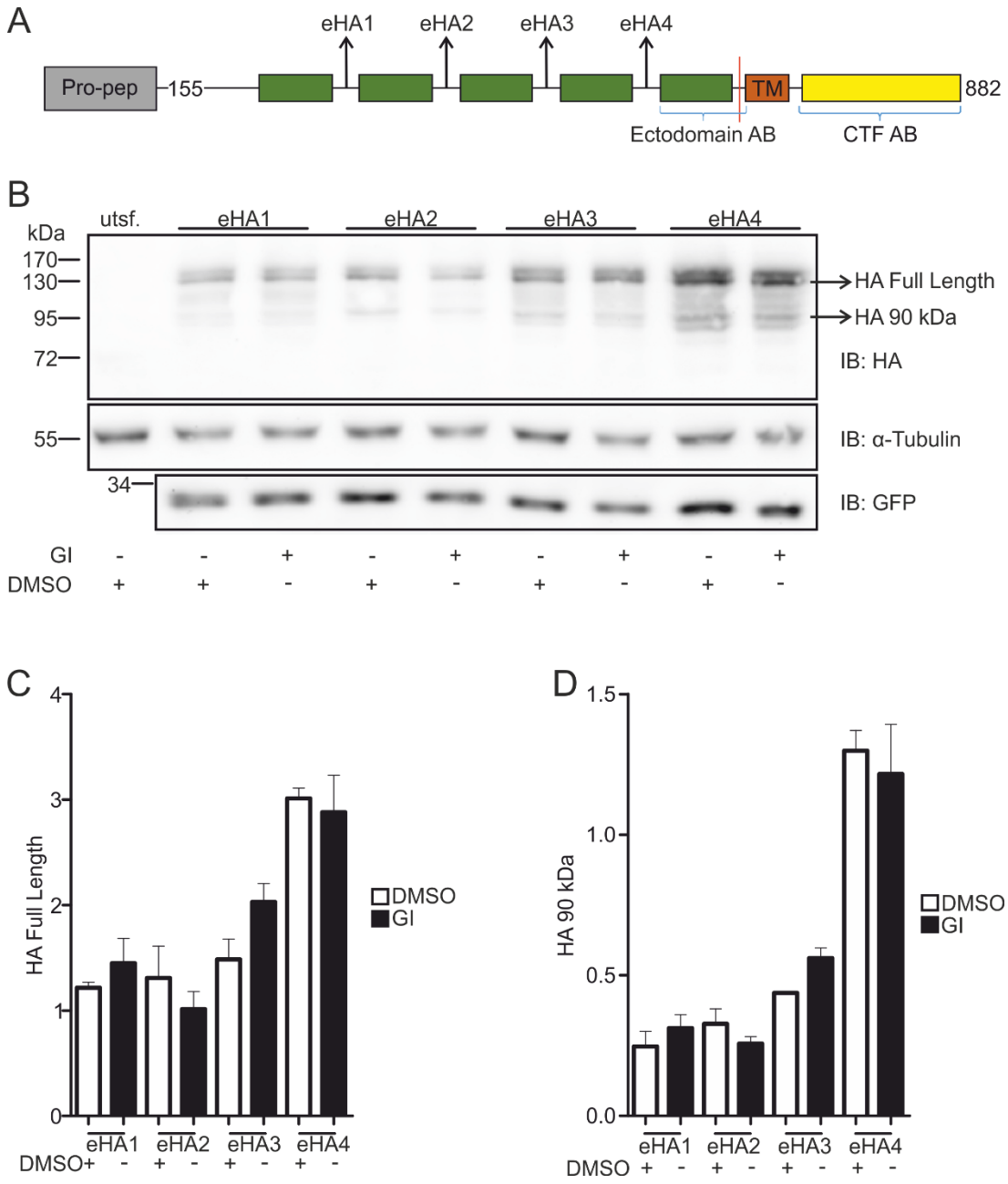

Figure 4.31. Additional fragments of E-cadherin are not dependent on activity of ADAM10.

A: Scheme of the end product for the transfected HA-tagged versions of E-cadherin. Pro-pep: pro-peptide; TM: transmembrane domain. B: A549 cells were seeded on 6-well plates, grown until confluence, starved with medium containing 0.5% FCS media and transfected with tagged versions of E-cadherin overnight. Afterwards, cells were further starved with medium containing 0% FCS before incubating with 10 µM GI or 0.1% DMSO for 30 min. Subsequently, cells were lysed and lysates were afterwards subjected to a Western blot against an HA antibody, an α-tubulin as a loading control and a GFP antibody as a control for transfection. Marked bands were quantified via densitometry and graphed in C and D. Quantitative data are shown as mean + SD. Data were normalized to GFP. Statistical analysis was performed with a one sample t-test. Asterisks with no connecting line represent differences with control group (* $p < 0.05$, ** $p < 0.01$).

4.3 Calcium-related events from *P. aeruginosa* on ADAM10 activity

To assess the effects on ADAM10 activity following natural stimuli or under pathophysiological conditions, experiments were performed after infection with the opportunistic, Gram-negative bacteria P. aeruginosa. Stimulation with a natural stimulus is intended to provide a contrast to the artificial stimulations observed previously with chemical reagents such as ionomycin, trifluoperazine, or ophiobolin A. At first glance, the expression of ADAM10 after 4 h of infection with P. aeruginosa was investigated via Western blot. Additionally, the role played by the PQS quorum sensing system, responsible for the production of virulence factors like proteases, toxins and biofilm formation components (Chadha, Harjai and Chhibber, 2021), was assessed through its blockage via the inhibition of the PqsR enzyme with two different PQS inhibitors, 1635 and 2050, applied directly to the bacteria. Given that the production of several of these virulence factors typically occurs at the end of the bacterial growth curve and is therefore considered a secondary metabolite, different times of inhibition were applied, including together with the infection, 30 min before infecting cells and overnight (12 h before infection).

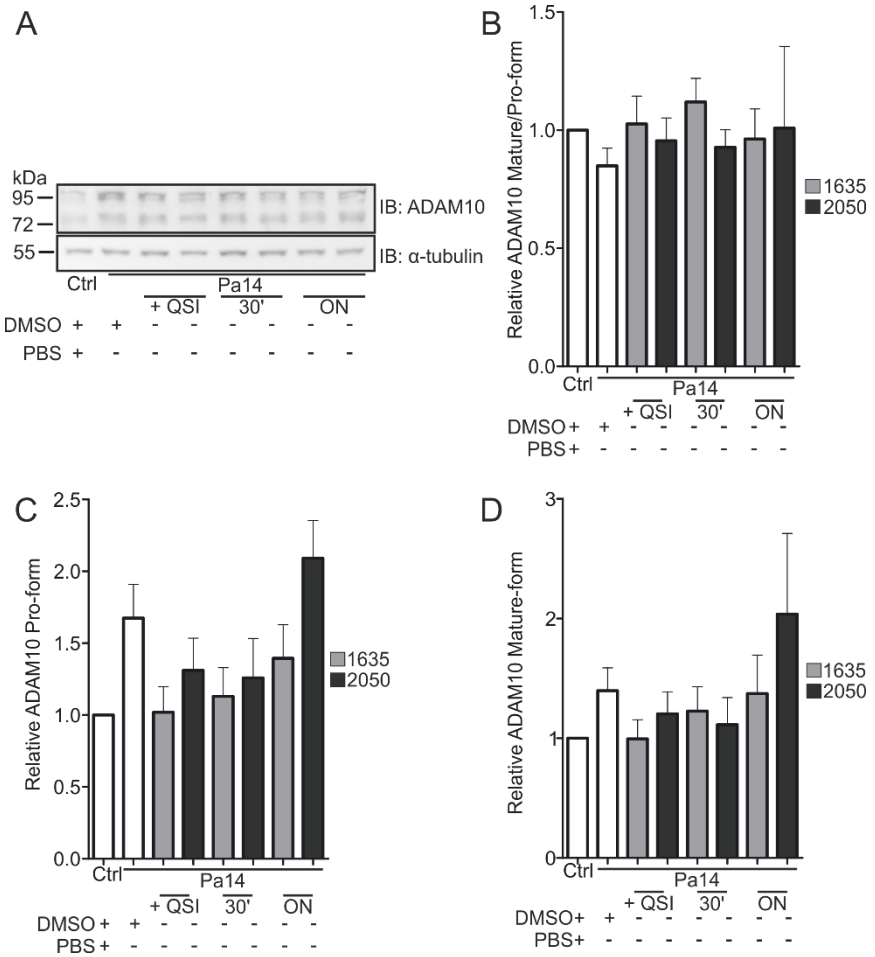

Figure 4.32. Infection of A549 with *P. aeruginosa* does not affect expression of ADAM10.

A549 cells were seeded on 6-well plates, grown until confluence and starved with medium containing 0.5% FCS media overnight. Afterwards, cells were further starved with medium containing 0% FCS for 1 h. Cells were incubated with 20 µM 1635 and 2050 quorum sensing inhibitors or 0.1% DMSO (vehicle control) for 30 min, followed by an infection with *Pseudomonas aeruginosa* 14 that was previously incubated with 1635 or 2050 at same time of infection, 30 min prior to infection or overnight (12 h prior to infection) in a multiplicity of infection (MOI) of 2.5 or PBS as vehicle control for 4 h. Subsequently, cells were lysed and lysates were afterwards subjected to a Western blot against a C-terminal ADAM10 antibody and α-tubulin as a loading control. Bands were quantified via densitometry. Quantitative data are shown as mean + SD. Data were normalized to first lane. Statistical analysis was performed with a one sample t-test.

No changes in the expression of both pro-form or mature form could be observed, neither did any significant change in the mature to pro-form ratio of ADAM10 could be observed (Fig. 4. 32). Despite these results, an activity increase cannot be discarded since it has been observed in previous results that an increased expression of ADAM10 might not necessarily mediate an activity increase (Fig 4. 11; Fig. 4. 21).

4.3.1 P. aeruginosa infection promotes ADAM10 activity

Although no change in ADAM10 expression was observed, significant changes in protease activation could still occur, as a change in activity is not necessarily paired with increased expression. Therefore, AP assays in these same conditions were performed. A P. aeruginosa mutant incapable of producing pyocyanin was also utilized. Pyocianin is an important virulence factor produced by the PQS pathway capable of acting as a reactive oxygen species generator, thus promoting oxidative stress in the host and increasing infectivity (Abdelaziz et al., 2023).

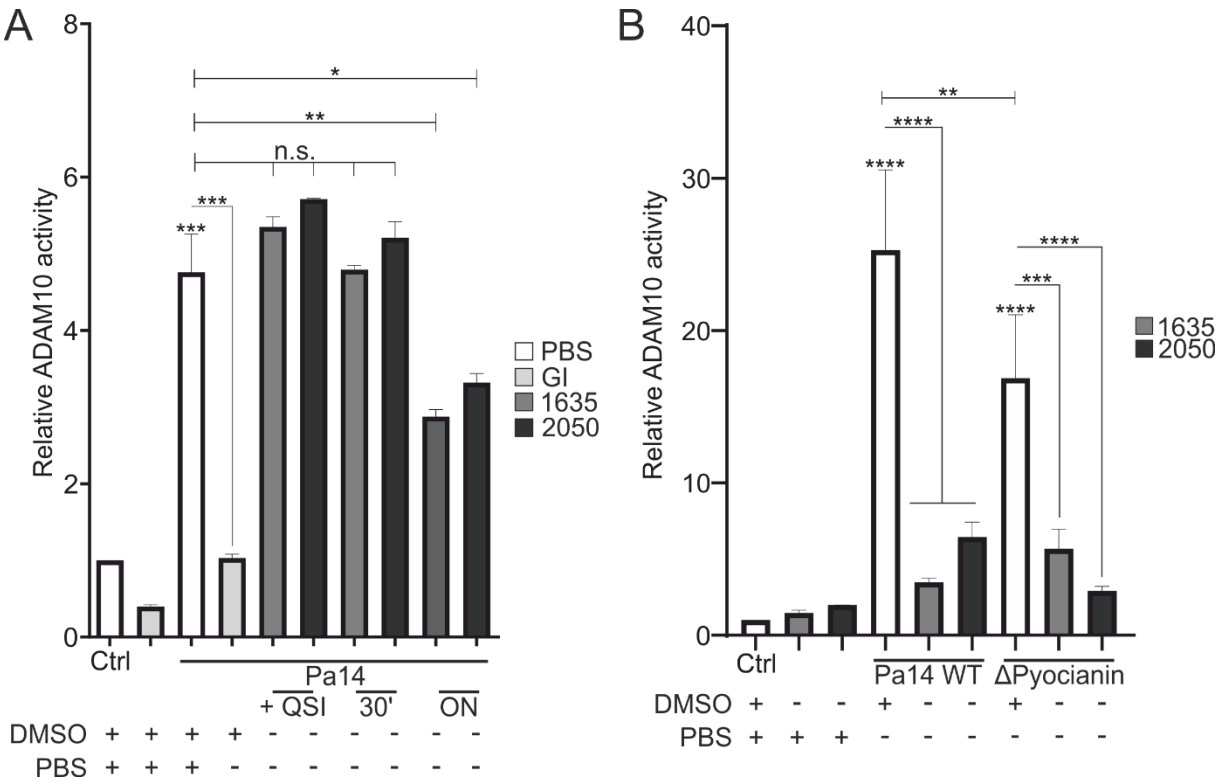

Figure 4.33. Activity increase of ADAM10 by *P. aeruginosa* infection is inhibited by pretreatment with PQS inhibitors.

A549 cells were transfected with AP-BTC overnight. Afterwards, cells were seeded on 6-well plates, grown until confluence and starved with medium containing 0.5% FCS overnight before further starving with medium containing 0% FCS and incubating with 10 µM GI, 20 µM 1635, 2050 quorum sensing inhibitors or 0.1% DMSO (vehicle control) for 30 min and then infected with *P. aeruginosa* 14 or *P. aeruginosa* 14 without Pyocianin expression (B) that were previously incubated with 1635 or 2050 at same time of infection, 30 min prior to infection or overnight (12 h prior to infection) in a multiplicity of infection of 2.5 or PBS as vehicle control for 4 h. Subsequently AP activity from supernatant and cell lysates was measured. Quantitative data are shown as mean + SD. Data were normalized to first lane. Statistical analysis was performed with a one sample t-test. Asterisks with no connecting line represent differences with control and those with lines represent differences among groups (* $p < 0.05$, ** $p < 0.01$, *** $p < 0.001$).

A significant increase in ADAM10 activity was observed after 4 hours of infection with P. aeruginosa. This activity increase was simultaneously impaired when using the ADAM10 inhibitor GI, thus underlining the role played by ADAM10 in this process and additionally, increasing the incubation time with the quorum sensing inhibitors 1635 and 2050 halves the promoted activity of P. aeruginosa, mainly when incubated overnight, showing an increased inhibiting activity over time (Fig. 4. 33A). Furthermore, infection with a pyocyanin mutant of P. aeruginosa did not wholly ablate the increased activity of WT Pseudomonas, as observed by the activity of both WT and mutant strains when inhibited with PQS inhibitors (Fig. 4. 33B). A feasible explanation is the existence of additional virulence factors that promote the activity of ADAM10, which are also related to the PQS quorum sensing machinery.

4.3.2 P. aeruginosa infection shows an overtime Ca^{2+} entry

Other virulence factors from P. aeruginosa could also be related to both Ca^{2+} entry and the orchestration of infection. Therefore, Ca^{2+} imaging measurements were performed with the online addition of bacterial particles that have been incubated with 1635 and 2050 quorum sensing inhibitors. The measurements were performed after the bacteria was grown for 3 h with a culture starting at an 0D600 of 0.05.

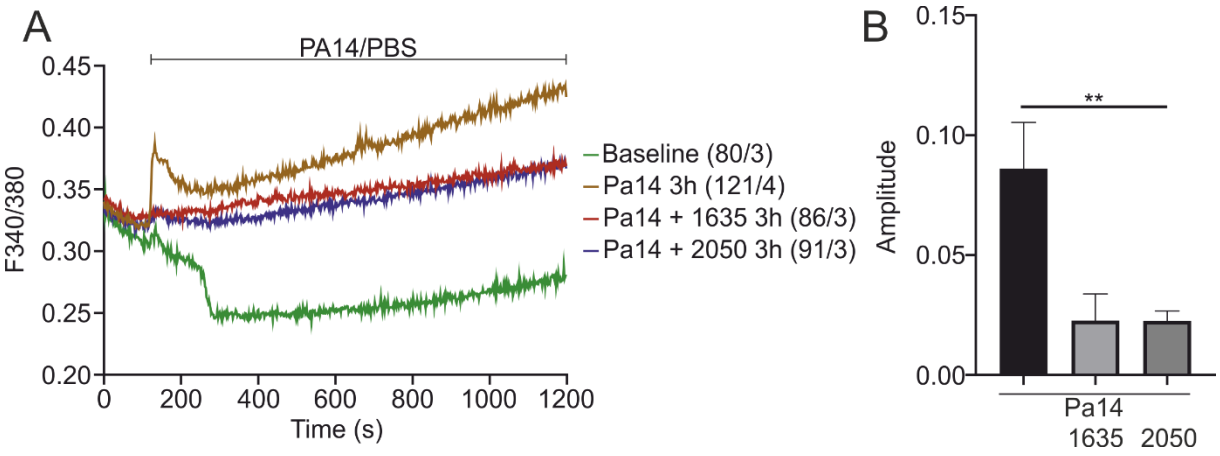

Figure 4.34. Infection with *P. aeruginosa* pretreated with PQS inhibitors abrogates Ca^{2+} influx promoted by infection.

A: A549 cells were seeded and grown to a 70% confluence on 6-well plates containing previously poly-L-Lysine coated coverslips. Cells were then loaded with 4 µM Fura2-AM for 30 min. Calcium imaging experiments were performed with addition of $4{,}6*10^7$ CFUs of *P. aeruginosa* 14 with and without pretreatment with PQS inhibitors 1635 or 2050 or PBS after 2 min of baseline reading. B: Amplitude as difference between peak and lowest value between 118 and 300 s was calculated and plotted. Quantitative data are shown as mean + SD. Statistical analysis was performed with a one sample t-test. Asterisks or numerals with no connecting line represent differences with control and those with lines represent differences among groups (* $p < 0.05$, ** $p < 0.01$).

The sole bacterial particle was already capable of promoting a Ca^{2+} influx that could be translated to an eventual activation of ADAM10. Additionally, this activity is related to the production of PQS-derived virulence factors since the treatment of P. aeruginosa with both PQS inhibitors completely ablated the Ca^{2+} entry (Fig. 4. 34).

5 Discussion

This thesis investigates whether specific Ca^{2+} concentrations are sufficient to activate ADAM10 and whether this activation depends solely on these conditions or also requires time to reach significant activity levels. Additionally, the role played by additional membrane-unbounded forms, as well as the influence of Ca^{2+} entry through specific entry points, such as certain members of the TRP channels or after SOCE promotion, was also investigated. Finally, the role played by natural stimuli, such as infection with *P. aeruginosa* and its prominent quorum sensing (QS) communication system, in coordination with Ca^{2+} entry, was also investigated. It was observed that specific concentrations of ionomycin would promote Ca^{2+} entry, serving as a threshold for the activation of ADAM10 in a time-independent manner. Ca^{2+} proved to be necessary for the release of mature ADAM10 in exosomes, although increased activation is observed at 1 h, while CaM inhibition seems to evoke faster activation responses. Furthermore, Ca^{2+} entry through specific members, such as the canonical members of the TRP channels, would specifically activate ADAM10, while entry through others, like TRPM3, would not.

The importance of ADAM10 in various diseases and conditions has been reported in several studies. For example, a protective effect promoted by the α-secretase activity of ADAM10 in AD has been observed *in vivo* (Guo *et al.*, 2019; Rangasamy *et al.*, 2023). Given the importance of ADAM proteases for normal physiological functions and developmental processes, it is challenging to directly attenuate or increase their activity, as such a treatment would likely affect normal physiological functions related to signaling and housekeeping. The importance of ADAM10 and ADAM17 is reflected in the fact that their knockout *in vivo* has lethal consequences (Peschon *et al.*, 1998; Zhang *et al.*, 2010). Ca^{2+}-dependent regulation of ADAM10. For these reasons, a better understanding of this protease is paramount to better target it in the context of further translational studies.

5.1.1 Differential effect on ADAM10 by Ca^{2+} related agonists

Activation of ADAM10 and ADAM17 by Ca^{2+} entry elicited by ionophores have been related to the scramblase function of Ca^{2+}-activated Cl^- channels known as anoctamins (Leitzke *et al.*, 2022). Researchers have also found that this effect can occur as a product of ionophore stimulation. In particular, ADAM10 activation was correlated with the externalization of PE to the outer leaflet of the cellular membrane and its association with a positively charged stalk region of ADAM10 (Bleibaum *et al.*, 2019), however, most experiments performed in these studies were conducted under the influence of a unique concentration of ionomycin and do not assess the effect of a concentration modulation. Furthermore, although the use of an ionophore appears to promote an increase in Ca^{2+}, few studies have followed up on this effect by measuring Ca^{2+} levels in conjunction with the rise in ADAM activity. On the other hand, the effect elicited by trifluoperazine, a known CaM inhibitor, on the action of ADAM10 has been associated with the dissociation of CaM from a CaMBD located in the C-terminal tail of the protease (Nagano *et al.*, 2004). It has been proposed that Ca^{2+} influx would provoke the dissociation of CaM from ADAM10, given that it has a lesser affinity for it (Reboud *et al.*, 2017). In these studies, the concentration of trifluoperazine was similar to the concentration used in the current work. It is also essential to consider that the CaMBD on ADAM10 is of the IQ type, which is Ca^{2+}-independent, where one would find CaM binding without the participation of Ca^{2+} ions (Horiuchi *et al.*, 2007). These studies did not mention any additional effect that the dissociation might have elicited from one of the many other interacting proteins of CaM. In spite of the possibility of a multicausal effect by trifluoperazine on the activity of ADAM10 almost no further studies assessing ADAM10s' activity have been performed with additional CaM inhibitors like ophiobolin A. An increase in ADAM10 activity has been observed in this work after CaM inhibition with this compound. Thus, a role played by CaM on the activity promotion of ADAM10 seems more feasible.

Some reports have already proposed that the presence of extracellular Ca^{2+} is a prerequisite for particular cleavage by ADAMs, as well as under specific stimulation conditions, such as the use of ionomycin. For example, an ionomycin-induced cleavage of E-cadherin has been shown to become ablated when depleting Ca^{2+} from extracellular media (Ito *et al.*, 1999). On the other hand, BAPTA-AM mediated chelation of intracellular Ca^{2+} together with the depletion of extracellular Ca^{2+} completely inhibited the cleavage of TNFR by ADAM10 after diosgenin stimulation (Yang et al., 2017), while BAPTA-AM chelation of intracellular Ca^{2+} appeared to not affect E-cadherin or AP-BTC cleavage by ADAM10 in this study, pointing towards a requirement for extracellular Ca^{2+} ions for ADAM10 activation. In another study, cleavage of TLR4 was also inhibited by treatment with BAPTA-AM but not by the depletion of extracellular Ca^{2+} after treatment with EGCG, after which extracellular Ca^{2+} influx, as well as intracellular store efflux, was observed (Baek *et al.*, 2019). Thus, it is possible that specific treatments, differing in their Ca^{2+} response, may exhibit differential effects on the activation of ADAM proteases. This might also be related to a differential substrate sensitivity towards ADAM10-mediated cleavage.

The distinction of the origin of the Ca^{2+} transients that elicit an activity increase has rarely been made. To elucidate whether passive efflux from intracellular stores is involved, the activity of ADAM10 was tested after thapsigargin stimulation, which inhibits SERCA. For instance, prolonged incubation times (24 h) with 300 nM thapsigargin were used in a study to assess ADAM17 activity. Although this investigation did correlate a thapsigargin stimulation with an increased expression and activity of ADAM17, the effect was related to the unfolded protein response elicited by the compounds given the more extended times of incubation (Rzymski *et al.*, 2012). In another study, thapsigargin stimulation failed to show an activity increase of ADAM17 on HER4-JM-a in contrast to the agonism exhibited by PMA on ADAM17(Rio *et al.*, 2000). Similar longer incubations with thapsigargin were performed to assess RAGE shedding by ADAM10 but instead failed to elicit any response, although such a cleavage was indeed observed after TNF-α stimulation (Miyoshi *et al.*, 2019), thus setting a contrast with the agonism of longer thapsigargin incubations on ADAM17 and ADAM10. This might be explained through the generation of reactive oxygen species as a product of an ER-stress response onto ADAM17 (Rzymski *et al.*, 2012). Since the focus of the present work was to assess the response of ADAM10 to Ca^{2+} transients, shorter incubation times were used to determine ADAM10 activity, given that 1 h is more than enough to observe a Ca^{2+} increase as observed in the calcium imaging experiments. Still, as in the studies mentioned earlier, thapsigargin and a consequent passive efflux of Ca^{2+} from intracellular stores did not lead to an increase in ADAM10 activity. Since the Ca^{2+} levels reached in this experiment do not reach those with ionomycin, it is possible that the Ca^{2+} concentration did not reach the necessary threshold levels to promote ADAM10s' action, whenever there is an incubation with thapsigargin.

A further aspect that has not been thoroughly investigated is the time dependency of these compounds, as most studies use both unique times and concentrations for their experiments. For example, Romero et al., 2020 use times of ionomycin stimulation from only 45 minutes, other studies like Dang et al., 2011 present more than just one time point at 5, 15 and 30 min; although it has been observed in this work that even shorter times already elicit strong activations of ADAM10 with specific concentrations since only 1 min showed a substantial activity increase with concentrations higher than 0.6 µM. Still, in general, most studies have a set time of not more than 1 h (Schulz *et al.*, 2008; Herzog *et al.*, 2014; Maretzky *et al.*, 2015). Although different concentrations have been used for trifluoperazine and ionomycin, the Ca^{2+} entry aspect elicited by the content of these reagents has rarely been investigated. As for the stimulation with trifluoperazine, different times of stimulation with this reagent have been tested in Anders et al., 2006 regarding its agonism on ADAM10, which is not only time-dependent but also dose-dependent, as evidenced by the cleavage of a receptor protein tyrosine

phosphatase. Taken together, these findings highlight that ADAM10 activation is not only concentration-dependent but also tightly regulated by stimulation time, suggesting that both parameters must be considered when interpreting activation dynamics. This time dependency provides the basis for investigating whether specific Ca^{2+} concentration thresholds further modulate ADAM10 activity.

5.1.2 Ca^{2+} concentration threshold on ADAM10 activation

It has been shown that trifluoperazine by itself promotes the efflux of Ca^{2+} from internal stores through the disinhibition of IP_3R and the agonism on RyR (Qin *et al.*, 2009; Kang *et al.*, 2017). As both are CaM inhibitors, ophiobolin A is expected to elicit a similar response. This is seen in Ca^{2+} measurements with 100 µM trifluoperazine in the absence of extracellular Ca^{2+}, where a steady increase occurs. However, unlike the transient rise triggered by thapsigargin, this sustained elevation may be nonspecific—especially given the use of EGTA, which depletes extracellular Ca^{2+}. Additionally, the Ca^{2+} increase promoted by ophiobolin A was not as high as that with trifluoperazine, although it remained steady throughout the measurement. On the other hand, this effect has been reported by Kang et al., 2017 with the use of the same concentration. However, in this study, previous stimulation with thapsigargin and depletion of internal stores ablated the Ca^{2+} increase in the measurements, suggesting that there might be some differences between the U87MG glioblastoma cells and the A549 cells. It is, therefore, possible that this elicited cleavage might be independent of Ca^{2+} and have a more direct interaction with CaM inhibition.

Given recent advances in the field, where it has been proven that Ca^{2+}, as a secondary messenger, acts in a time- and space restricted manner (Pinton *et al.*, 2008; Mulier, Vriens and Voets, 2017; Barak and Parekh, 2020a) and that different concentrations of certain ionophores like ionomycin elicit different effects, the regulation of ADAM10's activity by Ca^{2+} signaling grows in importance. A lower concentration of ionomycin of 1 µM promoted the release from internal stores without eliciting an apoptotic response, whereas higher concentrations of ionomycin (10 µM) showed a biphasic Ca^{2+} increase accompanied by an apoptotic effect (Gutiérrez *et al.*, 1999). Such a biphasic increase has been confirmed in this study when stimulating with 10 µM ionomycin, but not with lower concentrations, where it is most likely that, at least initially, a depletion of intracellular stores is taking place. Since the majority of studies where ionomycin has been used as a promoter of ADAM10 activity involved a fixed concentration of the reagent, it was necessary to assess the differential effect of a range of concentrations together with Ca^{2+} measurements. For instance, 1 µM ionomycin was enough to promote the cleavage of IL-1R by ADAM10 after incubation with GI (Lokau and Garbers, 2021). 1 µM and 2.5 µM ionomycin were also used to promote the cleavage of programmed death ligand 1 (PD-L1) and 2.5 µM ionomycin also increased the activity of ADAM10 on HB-EGF in MEF cells (Dang *et al.*, 2011). Although these studies did not assess ranges of concentrations, particularly those involving concentrations lower than 1 µM, they all confirm an increased activity with ranges of concentration between 1 µM and 2.5 µM, as seen in this thesis. An AP assay with an HB-EGF-AP substrate performed involved a concentration range of 0.1 µM to 1 µM ionomycin, with and without the presence of EGTA (Dethlefsen *et al.*, 1998). As observed in this work, the activity of ADAM10 exhibits a dose-dependent response even at these lower concentrations. However, no Ca^{2+} measurements were performed to confirm the presence of an increase in intracellular Ca^{2+} since it has been observed that 0.1 µM ionomycin does not promote a Ca^{2+} increase. The use of EGTA confirms the necessity for the presence of extracellular Ca^{2+} in the ionomycin-promoted increase in ADAM10 activity. Throughout the literature, various substrates have been used to assess the activities of ADAMs, and it is known that the specificity of different metalloproteinases to their substrates varies. For instance, cleavage of the homotypic cell-cell adhesion molecule cadherin-11, as well as a cleavage of N-cadherin by ADAM10, was observed after stimulation with 5 µM ionomycin for 1 h and 30 min (Uemura *et al.*, 2006; Noss *et*

al., 2015). It is worth mentioning that E-cadherin and N-cadherin share a high degree of homology (97.82% when aligned with Uniprot.org). The sole difference in their topology being that E-cadherin binds to the short isoform of p120 catenin, while N-cadherin binds to the larger one. Cleavage of E-cadherin in contrasting conditions of Ca^{2+} presence and absence was observed and attributed to ADAM10 (Ito *et al.*, 1999). Interestingly, an elevated concentration of 10 µM ionomycin was used, but with shorter times of 10 min, which exhibited a faster activation. However, in this thesis, a significantly faster activation of 1 min has also been observed. Additionally, presence or absence was achieved with the nominal addition of 2 mM $CaCl_2$ in TBS. However, a trend of E-cadherin cleavage was observed at a much lower extracellular Ca^{2+} concentration, starting with 0.1 mM $CaCl_2$. Regarding the Ca^{2+} concentration levels obtained during the ionomycin calibration curve, resting Ca^{2+} levels for A549 cells is 64,7 ± 2,5 nM (Padar *et al.*, 2004) which is close to the data obtained from the present study where the Ca^{2+} concentration calculated from the baseline (in this case 0.1 µM ionomycin) was 59.3 ± 2.9 nM.

Studies on further regulatory processes for ADAMs expression and subsequent activity are needed to gain a deeper understanding of the regulation of these proteins' activity at different levels. Such advancements would allow for the development of translational therapies that indirectly ascertain effects on ADAMs proteases, potentially resulting in fewer undesirable side effects. On that note, a time- and threshold-dependent Ca^{2+} entry for ADAMs activation, as well as a correlation between protease activity and specific Ca^{2+} entry points, represents a new regulatory stage in an already intricately and strongly regulated protease, not only at the expression level but also in its activity. Furthermore, new insights may be gained from assessing the activation of specific proteases by Ca^{2+} effectors, not only for proteases that have already shown such activation, like ADAM10, but also for others where these effects might not be as easily noticeable and may instead be related to the activity of soluble or exosome-related forms, such as ADAM8. In summary, the evidence indicates that ADAM10 activation is not only sensitive to ionomycin concentration and extracellular Ca^{2+} availability, but also to substrate specificity, underscoring the complexity of its regulation. This concentration- and substrate-dependent regulation provides a logical transition to the next section, which focuses on how Ca^{2+} influx and CaM inhibition differentially influence the release and soluble activity of ADAM10.

5.1.3 Soluble activity and release of ADAM10 is differentially regulated by Ca^{2+} influx and CaM inhibition

ADAM10 is released not only in exosomes, enabling trans activity (Aljohmani *et al.*, 2022), but also as a catalytically active soluble form with distinct cleavage specificity compared to its membrane-bound counterpart (Tousseyn *et al.*, 2009; Scharfenberg *et al.*, 2020). Several studies have correlated prolonged Ca^{2+} influx responses with an elevated release of exosomes. Indeed, in this work, longer incubation times with ionomycin did elicit the release of ADAM10-containing exosomes. However, it is unclear whether the activity observed in the FRET assays also includes the action of soluble forms, particularly considering that their release is typically dependent on the action of other proteases that might be indirectly activated via stimulation with ionomycin or CaM inhibition with trifluoperazine (Scharfenberg *et al.*, 2020). A direct correlation between exosome release and calcium-dependent events has been shown for some cells (Savina *et al.*, 2003). For example, a Ca^{2+}-dependent SNAP receptor is required for membrane fusion in cancer cells, as depletion of Munc13-4, a SNAP protein, led to reduced size CD63+ multivesicular bodies in breast cancer cells. On the other hand, the permeabilization of cellular membranes may lead to their repair and further activation of Ca^{2+}-dependent plasmatic membrane proteins, such as Annexin 6, which has been shown to participate in this process (Williams et al., 2023). The dependency of ADAMs' release in exosomes on intracellular Ca^{2+} is further supported by a study in which the use of BAPTA-AM prevented exosomal ADAM17

release in A549 cells (Groth *et al.*, 2016b). These effects likely result from prolonged incubation with a Ca^{2+} ionophore like ionomycin, as shown in this study, which observed both increased ADAM10 activity and elevated levels of ADAM10-containing exosomes. In this case, an increased expression of the tetraspanin CD9 is also observed in released exosomes. It is known that several subtypes of tetraspanins can interact with ADAM and consequently alter its substrate specificity, encompassing an additional level of regulation of these proteases (Harrison, Koo and Tomlinson, 2021). Particularly, the tetraspanin CD9 has also been observed to co-localize and thus regulate ADAM10's activity (Arduise *et al.*, 2008; Lu *et al.*, 2020). Although an ablation of exosome release after SOCE inhibition with YM58483 as well as with use of siRNA against STIM1 and Orai1 in breast cancer cells was reported(Didiasova *et al.*, 2015), stimulation with thapsigargin and a subsequent depletion of intracellular stores did not promote any activity of any ADAM10 form, membrane unbounded ones included. A recent study highlighting the significance of calcium/calmodulin-dependent kinase 1 (CAMK1) in the AMP-activated protein kinase (AMPK) signaling pathway and its subsequent attenuation of lipid accumulation found that lipid accumulation increased after CAMK1 knockdown (Yang *et al.*, 2023). However, it is unclear whether inhibiting CaM and inducing lipid accumulation would result in increased exosome secretion, especially at faster rates, as observed in this work with shorter incubation times using trifluoperazine. Altogether, these findings suggest that ADAM10 release, whether as exosomal or soluble forms, is shaped by the interplay of Ca^{2+} influx and CaM inhibition, which adds another dimension to the regulation of its proteolytic activity. Building on this, it becomes essential to explore how the spatial localization of Ca^{2+} entry sites further refines ADAM10 activation, which is addressed in the next section.

5.1.4 Microdomain localization of Ca^{2+} entry points on ADAM10 activity

Due to the increase of activity after treatment with Ca^{2+} ionophores like ionomycin, it is also expected that a Ca^{2+} influx through more physiological means would also promote the activation of ADAM10. Recently, a study proposed the shedding of EGFR ligands as a feasible readout for the activation of TRP channels using a TGFα-AP cleavage approach. However, researchers failed to provide Ca^{2+} measurement data that might support the gating hypothesis of the investigated channels (Tatsumi *et al.*, 2023). Still, authors utilize a wide array of different channels agonists with a strong TGFα-AP cleavage and an AP-BTC cleavage with TRPV1 and TRPV3 but not with agonism on other channels like TRPA1, thus supporting the hypothesis stated in this work that in (patho)physiological conditions, this effect might be subjected to some sort of regulation like a spatial control. This is further supported by the premise that Ca^{2+} microdomains and transient, temporal Ca^{2+} influxes are a product of these microdomains.

To exemplify, Ca^{2+} microdomains are generated as a product of the gating of several TRP channels like TRPA1, TRPV1 and TRPV4 (Nelson *et al.*, 2013; Senning and Gordon, 2015; Sullivan *et al.*, 2015). Additionally, Ca^{2+} transients generated by CRAC complexes and ER-PM junctions were also observed (Barak and Parekh, 2020b). However, it is unlikely that such gating would activate ADAM10 in A549 cells, given that in this study, CRAC gating after internal store depletion with thapsigargin and Ca^{2+} readdition failed to promote ADAM10 activation. Following this line, the fact that some TRPC channels are found in SOCE complexes, forming heteromeric channels with Orai1 (Liao *et al.*, 2007; Sánchez-Hernández *et al.*, 2010) means that the activation observed in this work by TRPC4 and TRPC5 is not a result of gating of TRPC channels from ER-PM junctions but other membrane domains independent of the SOCE machinery. Namely, TRPC4 and TRPC5 have been found in detergent-resistant membrane fractions and to be excluded from the membrane after cholesterol depletion in platelets. It was then proposed that TRPC4 and TRPC5, together with TRPC1 might form heteromultimers in lipid rafts (Brownlow and Sage, 2005). However, an AD model has been proposed, in which the amyloidogenic processing of APP occurs in lipid rafts while the non-amyloidogenic processing occurs in low-

cholesterol zones of the membrane since ADAM10 was found to remain soluble after detergent extraction (Cordy *et al.*, 2003). This incongruence could be attributed to the differences in cell lines and models used across the various studies. However, further research is needed to investigate mechanistic studies on the activation of ADAM10 following the gating and activation of TRP channels. Additionally, the lack of co-immunoprecipitation of TRPC4 or TRPC5 with ADAM10 suggests that the interaction between these proteins is transient; therefore, further tests would need to be conducted in the presence of crosslinkers or other experimental modalities that promote a more stable interaction between these proteins. In conclusion, the regulation of ADAM10 through Ca^{2+} microdomains and TRP channel activity appears to depend on the spatial localization of these entry points and their transient interactions, underscoring the importance of membrane compartmentalization in ADAM10 activation. This spatial regulation connects directly to the following section, which examines how ADAM10 contributes to the processing of specific substrates, with a focus on E-cadherin.

5.2 Processing of E-cadherin by ADAM10 and other proteases

One of the first investigations performed on the cleavage of E-cadherin by a putative metalloproteinase was done by Ito et al., 1999, where the researchers found that the production of soluble fragments of E-cadherin was inhibited after treatment with hydroxamic acid-based metalloproteinase inhibitors BB2516 and CGS27023A in experiments using an array of different types of protease inhibitors. Since then, the processing and degradation of E-cadherin by several other proteases, both endogenous and exogenous, in patho- and physiological conditions have been investigated. It will be later that this effect would be pinpointed to the activity of ADAM10 where, as observed in this thesis, both the known ADAM10 inhibitor GI and shRNA KD of ADAM10 elicited an inhibition of the C-terminal fragment production (Maretzky *et al.*, 2005). Although Ito et al., 1999 perform an identification of the C-terminal fragment with a purification step using an agarose column followed by an automated N-terminal amino acid sequence analysis, a different focus was chosen for the current work since a tagged version of E-cadherin was produced and transfected into A549 cells. Confirmation of the C-terminal fragment generation is achieved by detecting the C-terminally tagged V5 tail using Western blot analysis.

Action on E-cadherin by cysteine proteases was observed in several studies (Steinhusen *et al.*, 2001; Yoo *et al.*, 2012; Konze *et al.*, 2014), where the generation of a 100kDa fragment is observed. Such an effect is also observed in the present work since incubation with iodoacetamide, a known cysteine protease inhibitor, abolishes the production of this fragment. Interestingly, generation of the 100kDa fragment is only observed when cells are also treated with GI, so it is possible that cysteine protease require longer times to perform their action on E-cadherin and might, therefore, have a lower affinity to substrate-cadherin than ADAM10. Another possibility could be that the actual substrate for the activity of cysteine proteases is a middle product generated by an inhibited cleavage of E-cadherin mediated by ADAM10. Additionally, this effect is also observed when ionomycin is used as an agonist. On this line, it has been proven that several cysteine proteases are also stimulated by Ca^{2+} entry into the cell. This is exemplified by the action of caspases, known cysteine proteases that act as apoptosis executors and are put into action by Ca^{2+} influx into the cell (Fan *et al.*, 2005).

In pathophysiological conditions such as pathogen entry, E-cadherin cleavage and further colonization is a strategy used by many bacteria. For example, Ca^{2+} binding to the extracellular side of E-cadherin is key for the protection of this region from cleavage by *Helicobacter pylori* serine protease HtrA (Schmidt *et al.*, 2016). Coincidentally, this cleavage site is the same one of ADAM10 in the production of the CTF (Hu *et al.*, 2016). However, in the absence of infection conditions, the lack of extracellular Ca^{2+} does not promote even constitutive cleavage of E-cadherin by ADAM10. Therefore, the protective effect caused by Ca^{2+} may occur only in pathological conditions or under a stimulated response of ADAM10.

Altogether, these findings highlight that E-cadherin processing results from the coordinated actions of ADAM10 and other proteases, with calcium signals serving as both activators and modulators of cleavage specificity. This proteolytic regulation in cellular adhesion becomes especially relevant in pathological contexts, thereby providing a direct link to the next section on ADAM10 activation during infection and disease.

5.3 Activation of ADAM10 in pathophysiological conditions

Infection with *P. aeruginosa* promotes its entry through the indirect activation of endogenous proteases, such as ADAM10, following the elicitation of Ca^{2+} entry by *P. aeruginosa*. In the current work, such activation of ADAM10 after P. aeruginosa infection is observed, accompanied by a Ca^{2+} influx shortly after infection. This cytosolic Ca^{2+} increase may be induced by the action of exotoxin A (Aljohmani et al., 2022) or other quorum-sensing-related virulence factors since an interplay among different quorum-sensing systems has been identified in *P. aeruginosa* (Lee and Zhang, 2015). A decrease in ADAM10 activity is observed when the bacteria is preincubated with PQS quorum sensing inhibitors. Considering that longer times of preincubation with the inhibitors elicit more potent ADAM10 inhibition, it is likely that the production of secondary metabolites, which might act either directly on ADAM10's activation or indirectly, e.g., through Ca^{2+} entry promotion, is related to the activity promotion of ADAM10. Several virulence factors are characteristically produced during the later stages of bacterial growth and are therefore considered secondary metabolites (Sánchez-Jiménez, Llamas and Marcos-Torres, 2023). Furthermore, some virulence factors, such as the Ca^{2+}-regulated β-propeller protein CarP, are regulated via quorum sensing, as a triple deletion of the rhlI, lasI and pqsA synthases ablates their production (King *et al.*, 2021).

Ca^{2+} imaging experiments performed show an increase of cytosolic Ca^{2+} with freshly cultured bacterial particles, which is significantly decreased when using PQS quorum sensing inhibitors. The Ca^{2+} homeostasis deregulation that arises from the particles alone might serve as a promoting effect for the activity of pathogen-produced virulence factors that will be exerted in later stages of the infection process since it has been shown that Ca^{2+} promotes the activity of specific proteases like Elastase B (Keskin and Kahraman, 2021). This is supported by the fact that Ca^{2+} levels are elevated in pulmonary fluid and nasal secretions of patients with cystic fibrosis, serving as an environmental trigger for the pathogenicity of *P. aeruginosa* (King *et al.*, 2021). However, other components of *P. aeruginosa* must be considered. For example, researchers have suggested that both the quorum sensing machinery and the attachment of bacterial cells to the host through the cell-surface associated protein PilY1 are necessary for surface activation of virulence, though in this cited work only quorum sensing mutants of the *LasR* system were utilized and the involvement of other QS systems would have to be taken into account as well (Siryaporn *et al.*, 2014). Other components, such as Ca^{2+}-dependent sugar-binding lectins, are also being considered as novel targets for the binding processes of *P. aeruginosa* onto host cells (Grishin *et al.*, 2015; Passos da Silva *et al.*, 2019). Further research is needed to assess the pathophysiological consequences brought about by lectin-based recognition. Additionally, it is important to note that some experiments performed with heat-inactivated *P. aeruginosa* suggest a more active participation of the secreted virulence factors like exotoxin A in the infection process rather than the bacterial particles themselves (Aljohmani *et al.*, 2022). This could further confirm the hypothesis that early increases in Ca^{2+} concentrations serve as a trigger for further infection mechanisms.

6 References

Abdallah, M.A., Pfestorf, M. and Döring, G. (1989) 'Pseudomonas aeruginosa pyoverdin: structure and function.', *Antibiotics and chemotherapy*, 42, pp. 8–14. Available at: https://doi.org/10.1159/000417597.

Abdelaziz, A.A. *et al.* (2023) 'Pseudomonas aeruginosa's greenish-blue pigment pyocyanin: its production and biological activities', *Microbial Cell Factories*, 22(1), pp. 1–14. Available at: https://doi.org/10.1186/s12934-023-02122-1.

Agbowuro, A.A. *et al.* (2018) 'Proteases and protease inhibitors in infectious diseases', *Medicinal Research Reviews*, 38(4), pp. 1295–1331. Available at: https://doi.org/10.1002/med.21475.

Aitken, A. (1999) 'Protein consensus sequence motifs', *Applied Biochemistry and Biotechnology - Part B Molecular Biotechnology*, 12(3), pp. 241–253. Available at: https://doi.org/10.1385/mb:12:3:241.

Akbulut, Y. *et al.* (2015) 'Englerin a is a potent and selective activator of TRPC4 and TRPC5 calcium channels', *Angewandte Chemie - International Edition*, 54(12), pp. 3787–3791. Available at: https://doi.org/10.1002/anie.201411511.

Alexander, S.P.H., Mathie, A. and Peters, J.A. (2009) 'Transient receptor potential (TRP) cation channels', *Br J Pharmacol*, pp. 148–155. Available at: https://doi.org/10.1111/j.1476-5381.2009.00503_16.x.

Aljohmani, A. *et al.* (2022) 'Pseudomonas aeruginosa Triggered Exosomal Release of ADAM10 Mediates Proteolytic Cleavage in Trans'.

Ambudkar, I.S., de Souza, L.B. and Ong, H.L. (2017) 'TRPC1, Orai1, and STIM1 in SOCE: Friends in tight spaces', *Cell Calcium*. Elsevier Ltd, pp. 33–39. Available at: https://doi.org/10.1016/j.ceca.2016.12.009.

Amrita, S., Hughes, T.E. and Moiseenkova-Bell, V.Y. (2018) 'Transient Receptor Potential (TRP) Channels', *Rhabdoviruses*, 1, pp. 107–117. Available at: https://doi.org/10.1201/9781351076388.

Anders, L. *et al.* (2006) 'Furin-, ADAM 10-, and -Secretase-Mediated Cleavage of a Receptor Tyrosine Phosphatase and Regulation of β-Catenin's Transcriptional Activity', 26(10), pp. 3917–3934. Available at: https://doi.org/10.1128/MCB.26.10.3917.

Arai, J. *et al.* (2023) 'The immunological role of ADAMs in the field of gastroenterological chronic inflammatory diseases and cancers: a review', *Oncogene*, 42(8), pp. 549–558. Available at: https://doi.org/10.1038/s41388-022-02583-5.

Araki, K. *et al.* (2011) 'E/N-cadherin switch mediates cancer progression via TGF-β-induced epithelial-to-mesenchymal transition in extrahepatic cholangiocarcinoma', *British Journal of Cancer*, 105(12), pp. 1885–1893. Available at: https://doi.org/10.1038/bjc.2011.452.

Arduise, C. *et al.* (2008) 'Tetraspanins regulate ADAM10-mediated cleavage of TNFα and EGF', 181(33), pp. 7002–7013.

Baek, C.H. *et al.* (2019) 'Epigallocatechin-3-gallate downregulates lipopolysaccharide signaling in human aortic endothelial cells by inducing ectodomain shedding of TLR4', *European Journal of Pharmacology*, 863(September), p. 172692. Available at: https://doi.org/10.1016/j.ejphar.2019.172692.

Barak, P. and Parekh, A.B. (2020a) 'Signaling through ca^{2+} microdomains from store-operated crac channels', *Cold Spring Harbor Perspectives in Biology*, 12(7), pp. 1–18. Available at: https://doi.org/10.1101/cshperspect.a035097.

Barak, P. and Parekh, A.B. (2020b) 'Signaling through Ca^{2+} microdomains from store-operated crac channels', *Cold Spring Harbor Perspectives in Biology*, 12(7), pp. 1–18. Available at: https://doi.org/10.1101/cshperspect.a035097.

Becker, A. *et al.* (2020) 'Control of Insulin Release by Transient Receptor Potential Melastatin 3 (TRPM3) Ion Channels', *Cellular Physiology and Biochemistry*, 54(6), pp. 1115–1131. Available at: https://doi.org/10.33594/000000304.

Bleibaum, F. *et al.* (2019) 'ADAM10 sheddase activation is controlled by cell membrane asymmetry', *Journal of Molecular Cell Biology*, 11(11), pp. 979–993. Available at: https://doi.org/10.1093/jmcb/mjz008.

Bode, W., Gomis-Rüth, F.X. and Stöckler, W. (1993) 'Astacins, serralysins, snake venom and matrix metalloproteinases exhibit identical zinc-binding environments (HEXXHXXGXXH and Met-turn) and topologies and should be grouped into a common family, the "metzincins"', *FEBS Letters*, 331(1–2), pp. 134–140. Available at: https://doi.org/10.1016/0014-5793(93)80312-I.

Bodnar, D. *et al.* (2017) 'STIM-TRP pathways and microdomain organization: Ca^{2+} influx channels: The orai-STIM1-TRPC complexes', in *Advances in Experimental Medicine and Biology*. Springer New York LLC, pp. 139–157. Available at: https://doi.org/10.1007/978-3-319-57732-6_8.

Bouron, A., Kiselyov, K. and Oberwinkler, J. (2015) 'Permeation, regulation and control of expression of TRP channels by trace metal ions', *Pflugers Archiv European Journal of Physiology*. Springer Verlag, pp. 1143–1164. Available at: https://doi.org/10.1007/s00424-014-1590-3.

Brownlow, S.L. and Sage, S.O. (2005) 'Transient receptor potential protein subunit assembly and membrane distribution in human platelets', *Thrombosis and Haemostasis*, 94(4), pp. 839–845. Available at: https://doi.org/10.1160/TH05-06-0391.

Bruce, J.I.E. and James, A.D. (2020) 'Targeting the calcium signalling machinery in cancer', *Cancers*, 12(9), pp. 1–34. Available at: https://doi.org/10.3390/cancers12092351.

Caescu, C.I., Jeschke, G.R. and Turk, B.E. (2009) 'Active site determinants of substrate recognition by the metalloproteinases TACE and ADAM10', *Biochem J*, 424(1), pp. 79–88. Available at: https://doi.org/10.1042/BJ20090549.

Campbell, H.K., L, M.J. and DeMali, K.A. (2017) 'Interplay Between Tight Junctions & Adherens Junctions', *Physiology & behavior*, 176(10), pp. 139–148. Available at: https://doi.org/10.1016/j.yexcr.2017.03.061.Interplay.

Carriquí-Madroñal, B. *et al.* (2023) 'The matrix metalloproteinase ADAM10 supports hepatitis C virus entry and cell-to-cell spread via its sheddase activity', *PLoS Pathogens*, 19(11), pp. 1–24. Available at: https://doi.org/10.1371/journal.ppat.1011759.

Catterall, W.A. (2011) 'Voltage-gated calcium channels', *Cold Spring Harb Perspect Biol*, pp. 1–4. Available at: https://doi.org/10.1101/cshperspect.a003947.

Chadha, J., Harjai, K. and Chhibber, S. (2021) 'Revisiting the virulence hallmarks of Pseudomonas aeruginosa: a chronicle through the perspective of quorum sensing', *Environmental Microbiology* [Preprint]. Available at: https://doi.org/10.1111/1462-2920.15784.

Chang, C. and Werb, Z. (2001) 'The many faces of metalloproteases: Cell growth, invasion, angiogenesis and metastasis', *Trends in Cell Biology*, 11(11). Available at: https://doi.org/10.1016/S0962-8924(01)02122-5.

Chang, C.L., Chen, Y.J. and Liou, J. (2017) 'ER-plasma membrane junctions: Why and how do we study them?', *Biochimica et Biophysica Acta - Molecular Cell Research*. Elsevier B.V., pp. 1494–1506. Available at: https://doi.org/10.1016/j.bbamcr.2017.05.018.

Chong, G., Kimyon, Ö. and Manefield, M. (2013) 'Quorum Sensing Signal Synthesis May Represent a Selective Advantage Independent of Its Role in Regulation of Bioluminescence in Vibrio fischeri', *PLoS ONE*, 8(6). Available at: https://doi.org/10.1371/journal.pone.0067443.

Chubanov, V. *et al.* (2005) 'Emerging roles of TRPM6/TRPM7 channel kinase signal transduction complexes', *Naunyn-Schmiedeberg's Archives of Pharmacology*, 371(4), pp. 334–341. Available at: https://doi.org/10.1007/s00210-005-1056-4.

Chubanov, V. *et al.* (2023) 'TRPM channels in health and disease', *Nature Reviews Nephrology*, 20(March), pp. 175–187. Available at: https://doi.org/10.1038/s41581-023-00777-y.

Cordy, J.M. *et al.* (2003) 'Exclusively targeting β-secretase to lipid rafts by GPI-anchor addition up-regulates β-site processing of the amyloid precursor protein', *Proceedings of the National Academy of Sciences of the United States of America*, 100(20), pp. 11735–11740. Available at: https://doi.org/10.1073/pnas.1635130100.

Dang, M. *et al.* (2011) 'Epidermal Growth Factor (EGF) ligand release by substrate-specific A disintegrin and metalloproteases (ADAMs) involves different protein kinase C (PKC) isoenzymes depending on the stimulus', *Journal of Biological Chemistry*, 286(20), pp. 17704–17713. Available at: https://doi.org/10.1074/jbc.M110.187823.

Dash, S., Duraivelan, K. and Samanta, D. (2021) 'Cadherin-mediated host–pathogen interactions', *Cellular Microbiology*. Blackwell Publishing Ltd. Available at: https://doi.org/10.1111/cmi.13316.

Desai, R.A. *et al.* (2009) 'Cell polarity triggered by cell-cell adhesion via E-cadherin.', *Journal of cell science*, 122(Pt 7), pp. 905–911. Available at: https://doi.org/10.1242/jcs.028183.

Dethlefsen, S.M. *et al.* (1998) *Extracellular Calcium Influx Stimulates Metalloproteinase Cleavage and Secretion of Heparin-Binding EGF-Like Growth Factor Independently of Protein Kinase C*, *J. Cell. Biochem*.

Didiasova, M. *et al.* (2015) 'STIM1/ORAI1-mediated Ca^{2+} influx regulates enolase-1 exteriorization', *Journal of Biological Chemistry*, 290(19), pp. 11983–11999. Available at: https://doi.org/10.1074/jbc.M114.598425.

Dombroski, J.A. *et al.* (2021) 'Channeling the Force: Piezo1 Mechanotransduction in Cancer Metastasis', *Cells*, 10(2815), pp. 282–294. Available at: https://doi.org/https://doi.org/10.3390/cells10112815.

Edwards, D.R., Handsley, M.M. and Pennington, C.J. (2009) 'The ADAM metalloproteinases', *Molecular Aspects of Medicine*, pp. 258–289. Available at: https://doi.org/10.1016/j.mam.2008.08.001.

Emrich, S.M. *et al.* (2023) 'Orai3 and orai1 mediate crac channel function and metabolic reprogramming in b cells', *eLife*, 12, pp. 1–33. Available at: https://doi.org/10.7554/eLife.84708.

Endres, K. *et al.* (2003) 'Tumor necrosis factor-α converting enzyme is processed by proprotein-convertases to its mature form which is degraded upon phorbol ester stimulation', *European Journal of Biochemistry*, 270(11), pp. 2386–2393. Available at: https://doi.org/10.1046/j.1432-1033.2003.03606.x.

Eschenbrenner, E. *et al.* (2020) 'TspanC8 tetraspanins differentially regulate ADAM10 endocytosis and half-life', *Life Science Alliance*, 3(1). Available at: https://doi.org/10.26508/lsa.201900444.

Evans, J.P. (2001) 'Fertilin β and other ADAMS as integrin ligands: Insights into cell adhesion and fertilization', *BioEssays*, 23(7), pp. 628–639. Available at: https://doi.org/10.1002/bies.1088.

Evans, J.P., Schultz, R.M. and Kopf, G.S. (1998) 'Roles of the disintegrin domains of mouse fertilins α

and β in fertilization', *Biology of Reproduction*, 59(1), pp. 145–152. Available at: https://doi.org/10.1095/biolreprod59.1.145.

Fan, T.J. *et al.* (2005) 'Caspase family proteases and apoptosis', *Acta Biochimica et Biophysica Sinica*, 37(11), pp. 719–727. Available at: https://doi.org/10.1111/j.1745-7270.2005.00108.x.

Feske, S. *et al.* (2006) 'A mutation in Orai1 causes immune deficiency by abrogating CRAC channel function.', *Nature*, 441(7090), pp. 179–185. Available at: https://doi.org/10.1038/nature04702.

Frühwald, J. *et al.* (2012) 'Alternative splicing of a protein domain indispensable for function of transient receptor potential melastatin 3 (TRPM3) ion channels', *Journal of Biological Chemistry*, 287(44), pp. 36663–36672. Available at: https://doi.org/10.1074/jbc.M112.396663.

Galindo-Murillo, R. and Cheatham, T.E. (2014) 'DNA binding dynamics and energetics of cobalt, nickel, and copper metallopeptides', *ChemMedChem*, 9(6), pp. 1252–1259. Available at: https://doi.org/10.1002/cmdc.201402020.

Gallwitz, M. *et al.* (2012) 'The extended cleavage specificity of human thrombin', *PLoS ONE*, 7(2). Available at: https://doi.org/10.1371/journal.pone.0031756.

Giebeler, N. and Zigrino, P. (2016) 'A disintegrin and metalloprotease (ADAM): Historical overview of their functions', *Toxins*. MDPI AG. Available at: https://doi.org/10.3390/toxins8040122.

Grabowska, M.M. and Day, M.L. (2012) 'Soluble E-cadherin: More than a symptom of disease', *Frontiers in Bioscience*, 17(5), pp. 1948–1964. Available at: https://doi.org/10.2741/4031.

Griffin, P.J. and Fogarty, W.M. (1973) ' Physicochemical Properties of the Native, Zinc- and Manganese-Prepared Metalloprotease of Bacillus polymyxa ', *Applied Microbiology*, 26(2), pp. 191–195. Available at: https://doi.org/10.1128/am.26.2.191-195.1973.

Grishin, A. V. *et al.* (2015) 'Pseudomonas Aeruginosa lectins as targets for novel antibacterials', *Acta Naturae*, 7(2), pp. 29–41. Available at: https://doi.org/10.32607/20758251-2015-7-2-29-41.

Groth, E. *et al.* (2016a) 'Stimulated release and functional activity of surface expressed metalloproteinase ADAM17 in exosomes', *Biochimica et Biophysica Acta - Molecular Cell Research*, 1863(11), pp. 2795–2808. Available at: https://doi.org/10.1016/j.bbamcr.2016.09.002.

Groth, E. *et al.* (2016b) 'Stimulated release and functional activity of surface expressed metalloproteinase ADAM17 in exosomes', *Biochimica et Biophysica Acta - Molecular Cell Research*, 1863(11), pp. 2795–2808. Available at: https://doi.org/10.1016/j.bbamcr.2016.09.002.

Groves, M.D. *et al.* (2006) 'Phase II trial of temozolomide plus marimastat for recurrent anaplastic gliomas: A relationship among efficacy, joint toxicity and anticonvulsant status', *Journal of Neuro-Oncology*, 80(1), pp. 83–90. Available at: https://doi.org/10.1007/s11060-006-9160-y.

Grynkiewicz, G., Poenie, M. and Tsien, R.Y. (1985) 'A new generation of Ca^{2+} indicators with greatly improved fluorescence properties', *Journal of Biological Chemistry*, 260(6), pp. 3440–3450. Available at: https://doi.org/10.1016/s0021-9258(19)83641-4.

Guerra, E. *et al.* (2021) 'Trop-2 induces ADAM10-mediated cleavage of E-cadherin and drives EMT-less metastasis in colon cancer', *Neoplasia (United States)*, 23(9), pp. 898–911. Available at: https://doi.org/10.1016/j.neo.2021.07.002.

Guilbert, A. *et al.* (2009) 'Evidence that TRPM7 is required for breast cancer cell proliferation', *American Journal of Physiology - Cell Physiology*, 297(3), pp. 493–502. Available at: https://doi.org/10.1152/ajpcell.00624.2008.

Guo, H. *et al.* (2019) 'Vascular endothelial growth factor improves the cognitive decline of Alzheimer's disease via concurrently inducing the expression of ADAM10 and reducing the

expression of β-site APP cleaving enzyme 1 in Tg2576 mice', *Neuroscience Research*, 142, pp. 49–57. Available at: https://doi.org/10.1016/j.neures.2018.04.003.

Gutiérrez, A.A. *et al.* (1999) 'Activation of a Ca^{2+}-permeable cation channel by two different inducers of apoptosis in a human prostatic cancer cell line', *Journal of Physiology*, 517(1), pp. 95–107. Available at: https://doi.org/10.1111/j.1469-7793.1999.0095z.x.

Gwanyanya, A. and Mubagwa, K. (2022) 'Emerging role of transient receptor potential (TRP) ion channels in cardiac fibroblast pathophysiology', *Frontiers in Physiology*, 13(October), pp. 1–14. Available at: https://doi.org/10.3389/fphys.2022.968393.

Harada, S. *et al.* (1995) 'Complete Amino Acid Sequence of a Zinc Metalloendoprotease from Streptomyces caespitosus', *European Journal of Biochemistry*, 233(2), pp. 683–686. Available at: https://doi.org/10.1111/j.1432-1033.1995.683_2.x.

Harrison, N., Koo, C.Z. and Tomlinson, M.G. (2021) 'Regulation of adam10 by the tspanc8 family of tetraspanins and their therapeutic potential', *International Journal of Molecular Sciences*. MDPI AG. Available at: https://doi.org/10.3390/ijms22136707.

Herzog, C. *et al.* (2014) 'ADAM10 is the major sheddase responsible for the release of membrane-Associated meprin A', *Journal of Biological Chemistry*, 289(19), pp. 13308–13322. Available at: https://doi.org/10.1074/jbc.M114.559088.

Hoettecke, N. *et al.* (2010) 'Improved synthesis of ADAM10 inhibitor GI254023X', *Neurodegenerative Diseases*, 7(4), pp. 232–238. Available at: https://doi.org/10.1159/000267865.

Horiuchi, K. *et al.* (2007) 'Substrate Selectivity of Epidermal Growth Factor-Receptor Ligand Sheddases and their Regulation by Phorbol Esters and Calcium Influx □ D', *Molecular Biology of the Cell*, 18, pp. 176–188. Available at: https://doi.org/10.1091/mbc.E06.

Hou, L. *et al.* (2018) 'PAX2 may induce ADAM10 expression in renal tubular epithelial cells and contribute to epithelial-to-mesenchymal transition', *International Urology and Nephrology*, 50(9), pp. 1729–1741. Available at: https://doi.org/10.1007/s11255-018-1956-0.

Hu, Q.P. *et al.* (2016) 'Beyond a tumor suppressor: Soluble E-cadherin promotes the progression of cancer', *International Journal of Cancer*, 138(12), pp. 2804–2812. Available at: https://doi.org/10.1002/ijc.29982.

Huang, J., Bridges, L.C. and White, J.M. (2005) 'Selective Modulation of Integrin-mediated Cell Migration by Distinct ADAM Family Members', *Molecular Biology of the Cell*, 16(November), pp. 5356–5372. Available at: https://doi.org/10.1091/mbc.E05.

Ito, K. *et al.* (1999) 'Calcium influx triggers the sequential proteolysis of extracellular and cytoplasmic domains of E-cadherin, leading to loss of β-catenin from cell-cell contacts', *Oncogene*, 18(50), pp. 7080–7090. Available at: https://doi.org/10.1038/sj.onc.1203191.

Itsuki, K. *et al.* (2014) 'PLC-mediated PI(4,5)P2 hydrolysis regulates activation and inactivation of TRPC6/7 channels', *Journal of General Physiology*, 143(2), pp. 183–201. Available at: https://doi.org/10.1085/jgp.201311033.

J.A.M. Bard, Ellen A. Goodall, Eric R. Greene, Erik Jonsson, Ken C. Dong, and A.M. (2019) 'Structure and Function of the 26S Proteasome', *Physiology & behavior*, 46(2), pp. 248–256. Available at: https://doi.org/10.1146/annurev-biochem-062917-011931.Structure.

Jurado-Martín, I., Sainz-Mejías, M. and McClean, S. (2021) 'Pseudomonas aeruginosa: An audacious pathogen with an adaptable arsenal of virulence factors', *International Journal of Molecular Sciences*, 22(6), pp. 1–37. Available at: https://doi.org/10.3390/ijms22063128.

Kang, S.S.S. *et al.* (2017) 'Trifluoperazine, a well-known antipsychotic, inhibits glioblastoma invasion by binding to calmodulin and disinhibiting calcium release channel IP3R', *Molecular Cancer Therapeutics*, 16(1), pp. 217–227. Available at: https://doi.org/10.1158/1535-7163.MCT-16-0169-T.

Kapust, R.B. *et al.* (2002) 'The P1' specificity of tobacco etch virus protease', *Biochemical and Biophysical Research Communications*, 294(5), pp. 949–955. Available at: https://doi.org/10.1016/S0006-291X(02)00574-0.

Kashio, M. and Tominaga, M. (2022) 'TRP channels in thermosensation', *Current Opinion in Neurobiology*, 75, p. 102591. Available at: https://doi.org/10.1016/j.conb.2022.102591.

Keskin, Z.B. and Kahraman, H. (2021) 'Effect of calcium on Pseudomonas aeruginasa and Bacillus cereus metabolites.', *Brazilian journal of biology = Revista brasleira de biologia*, 82, p. e243189. Available at: https://doi.org/10.1590/1519-6984.243189.

Ketterer, C. *et al.* (2011) 'Genetic variation within the TRPM5 locus associates with prediabetic phenotypes in subjects at increased risk for type 2 diabetes', *Metabolism: Clinical and Experimental*, 60(9), pp. 1325–1333. Available at: https://doi.org/10.1016/j.metabol.2011.02.002.

Kim, H. *et al.* (2012) 'The roles of G proteins in the activation of TRPC4 and TRPC5 transient receptor potential channels', *Channels*, 6(5), pp. 333–343. Available at: https://doi.org/10.4161/chan.21198.

Kim, J. *et al.* (2019) 'TRPC1 as a negative regulator for TRPC4 and TRPC5 channels', *Pflugers Archiv European Journal of Physiology*, 471(8), pp. 1045–1053. Available at: https://doi.org/10.1007/s00424-019-02289-w.

King, M. *et al.* (2021) 'Calcium-Regulated Protein CarP Responds to Multiple Host Signals and Mediates Regulation of Pseudomonas aeruginosa Virulence by Calcium', *Applied and Environmental Microbiology*, 87(10), pp. 1–21. Available at: https://doi.org/10.1128/AEM.00061-21.

Kodakandla, G., Akimzhanov, A.M. and Boehning, D. (2023) 'Regulatory mechanisms controlling store-operated calcium entry', *Frontiers in Physiology*, 14(December). Available at: https://doi.org/10.3389/fphys.2023.1330259.

Konze, S.A. *et al.* (2014) 'Cleavage of e-cadherin and-catenin by calpain affects wnt signaling and spheroid formation in suspension cultures of human pluripotent stem cells', *Molecular and Cellular Proteomics*, 13(4), pp. 990–1007. Available at: https://doi.org/10.1074/mcp.M113.033423.

Lee, J. and Zhang, L. (2015) 'The hierarchy quorum sensing network in Pseudomonas aeruginosa', *Protein and Cell*, 6(1), pp. 26–41. Available at: https://doi.org/10.1007/s13238-014-0100-x.

Leitzke, S. *et al.* (2022) 'Influence of Anoctamin-4 and-9 on ADAM10 and ADAM17 Sheddase Function', *Membranes*, 12(2). Available at: https://doi.org/10.3390/membranes12020123.

Liao, Y. *et al.* (2007) 'Orai proteins interact with TRPC channels and confer responsiveness to store depletion', *PNAS*, 104(11), pp. 4682–4687. Available at: https://doi.org/https://doi.org/10.1073/pnas.0611692104.

Liou, J. *et al.* (2005) 'STIM Is a Ca^{2+} Sensor Essential for Ca^{2+} -Store-Depletion- Triggered Ca^{2+} Influx', *Current biology : CB*, 471(7336), pp. 68–73. Available at: https://doi.org/10.1016/j.cub.2005.05.055.STIM.

Liu, C.C. *et al.* (2018) 'Collagen XVII/laminin-5 activates epithelial-to-mesenchymal transition and is associated with poor prognosis in lung cancer', *Oncotarget*, 9(2), pp. 1656–1672. Available at: https://doi.org/10.18632/oncotarget.11208.

Lokau, J. and Garbers, C. (2021) 'Interleukin-6–interleukin-11 receptor chimeras reveal ionomycin-induced proteolysis beyond ADAM10', *FEBS Letters*, 595(24), pp. 3072–3082. Available at:

https://doi.org/10.1002/1873-3468.14230.

López-Otín, C. and Bond, J.S. (2008) 'Proteases: Multifunctional enzymes in life and disease', *Journal of Biological Chemistry*, 283(45), pp. 30433–30437. Available at: https://doi.org/10.1074/jbc.R800035200.

Lopez, J.J. *et al.* (2020) 'TRPC Channels in the SOCE Scenario', *Cells*. NLM (Medline). Available at: https://doi.org/10.3390/cells9010126.

de Lorenzo, V. (2015) 'Pseudomonas aeruginosa: The making of a pathogen', *Environmental Microbiology*, 17(1), pp. 1–3. Available at: https://doi.org/10.1111/1462-2920.12620.

Lu, W. *et al.* (2020) 'Tetraspanin CD9 interacts with α-secretase to enhance its oncogenic function in pancreatic cancer', *American Journal of Translational Research*, 12(9), pp. 5525–5537.

Lu, X. *et al.* (2005) 'Snake venom metalloproteinase containing a disintegrin-like domain, its structure-activity relationships at interacting with integrins.', *Current medicinal chemistry. Cardiovascular and hematological agents*, 3(3), pp. 249–260. Available at: https://doi.org/10.2174/1568016054368205.

Mala, R.B. *et al.* (1998) 'Molecular and Biotechnological Aspects of Microbial Proteases', *Microbiology and Molecular Biology Reviews*, 62(3), pp. 597–635.

Marcello, E. *et al.* (2007) 'Synapse-associated protein-97 mediates α-secretase ADAM10 trafficking and promotes its activity', *Journal of Neuroscience*, 27(7), pp. 1682–1691. Available at: https://doi.org/10.1523/JNEUROSCI.3439-06.2007.

Maretzky, T. *et al.* (2005) *ADAM10 mediates E-cadherin shedding and regulates epithelial cell-cell adhesion, migration, and-catenin translocation*. Available at: http://www.pnas.orgcgidoi10.1073pnas.0500918102.

Maretzky, T. *et al.* (2015) 'The cytoplasmic domain of a disintegrin and metalloproteinase 10 (ADAM10) regulates its constitutive activity but is dispensable for stimulated ADAM10-dependent shedding', *Journal of Biological Chemistry*, 290(12), pp. 7416–7425. Available at: https://doi.org/10.1074/jbc.M114.603753.

Marquart, M.E. (2021) 'Pathogenicity and virulence of Streptococcus pneumoniae: Cutting to the chase on proteases', *Virulence*, 12(1), pp. 766–787. Available at: https://doi.org/10.1080/21505594.2021.1889812.

Matthews, A.L. *et al.* (2017) 'Regulation of A disintegrin and metalloproteinase (ADAM) family sheddases ADAM10 and ADAM17: The emerging role of tetraspanins and rhomboids', *Platelets*. Taylor and Francis Ltd, pp. 333–341. Available at: https://doi.org/10.1080/09537104.2016.1184751.

McFadzean, I. and Gibson, A. (2002) 'The developing relationship between receptor-operated and store-operated calcium channels in smooth muscle', *British Journal of Pharmacology*, 135(1), pp. 1–13. Available at: https://doi.org/10.1038/sj.bjp.0704468.

Milla, M.E., Gonzales, P.E. and Leonard, J.D. (2006) 'The TACE Zymogen', *Cell Bioch. Biophy.*, 44, pp. 342–348.

Miller, M. *et al.* (2011) 'Identification of ML204, a novel potent antagonist that selectively modulates native TRPC4/C5 ion channels', *Journal of Biological Chemistry*, 286(38), pp. 33436–33446. Available at: https://doi.org/10.1074/jbc.M111.274167.

Minke, B. (2006) 'TRP channels and Ca^{2+} signaling', *Cell Calcium*. Elsevier Ltd, pp. 261–275. Available at: https://doi.org/10.1016/j.ceca.2006.05.002.

Miyoshi, A. *et al.* (2019) 'JNK and ATF4 as two important platforms for tumor necrosis factor-α–

stimulated shedding of receptor for advanced glycation end products', *FASEB Journal*, 33(3), pp. 3575–3589. Available at: https://doi.org/10.1096/fj.201701553RR.

Morgan, A.J. and Jacob, R. (1994) *Ionomycin enhances Ca^{2+} influx by stimulating store-regulated cation entry and not by a direct action at the plasma membrane*, *Biochem. J*.

Mueller, A.C. *et al.* (2021) 'Induction of ADAM10 by RT drives fibrosis, resistance, and EMT in pancreatic cancer', 81(12), pp. 3255–3269. Available at: https://doi.org/10.1158/0008-5472.CAN-20-3892.Induction.

Mulcahy, L.R., Isabella, V.M. and Lewis, K. (2014) 'Pseudomonas aeruginosa Biofilms in Disease', *Microbial Ecology*, 68(1), pp. 1–12. Available at: https://doi.org/10.1007/s00248-013-0297-x.

Mulier, M., Vriens, J. and Voets, T. (2017) 'TRP channel pores and local calcium signals', *Cell Calcium*. Elsevier Ltd, pp. 19–24. Available at: https://doi.org/10.1016/j.ceca.2017.04.007.

Murphy, G. (2011) 'Tissue inhibitors of metalloproteinases', *Genome Biology*, 12(11). Available at: https://doi.org/10.1186/gb-2011-12-11-233.

N Saha, D Robev, JP Himanen, B.N. (2017) 'ADAM proteases: Emerging role and targeting of the non-catalytic domains', *Physiology & behavior*, 176(3), pp. 139–148. Available at: https://doi.org/10.1159/000444169.Carotid.

Nagano, O. *et al.* (2004) 'Cell-matrix interaction via CD44 is independently regulated by different metalloproteinases activated in response to extracellular Ca^{2+} influx and PKC activation', *Journal of Cell Biology*, 165(6), pp. 893–902. Available at: https://doi.org/10.1083/jcb.200310024.

Nagase, H. (2001) 'Metalloproteases.', *Current protocols in protein science / editorial board, John E. Coligan ... [et al.]*, Chapter 21, pp. 1–13. Available at: https://doi.org/10.1002/0471140864.ps2104s24.

Nelson, M.T. *et al.* (2013) 'Elementary Ca^{2+}signals through endothelial TRPV4 channels regulate vascular function', *BMC Pharmacology and Toxicology*, 14(S1), pp. 597–601. Available at: https://doi.org/10.1186/2050-6511-14-s1-o23.

Nilius, B. and Owsianik, G. (2011) 'The transient receptor potential family of ion channels', *Genome Biology*, 12(3). Available at: https://doi.org/10.1186/gb-2011-12-3-218.

Norgard, R.J. *et al.* (2021) 'Calcium signaling induces a partial EMT', *EMBO reports*, 22(9), pp. 1–13. Available at: https://doi.org/10.15252/embr.202051872.

Noss, E.H. *et al.* (2015) 'Evidence for cadherin-11 cleavage in the synovium and partial characterization of its mechanism', *Arthritis Research and Therapy*, 17(1). Available at: https://doi.org/10.1186/s13075-015-0647-9.

Nunan, J. and Small, D.H. (2000) 'Regulation of APP cleavage by α-, β- and γ-secretases', *FEBS Letters*, 483(1), pp. 6–10. Available at: https://doi.org/10.1016/S0014-5793(00)02076-7.

O'Brien, R.J. and Wong, P.C. (2011) 'Amyloid precursor protein processing and alzheimer's disease', *Annual Review of Neuroscience*, 34, pp. 185–204. Available at: https://doi.org/10.1146/annurev-neuro-061010-113613.

Olsen, J. V., Ong, S.E. and Mann, M. (2004) 'Trypsin cleaves exclusively C-terminal to arginine and lysine residues', *Molecular and Cellular Proteomics*, 3(6), pp. 608–614. Available at: https://doi.org/10.1074/mcp.T400003-MCP200.

Padar, S. *et al.* (2004) 'Differential regulation of calcium homeostasis in adenocarcinoma cell line A549 and its Taxol-resistant subclone', *British Journal of Pharmacology*, 142(2), pp. 305–316. Available at: https://doi.org/10.1038/sj.bjp.0705755.

Pan, Y. *et al.* (2012) 'ADAM10 promotes pituitary adenoma cell migration by regulating cleavage of CD44 and L1', *Journal of Molecular Endocrinology*, 49(1), pp. 21–33. Available at: https://doi.org/10.1530/JME-11-0174.

Park, G. Bin *et al.* (2015) 'Regulation of ADAM10 and ADAM17 by sorafenib inhibits epithelial-to-mesenchymal transition in epstein-barr virus-infected retinal pigment epithelial cells', *Investigative Ophthalmology and Visual Science*, 56(9), pp. 5162–5173. Available at: https://doi.org/10.1167/iovs.14-16058.

Parsons, S.L., Watson, S.A. and Steele, R.J.C. (1997) 'Phase I/II trial of batimastat, a matrix metalloproteinase inhibitor, in patients with malignant ascites', *European Journal of Surgical Oncology*, 23(6), pp. 526–531. Available at: https://doi.org/10.1016/S0748-7983(97)93077-8.

Passos da Silva, D. *et al.* (2019) 'The Pseudomonas aeruginosa lectin LecB binds to the exopolysaccharide Psl and stabilizes the biofilm matrix', *Nature Communications*, 10(1), pp. 1–11. Available at: https://doi.org/10.1038/s41467-019-10201-4.

Patergnani, S. *et al.* (2020) 'Various aspects of calcium signaling in the regulation of apoptosis, autophagy, cell proliferation, and cancer', *International Journal of Molecular Sciences*, 21(21), pp. 1–27. Available at: https://doi.org/10.3390/ijms21218323.

Peier, A.M. *et al.* (2002) 'A TRP channel that senses cold stimuli and menthol', *Cell*, 108(5), pp. 705–715. Available at: https://doi.org/10.1016/S0092-8674(02)00652-9.

Peschon, J.J. *et al.* (1998) 'An essential role for ectodomain shedding in mammalian development', *Science*, 282(5392), pp. 1281–1284. Available at: https://doi.org/10.1126/science.282.5392.1281.

Philipp, S. *et al.* (1998) 'A novel capacitative calcium entry channel expressed in excitable cells', *EMBO Journal*, 17(15), pp. 4274–4282. Available at: https://doi.org/10.1093/emboj/17.15.4274.

Pinton, P. *et al.* (2008) 'Calcium and apoptosis: ER-mitochondria Ca^{2+} transfer in the control of apoptosis', *Oncogene*, pp. 6407–6418. Available at: https://doi.org/10.1038/onc.2008.308.

Prakriya, M. (2013) 'Store-operated Orai channels: structure and function.', *Current topics in membranes*, 71, pp. 1–32. Available at: https://doi.org/10.1016/B978-0-12-407870-3.00001-9.

Prakriya, M. and Lewis, R.S. (2015) 'Store-Operated Calcium Channels.', *Physiological reviews*, 95(4), pp. 1383–1436. Available at: https://doi.org/10.1152/physrev.00020.2014.

Prawitt, D. *et al.* (2000) 'Identification and characterization of MTR1, a novel gene with homology to melastatin (MLSN1) and the trp gene family located in the BWS-WT2 critical region on chromosome 11p15.5 and showing allele-specific expression', *Human Molecular Genetics*, 9(2), pp. 203–216. Available at: https://doi.org/10.1093/hmg/9.2.203.

Qin, J. *et al.* (2009) 'Trifluoperazine: A rynodine receptor agonist', *Pflugers Archiv European Journal of Physiology*, 458(4), pp. 643–651. Available at: https://doi.org/10.1007/s00424-009-0658-y.

Qu, B. *et al.* (2011) 'ORAI-mediated calcium influx in T cell proliferation, apoptosis and tolerance', *Cell Calcium*, 50(3), pp. 261–269. Available at: https://doi.org/10.1016/j.ceca.2011.05.015.

Raaflaub, J. (1956) 'Applications of Metal Buffers and Metal Indicators in Biochemistry', in *Methods of Biochemical Analysis*. (Methods of Biochemical Analysis), pp. 301–325. Available at: https://doi.org/https://doi.org/10.1002/9780470110195.ch10.

Radford, R.J. and Lippard, S.J. (2013) 'Chelators for Investigating Zinc Metalloneurochemistry', *Curr Opin Chem Biol.*, 17(2), pp. 129–136. Available at: https://doi.org/10.1016/j.cbpa.2013.01.009.

Raffaello, A. *et al.* (2016) 'Calcium at the center of cell signaling: interplay between endoplasmic reticulum, mitochondria and lysosomes', *Trends Biochem Sci.*, 176(12), pp. 1035–1049. Available at:

https://doi.org/10.1016/j.tibs.2016.09.001.

Ramachandran, R.P. *et al.* (2020) 'Mitochondrial Targeting of the Enteropathogenic Escherichia coli Map Triggers Calcium Mobilization, ADAM10-MAP Kinase Signaling, and Host Cell Apoptosis Downloaded from'. Available at: https://doi.org/10.1128/mBio.

Rangasamy, S.B. *et al.* (2023) 'Treadmill workout activates PPARα in the hippocampus to upregulate ADAM10, decrease plaques and improve cognitive functions in 5XFAD mouse model of Alzheimer's disease', *Brain, Behavior, and Immunity*, 109(312), pp. 204–218. Available at: https://doi.org/10.1016/j.bbi.2023.01.009.

Rather, M.A. *et al.* (2022) 'Quorum Quenching: A Drug Discovery Approach Against Pseudomonas aeruginosa', *Microbiological Research*, 264(April), p. 127173. Available at: https://doi.org/10.1016/j.micres.2022.127173.

Ratnikov, B.I. *et al.* (2014) 'Basis for substrate recognition and distinction by matrix metalloproteinases', *Proceedings of the National Academy of Sciences of the United States of America*, 111(40), pp. E4148–E4155. Available at: https://doi.org/10.1073/pnas.1406134111.

Rawlings, N.D., Barrett, A.J. and Bateman, A. (2012) 'MEROPS: The database of proteolytic enzymes, their substrates and inhibitors', *Nucleic Acids Research*, 40(D1), pp. 343–350. Available at: https://doi.org/10.1093/nar/gkr987.

Reboud, E. *et al.* (2017) 'Pseudomonas aeruginosa ExlA and Serratia marcescens ShlA trigger cadherin cleavage by promoting calcium influx and ADAM10 activation', *PLoS Pathogens*, 13(8). Available at: https://doi.org/10.1371/journal.ppat.1006579.

Rio, C. *et al.* (2000) 'Tumor necrosis factor-α-converting enzyme is required for cleavage of erbB4/HER4', *Journal of Biological Chemistry*, 275(14), pp. 10379–10387. Available at: https://doi.org/10.1074/jbc.275.14.10379.

Romero, Y., Wise, R. and Zolkiewska, A. (2020) 'Proteolytic processing of PD-L1 by ADAM proteases in breast cancer cells', *Cancer Immunology, Immunotherapy*, 69(1), pp. 43–55. Available at: https://doi.org/10.1007/s00262-019-02437-2.

Rzymski, T. *et al.* (2012) 'The unfolded protein response controls induction and activation of ADAM17/TACE by severe hypoxia and ER stress', *Oncogene*, 31(31), pp. 3621–3634. Available at: https://doi.org/10.1038/onc.2011.522.

Sánchez-Hernández, Y. *et al.* (2010) 'Store-operated Ca^{2+} entry is expressed in human endothelial progenitor cells', *Stem Cells and Development*, 19(12), pp. 1967–1981. Available at: https://doi.org/10.1089/scd.2010.0047.

Sánchez-Jiménez, A., Llamas, M.A. and Marcos-Torres, F.J. (2023) 'Transcriptional Regulators Controlling Virulence in Pseudomonas aeruginosa', *International Journal of Molecular Sciences*, 24(15). Available at: https://doi.org/10.3390/ijms241511895.

Savina, A. *et al.* (2003) 'Exosome release is regulated by a calcium-dependent mechanism in K562 cells', *Journal of Biological Chemistry*, 278(22), pp. 20083–20090. Available at: https://doi.org/10.1074/jbc.M301642200.

Scharfenberg, F. *et al.* (2020) 'Degradome of soluble ADAM10 and ADAM17 metalloproteases', *Cellular and Molecular Life Sciences*, 77(2), pp. 331–350. Available at: https://doi.org/10.1007/s00018-019-03184-4.

Schauperl, M. *et al.* (2015) 'Characterizing protease specificity: How many substrates do we need?', *PLoS ONE*, 10(11), pp. 1–17. Available at: https://doi.org/10.1371/journal.pone.0142658.

Schechter, I. and Berger, A. (1972) 'On the size of the active site in proteases: Pronase', *Biochemical and Biophysical Research Communications*, 46(5), pp. 1956–1960. Available at: https://doi.org/10.1016/0006-291X(72)90076-9.

Schmidt, T.P. *et al.* (2016) 'Calcium binding protects E-cadherin from cleavage by Helicobacter pylori HtrA', *Gut Pathogens*, 8(1), pp. 1–10. Available at: https://doi.org/10.1186/s13099-016-0112-6.

Schulz, B. *et al.* (2008) 'Disintegrin Metalloprotease (ADAM) 10 Regulates Endothelial Permeability and T Cell Transmigration by Proteolysis of Vascular Endothelial Cadherin', *Circulation Research*, 102(10), pp. 1192–1201. Available at: https://doi.org/10.1161/CIRCRESAHA.107.169805.Disintegrin.

Schütz, C. *et al.* (2021) 'A New PqsR Inverse Agonist Potentiates Tobramycin Efficacy to Eradicate Pseudomonas aeruginosa Biofilms', *Advanced Science*, 8(12), pp. 1–12. Available at: https://doi.org/10.1002/advs.202004369.

Seifert, A. *et al.* (2021) 'The metalloproteinase ADAM10 requires its activity to sustain surface expression', *Cellular and Molecular Life Sciences*, 78(2), pp. 715–732. Available at: https://doi.org/10.1007/s00018-020-03507-w.

Senning, E.N. and Gordon, S.E. (2015) 'Activity and Ca^{2+} regulate the mobility of TRPV1 channels in the plasma membrane of sensory neurons', *eLife*, 2015(4), pp. 1–20. Available at: https://doi.org/10.7554/eLife.03819.

Shimoda, M. (2019) 'Chapter Two - Extracellular vesicle-associated MMPs: A modulator of the tissue microenvironment', in G.S.B.T.-A. in C.C. Makowski (ed.). Elsevier, pp. 35–66. Available at: https://doi.org/https://doi.org/10.1016/bs.acc.2018.10.006.

Singh, J. *et al.* (2006) 'Annotation of androgen dependence to human prostate cancer-associated genes by microarray analysis of mouse prostate', *Cancer Letters*, 237(2), pp. 298–304. Available at: https://doi.org/10.1016/j.canlet.2005.06.008.

Siryaporn, A. *et al.* (2014) 'Surface attachment induces Pseudomonas aeruginosa virulence', *Proceedings of the National Academy of Sciences of the United States of America*, 111(47), pp. 16860–16865. Available at: https://doi.org/10.1073/pnas.1415712111.

Smith, T.M., Tharakan, A. and Martin, R.K. (2020) 'Targeting ADAM10 in Cancer and Autoimmunity', *Frontiers in Immunology*. Frontiers Media S.A. Available at: https://doi.org/10.3389/fimmu.2020.00499.

Song, M.Y. and Yuan, J.X.J. (2010) 'Introduction to TRP channels: Structure, function, and regulation', in *Advances in Experimental Medicine and Biology*, pp. 99–108. Available at: https://doi.org/10.1007/978-1-60761-500-2_6.

Souza, J.S.M. *et al.* (2020) 'The evolution of ADAM gene family in eukaryotes', *Genomics*, 112(5), pp. 3108–3116. Available at: https://doi.org/10.1016/j.ygeno.2020.05.010.

Steinhusen, U. *et al.* (2001) 'Cleavage and Shedding of E-cadherin after Induction of Apoptosis', *Journal of Biological Chemistry*, 276(7), pp. 4972–4980. Available at: https://doi.org/10.1074/jbc.M006102200.

Suguro, M. *et al.* (2006) 'Expression profiling analysis of the CD5+ diffuse large B-cell lymphoma subgroup: Development of a CD5 signature', *Cancer Science*, 97(9), pp. 868–874. Available at: https://doi.org/10.1111/j.1349-7006.2006.00267.x.

Sullivan, M.N. *et al.* (2015) 'Vascular biology: Localized TRPA1 channel Ca^{2+} signals stimulated by reactive oxygen species promote cerebral artery dilation', *Science Signaling*, 8(358), pp. 1–26. Available at: https://doi.org/10.1126/scisignal.2005659.

Svobodova, B. and Groschner, K. (2016) 'Mechanisms of lipid regulation and lipid gating in TRPC channels', *Cell Calcium*, 59(6), pp. 271–279. Available at: https://doi.org/10.1016/j.ceca.2016.03.012.

Tang, M.K.S.S. *et al.* (2018) 'Soluble E-cadherin promotes tumor angiogenesis and localizes to exosome surface', *Nature Communications*, 9(1). Available at: https://doi.org/10.1038/s41467-018-04695-7.

Tatsumi, M. *et al.* (2023) 'Ectodomain shedding of EGFR ligands serves as an activation readout for TRP channels.', *PloS one*, 18(1), p. e0280448. Available at: https://doi.org/10.1371/journal.pone.0280448.

Thiel, G. *et al.* (2017) 'Transient receptor potential TRPM3 channels: Pharmacology, signaling, and biological functions', *Pharmacological Research*, 124, pp. 92–99. Available at: https://doi.org/10.1016/j.phrs.2017.07.014.

Tousseyn, T. *et al.* (2009) 'ADAM10, the rate-limiting protease of regulated intramembrane proteolysis of notch and other proteins, is processed by ADAMS-9, ADAMS-15, and the γ-secretase', *Journal of Biological Chemistry*, 284(17), pp. 11738–11747. Available at: https://doi.org/10.1074/jbc.M805894200.

Trebak, M. and Putney, J.W.J. (2017) 'ORAI Calcium Channels.', *Physiology (Bethesda, Md.)*, 32(4), pp. 332–342. Available at: https://doi.org/10.1152/physiol.00011.2017.

Turk, B. (2006) 'Targeting proteases: Successes, failures and future prospects', *Nature Reviews Drug Discovery*, 5(9), pp. 785–799. Available at: https://doi.org/10.1038/nrd2092.

Uemura, K. *et al.* (2006) 'Characterization of sequential N-cadherin cleavage by ADAM10 and PS1', *Neuroscience Letters*, 402(3), pp. 278–283. Available at: https://doi.org/10.1016/j.neulet.2006.04.018.

Varin, J. *et al.* (2020) 'Identification and characterization of novel TRPM1 autoantibodies from serum of patients with melanoma-associated retinopathy', *PLoS ONE*, 15(4), pp. 1–15. Available at: https://doi.org/10.1371/journal.pone.0231750.

Veit, M. *et al.* (2018) 'Anoctamin-6 regulates ADAM sheddase function', *Biochimica et Biophysica Acta - Molecular Cell Research*, 1865(11), pp. 1598–1610. Available at: https://doi.org/10.1016/j.bbamcr.2018.08.011.

Van Der Velden, V.H.J. and Hulsmann, A.R. (1999) 'Peptidases: Structure, function and modulation of peptide-mediated effects in the human lung', *Clinical and Experimental Allergy*, 29(4), pp. 445–456. Available at: https://doi.org/10.1046/j.1365-2222.1999.00462.x.

Venkatachalam, K. and Montell, C. (2007) 'TRP channels', *Annual Review of Biochemistry*, pp. 387–417. Available at: https://doi.org/10.1146/annurev.biochem.75.103004.142819.

Van Der Vorst, E.P.C., Weber, C. and Donners, M.M.P.C. (2018) 'A Disintegrin and Metalloproteases (ADAMs) in Cardiovascular, Metabolic and Inflammatory Diseases: Aspects for Theranostic Approaches', *Thrombosis and Haemostasis*, 118(7), pp. 1167–1175. Available at: https://doi.org/10.1055/s-0038-1660479.

Wan, X. *et al.* (2022) 'cGAS-STING Pathway Performance in the Vulnerable Atherosclerotic Plaque', *Aging and Disease*, 13(6), pp. 1606–1614. Available at: https://doi.org/10.14336/AD.2022.0417.

Wang, H. *et al.* (2020) 'TRPC channels: Structure, function, regulation and recent advances in small molecular probes', *Pharmacol Ther.*, pp. 1–78. Available at: https://doi.org/10.1016/j.pharmthera.2020.107497.TRPC.

Wang, L.Y. and Augustine, G.J. (2015) 'Presynaptic nanodomains: A tale of two synapses', *Frontiers in*

Cellular Neuroscience, 8(JAN), pp. 1–10. Available at: https://doi.org/10.3389/fncel.2014.00455.

Wang, X. *et al.* (2018) 'E-cadherin bridges cell polarity and spindle orientation to ensure prostate epithelial integrity and prevent carcinogenesis in vivo', *PLoS Genetics*, 14(8), pp. 1–23. Available at: https://doi.org/10.1371/journal.pgen.1007609.

Werb, Z. (1997) 'ECM and cell surface proteolysis: Regulating cellular ecology', *Cell*, 91(4), pp. 439–442. Available at: https://doi.org/10.1016/S0092-8674(00)80429-8.

WHO Bacterial Priority Pathogens List, 2024: bacterial pathogens of public health importance to guide research, development and strategies to prevent and control antimicrobial resistance. Geneva: World Health Organization; 2024. Licence: CC BY-NC-SA 3.0 I (2024).

Williams, J.K. *et al.* (2023) 'Annexin A6 mediates calcium-dependent exosome secretion during plasma membrane repair', *eLife*, 12, pp. 1–24. Available at: https://doi.org/10.7554/eLife.86556.

Williams, R.J.P. (1992) 'Calcium and calmodulin', *Cell Calcium*, 13(6–7), pp. 355–362. Available at: https://doi.org/10.1016/0143-4160(92)90049-X.

Wu, L. and Chen, J. (2023) 'Type 3 IP3 receptor: Its structure, functions, and related disease implications', *Channels*, 17(1), pp. 1–15. Available at: https://doi.org/10.1080/19336950.2023.2267416.

Xie, J. *et al.* (2016) 'SOCE and cancer: Recent progress and new perspectives', *International Journal of Cancer*. Wiley-Liss Inc., pp. 2067–2077. Available at: https://doi.org/10.1002/ijc.29840.

Xie, Q. *et al.* (2021) 'Tspan5 promotes epithelial–mesenchymal transition and tumour metastasis of hepatocellular carcinoma by activating Notch signalling', *Molecular Oncology*, 15(11), pp. 3184–3202. Available at: https://doi.org/10.1002/1878-0261.12980.

Yang, F. *et al.* (2023) 'Human umbilical cord mesenchymal stem cell-derived exosomes ameliorate liver steatosis by promoting fatty acid oxidation and reducing fatty acid synthesis', *JHEP Reports*, 5(7), p. 100746. Available at: https://doi.org/10.1016/j.jhepr.2023.100746.

Yang, W.S. *et al.* (2017) 'Diosgenin, an Activator of 1,25D 3 -MARRS Receptor/ERp57, Attenuates the Effects of TNF-α by Causing ADAM10-Dependent Ectodomain Shedding of TNF Receptor 1', *Cellular Physiology and Biochemistry*, 43(6), pp. 2434–2445. Available at: https://doi.org/10.1159/000484396.

Yoo, C.B. *et al.* (2012) 'γ-Secretase-dependent cleavage of E-cadherin by staurosporine in breast cancer cells', *Cell Communication and Adhesion*, 19(1), pp. 11–16. Available at: https://doi.org/10.3109/15419061.2012.665969.

Yu, T.J. *et al.* (2021) 'PDSS1-mediated activation of CAMK2A-STAT3 signaling promotes metastasis in triple-negative breast cancer', *Cancer Research*, 81(21), pp. 5491–5505. Available at: https://doi.org/10.1158/0008-5472.CAN-21-0747.

Zhang, C. *et al.* (2010) 'Adam10 is essential for early embryonic cardiovascular development', *Developmental Dynamics*, 239(10), pp. 2594–2602. Available at: https://doi.org/10.1002/dvdy.22391.

7 Annex

7.1 List of Abbreviations

µg	Microgram
µL	Microliter

AD	Alzheimer's Disease
ADAM	A Disintegrin and Metalloproteinase
AJ	Adherens Junction
AP-BTC	Alkaline Phosphatase-Betacellulin
APP	Amyloid Precursor Protein
Ca^{2+}	Calcium
CaM	Calmodulin
CAMK	Calmodulin Kinase
CCD	Charge Couple Device
CFU	Colony Forming Units
CRAC	Calcium release-activated channel
CTF	C-terminal Fragment
DMEM	Dulbecco's Modified Eagle Medium
EGF	Epidermal Growth Factor
EGFR	Epidermal Growth Factor Receptor
EMT	Epithelial to Mesenchymal Transition
FCS	Fetal Calb Serum
GI	GI254023X
IP_3R	Inositol Triphosphate Receptor
iRhom	Inactive Rhomboid-like Protein
KD	Knockdown
kDa	Kilodalton
MMP	Matrix metalloproteinase
MOI	Multiplicity of Infection
NCX	Sodium-Calcium Exchanger
PS	Phosphatidylserine
PFA	Paraformaldehyde
PLC	Phospholipase C
PLL	Poli-L-Lysine
ROI	Region of Interest
SARAF	SOCE-associated regulatory Factor
SERCA	Sarcoplasmic/endoplasmic reticulum calcium ATPase
SH3	Src Homology Region-3
shRNA	Small hairpin RNA
SOAR	STIM-Orai activating region
SOCE	Store-Operated Calcium Entry
SSC	Systemic Sclerosis
STIM	Stromal Interaction Molecule
THY	Todd Hewitt Broth w/ 2% Yeast Extract
TIMP	Tissue Inhibitor of Metalloproteinases
TRP	Transient Receptor Potential
Tspan	Tetraspanin
VGCC	Voltage-Gated Calcium Channel
WB	Western blot
WT	Wild-Type

7.2 List of Figures

7.3 List of tables

8 Acknowledgment

A doctor thesis is at many points written and referred to as a singular work. Wrongly suggesting that we students perform all the work, everytime. In reality, this cannot be further away from the truth since many people either directly or indirectly have helped me in mine. To them, I dedicate these words.

To my newly found family in Germany, those who, for a student far from home, became a second family supporting me whenever they could. To Nina and Maria, not only for their superb technical assistance in the lab which helped me with everything included in this thesis, but also for their day-to-day support. To my colleagues and friends, Ahmad and Mariana, it has been a pleasure laughing, gossiping and of course, working and collaborating with you during my years in the lab, I am sure life will still keep us around. Finally and not least thank you Daniela for nurturing me and preparing me for my professional future, your dedication to your work, capability of keeping up with everything involved and at the same time maintaining your characteristic positive attitude is an example I will try to replicate in my future endeavors. To my colleagues from the department of pharmacology and toxicology for their help, readiness, scientific insights and collaborations, which helped me go through the line, whenever I was in need of assistance I knew I could count with Uli Wissenbach Andreas Beck, Stephan Philipp, Adolfo Cavalié, Heidi Löhr and Veit Flockerzi. To my family back home, dad, mom and brothers and sister. Every single minute put out during my work was done with all of you in mind, thank you all for molding me into who I am today. None of it would have been possible without you. And lastly, I would like to thank my partner Lara, for supporting me in every way possible during my studies. Your love and support made everything easier. You help me do better and overcome myself, trying to put out the best version there is of me every day, so thank you.

9 Publications

- Cook, L., Gharzia, F.G., Bartsch, J.W. and Yildiz, D. (2024), A jack of all trades – ADAM8 as a signaling hub in inflammation and cancer. FEBS J, 291: 3989 4008. https://doi.org/10.1111/febs.17034

- Aljohmani A, Heinze H, Gharzia FG, Reda B, Abdrabou AMM, Becker SL, Bischoff M, Hannig M, Yildiz D. Extracellular Release of a Disintegrin and Metalloproteinase Correlates With Periodontal Disease Severity. J Clin Periodontol. 2025 Feb;52(2):237-248. doi: 10.1111/jcpe.14073. Epub 2024 Sep 24. PMID: 39317350; PMCID: PMC11743067.

- Gharzia, F.G., Aljohmani, A., Beck, A. *et al.* Regulation of ADAM10 activity through microdomain-dependent intracellular calcium changes. *Cell Commun Signal* **22**, 531 (2024). https://doi.org/10.1186/s12964-024-01891-5.

- Federico Guillermo Gharzia, Lukas Exner-Brown, Erik Kosche, Martin Empting, Daniela Yildiz. Quorum Sensing Inhibition - Interference with the host-pathogen-interaction exemplified for regulated proteolysis (in preparation).

10 Resume

The curriculum vitae was removed from the electronic version of the doctoral thesis for reasons of data protection.